

**The Physics and Chemistry of Semiconductor Nanocrystals in Sol-gel
Derived Optical Microcavities**

by

Yinthai Chan

B.S. Chemistry
University of California, Berkeley, 2001

Submitted to the Department of Chemistry
in Partial Fulfillment of the Requirements for the Degree of

DOCTOR OF PHILOSOPHY

at the

MASSACHUSETTS INSTITUTE OF TECHNOLOGY

June 2006

© 2006 MASSACHUSETTS INSTITUTE OF TECHNOLOGY
All Rights Reserved

Signature of Author _____

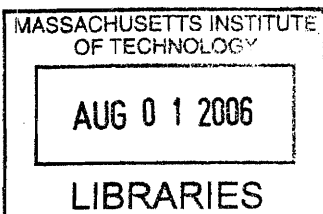
Department of Chemistry
May 11, 2006

Certified by _____

Moungi G. Bawendi
Professor of Chemistry
Thesis Supervisor

Accepted by _____

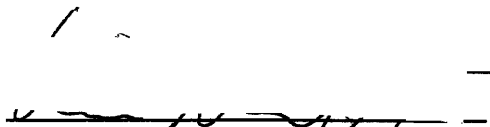
Robert W. Field
Chairman, Department Committee on Graduate Students



ARCHIVES

This doctoral thesis has been examined by a committee of the Department of Chemistry as follows:

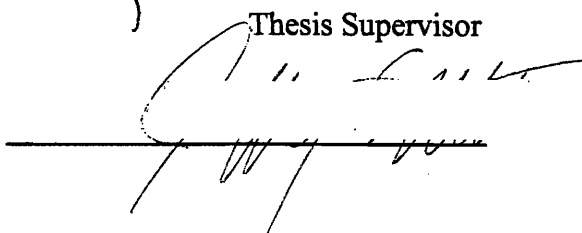
Professor Andrei Tokmakoff


Chairman

Professor Mounji G. Bawendi


Thesis Supervisor

Professor Jeffrey I. Steinfeld



The Physics and Chemistry of Semiconductor Nanocrystals in Sol-gel Derived Optical Microcavities

by

Yinthai Chan

Submitted to the Department of Chemistry on May 11, 2006 in Partial Fulfillment of the Requirements for the Degree of Doctor of Philosophy in Chemistry

ABSTRACT

The incorporation of semiconductor nanocrystals (NCs) into sol-gel derived matrices presents both novel applications as well as a robust platform in which to investigate the nonlinear optical properties of NCs. This thesis summarizes our present understanding of the chemistry of the incorporation process and the applications and underlying optical physics that was gleaned from studying these NC-doped sol-gel structures. Chapter 2 describes the synthesis of NC-doped core-shell silica microsphere composites of tunable size and emission wavelength, as well as their subsequent use for *in-vivo* imaging of blood vessels. This chapter illustrates how an appreciation of the kinetics of the Stöber process allowed for the achievement of highly monodisperse microsphere composites with a uniform incorporation of NCs. Chapter 3 reviews the requirements for achieving stimulated emission in CdSe NCs and details the development of NC-based lasers through sol-gel derived microcavities, from distributed feedback (DFB) grating structures to spherical microresonators exhibiting whispering-gallery mode lasing. Chapter 4 compares and explicates the differences between silica and titania as host matrices for NCs in terms of their chemical stability in the presence of solvents. This chapter explores the possibility of integrating NC-based microcavity lasers with microfluidic networks, thus providing the potential to dynamically tune the optical properties of the laser through interaction with different solvent environments on a miniaturized scale. Extension of the spectral window of NC-based gain media is discussed in Chapter 5, where extremely fast non-radiative Auger relaxation processes encountered in blue-emitting CdSe NCs may be circumvented by employing an alternative semiconductor NC, CdS/ZnS. Through judicious chemistry CdS/ZnS NCs may be uniformly incorporated into a sol-gel derived microcavity to provide room temperature lasing at blue wavelengths. Finally, our investigation into the optical physics of NCs in sol-gel derived microcavities is summarized in Chapter 6, which describes our observation of stimulated emission from multiexcitonic states in CdSe/ZnS NCs incorporated into a titania matrix. We employ transient photoluminescence to optically characterize the emission from these multiexcitonic states, which we attribute to $1P_{3/2}$ - $1P_e$ transitions. A DFB structure is introduced onto the CdSe/ZnS-titania composite to facilitate simultaneous lasing at two distinct wavelengths.

Thesis Supervisor: Mounji G. Bawendi, Ph.D.
Title: Professor of Chemistry

To my family

Table of Contents

Title page	1
Signature page.....	3
Abstract.....	5
Dedication.....	7
Table of contents.....	9
List of figures.....	11
Chapter 1: Introduction	
1.1: A brief introduction to semiconductor nanocrystals.....	15
1.1.1: Electronic structure and optical properties	16
1.1.2: Synthesis.....	20
1.1.3: Surface passivation.....	22
1.2: An introduction to sol-gel chemistry.....	24
1.3: Silica microspheres.....	25
1.3.1: Motivation.....	25
1.3.2: Synthesis.....	25
1.3.3: The challenge of doping silica microspheres with NCs.....	30
1.4: Titania thin films.....	31
1.4.1: Motivation: NCs as gain media.....	31
1.4.2: The need for sol-gel derived films.....	35
1.4.3: Further development and challenges.....	36
1.5: Thesis overview.....	37
1.6: References.....	39
Chapter 2: Incorporation of NCs into Core-Shell Silica Microspheres	
2.1: Introduction.....	43
2.2: Strategy for incorporating NCs into microspheres.....	46
2.3: Experimental.....	50
2.3.1: Silica overcoated microspheres.....	50
2.3.2: Titania overcoated microspheres.....	50
2.3.3: Bare silica microspheres.....	51
2.3.4: Sample preparation and characterization.....	51
2.4: Results.....	53
2.4.1: On the coating process.....	53
2.4.2: Characterization by transmission electron microscopy.....	54
2.4.3: Characterization by fluorescence microscopy.....	56
2.4.4: Emission characterization, loading fraction and quantum yield.....	58
2.4.5: Characterization by wavelength dispersive spectroscopy.....	61
2.4.6: Extension of coating procedure to titania.....	61
2.5: Application to <i>in-vivo</i> imaging.....	63
2.6: Conclusions.....	64
2.7: References.....	66

Chapter 3: On the development of CdSe/ZnS NC lasers	
3.1: Chapter overview.....	69
3.2: Soft-Lithographically Embossed Distributed-Feedback NC Lasers.....	70
3.2.1: Motivation.....	70
3.2.2: Experimental.....	71
3.2.3: Characterization by Atomic Force Microscopy.....	74
3.2.4: Optical characterization.....	77
3.2.5: Conclusions.....	79
3.3: Semiconductor NC/Microsphere Resonator Composites.....	80
3.3.1: Introduction.....	80
3.3.2: Experimental.....	82
3.3.3: Materials characterization.....	83
3.3.4: Optical characterization.....	87
3.3.5: Quality factor, threshold and stability characterization.....	89
3.3.6: Fitting with Mie theory.....	91
3.3.7: Conclusions.....	92
3.4: Chapter conclusion.....	93
3.5: References.....	94
Appendix A – Notes on the synthesis of core and core-shell NCs and their incorporation into titania matrices.....	97
Chapter 4: A Solvent-Stable NC-based Laser	
4.1: Chapter overview.....	103
4.2: Introduction.....	105
4.3: Initial attempts.....	107
4.4: Experimental.....	113
4.4.1: Preparation of NC-silica sols.....	113
4.4.2: Preparation of Distributed-Feedback NC-silica structures.....	113
4.4.3: Preparation of NC-silica Microsphere Resonator structures.....	114
4.5: Results.....	114
4.5.1: The incorporation process.....	114
4.5.2: Optical characterization.....	117
4.5.3: Effects of amines on lasing.....	120
4.6: Conclusions.....	124
4.7: References.....	125
Chapter 5: A Blue Nanocrystal Laser: The Case of CdS/ZnS	
5.1: Chapter overview.....	127
5.2: Introduction.....	128
5.3: Experimental.....	129
5.3.1: Synthesis of CdS/ZnS NCs.....	129
5.3.2: Incorporation of CdS/ZnS into silica waveguides.....	132
5.3.3: Coupling the NC-silica composites to microspheres.....	132
5.4: Results and discussion.....	133
5.4.1: On the incorporation process.....	133

5.4.2: Tunable ASE at room temperature.....	135
5.4.3: Photostability study.....	136
5.4.4: Variable stripe length measurements.....	138
5.4.5: Coupling to a feedback structure.....	139
5.5: Conclusion.....	142
5.6: References.....	143
Appendix A – Incorporating core CdS NCs into silica films.....	145
Appendix B – Achieving ASE from CdS/ZnS-silica composites using a nanosecond excitation source.....	147
Chapter 6: Stimulated Emission from Multiexcitonic States in CdSe/ZnS NCs	
6.1: Introduction.....	149
6.2: Experimental.....	152
6.2.1: Synthesis of core and core-shell CdS/ZnS NCs.....	152
6.2.2: Incorporation into titania and fabrication of NC-titania DFBs.....	152
6.2.3: Optical measurements.....	153
6.3: Characterization of the multiexcitonic transition.....	154
6.3.1: Transient photoluminescence measurements.....	154
6.3.2: Lifetime measurements.....	157
6.3.3: Analysis of the energy splitting, Δ	159
6.3.4: Analysis of the power dependence of the emission bands.....	161
6.3.5: Amplified spontaneous emission measurements.....	168
6.3.6: Variable stripe length measurements.....	172
6.4: Lasing from multiexcitonic states in NCs.....	177
6.5: Summary and conclusions.....	179
6.6: References.....	181
Chapter 7: Concluding remarks.....	183
Curriculum Vitae.....	189
Acknowledgements.....	193

List of Figures

Fig. 1.1: Electronic density of states of quantum confined semiconductors.....	16
Fig. 1.2: Size dependent optical properties of CdSe NCs.....	18
Fig. 1.3: Illustration of the electronic structure of CdSe NCs.....	19
Fig. 1.4: Experimental setup for the synthesis of CdSe NCs.....	21
Fig. 1.5: TEM image of CdSe NCs.....	21
Fig. 1.6: SEM images of Stöber silica microspheres.....	28
Fig. 1.7: Histograms of TEM images of Stöber spheres.....	29
Fig. 1.8: Gain profiles of quantum confined semiconductors.....	32
Fig. 1.9: Conditions for optical gain in NCs.....	33
Fig.1.10: ASE from close-packed films of CdSe at 80 K.....	35
Fig. 2.1: Initial attempts at incorporating NCs into Stöber spheres.....	46
Fig. 2.2: SEM and fluorescence microscope images of initial attempts.....	47
Fig. 2.3: Schematic of an improved strategy.....	49
Fig. 2.4: TEM image of overcoated NC-silica microspheres.....	55
Fig. 2.5: Histogram depicting size distribution of microspheres.....	55
Fig. 2.6: Fluorescence microscope images of NC-silica microspheres.....	56
Fig. 2.7: Close-packing of NC-silica microspheres.....	57
Fig. 2.8: NC-silica microspheres of different sizes and colors.....	58
Fig. 2.9: Emission profiles of NC-silica microspheres.....	60
Fig.2.10: Emission profile before and after incorporation into microspheres.....	60
Fig.2.11: Fluorescence microscope image of titania coated silica microspheres...	62
Fig.2.12: TEM image of titania coated silica microspheres.....	62
Fig.2.13: <i>In-vivo</i> image of NC-microspheres circulating blood vessels.....	64
Fig. 3.1: Schematic for embossing NC-titania films with a grating structure.....	74
Fig. 3.2: AFM image of an embossed NC-titania film.....	75
Fig. 3.3: AFM images of a multi-layer embossed NC-titania structure.....	76
Fig. 3.4: Lasing from an embossed NC-titania DFB film.....	78
Fig. 3.5: Lasing from a multi-layer DFB NC-titania heterostructure.....	78
Fig. 3.6: SEM/fluorescence microscope images of NC-titania microspheres.....	85
Fig. 3.7: Necking between NC-titania microsphere resonators.....	86
Fig. 3.8: WGM lasing spectra.....	88
Fig. 3.9: Histogram of lasing thresholds.....	90
Fig.3.10: Photostability of lasing from a NC-titania microsphere resonator.....	90
Fig.3.11: Fits of the lasing transitions using Mie theory.....	92
Fig.3.A.1: Absorption/emission spectra of CdSe synthesized from Cd(acac) ₂	100
Fig.3.A.2: Absorption/emission spectra of a very large CdSe NC sample.....	101
Fig. 4.1: NC-titania film exposed to water.....	106
Fig. 4.2: Incorporation process of NCs into titania and silica.....	108
Fig. 4.3: NC-silica film without thermal annealing.....	110
Fig. 4.4: NC-silica film without thermal annealing exposed to water.....	111
Fig. 4.5: NC-silica film annealed at 80°C.....	112
Fig. 4.6: NC-silica film annealed at 200°C.....	112
Fig. 4.7: Thermally annealed NC-silica film exposed to water.....	116
Fig. 4.8: AFM image of a NC-silica film.....	116

Fig. 4.9: Thermally annealed NC-silica film exposed to water.....	118
Fig.4.10: Lasing in water from a NC-silica DFB film.....	119
Fig.4.11: WGM lasing in ethanol from a NC-silica microsphere resonator.....	119
Fig.4.12: Schematic of a NC-silica/PDMS construct.....	120
Fig.4.13: Photograph of the NC-silica/PDMS construct.....	121
Fig.4.14: ASE data from VSL measurements.....	122
Fig.4.15: Lifetime measurements on a NC-silica film.....	123
Fig.4.16: Effect of amines on lasing intensity.....	124
Fig. 5.1: Absorption/emission spectra of CdS and CdS/ZnS NCs.....	131
Fig. 5.2: AFM image of a CdS/ZnS-silica film.....	135
Fig. 5.3: Fluorescence and ASE spectra of CdS/ZnS-silica films.....	136
Fig. 5.4: Photostability of ASE in a CdS/ZnS-silica film.....	137
Fig. 5.5: VSL measurements on a CdS/ZnS-silica film.....	139
Fig. 5.6: Fluorescence microscope image of a CdS/ZnS-silica microsphere.....	140
Fig. 5.7: WGM lasing from a CdS/ZnS-silica microsphere.....	141
Fig. 5.8: Intensity versus pump power curve.....	141
Fig.5.A.1: Emission spectrum of a CdS-silica film.....	146
Fig.5.A.2: Room temperature ASE from a CdS-silica film.....	146
Fig.5.B.1: Excitation of CdS/ZnS-silica films with a Nd:YAG.....	148
Fig. 6.1: Relaxation dynamics of multiexciton states in CdSe NCs.....	151
Fig. 6.2: 3D transient PL spectrum.....	155
Fig. 6.3: Transient PL spectra of 2.3 nm CdSe NCs.....	155
Fig. 6.4: Transient PL spectra of 4.3 nm CdSe NCs.....	156
Fig. 6.5: Transient PL band-edge spectra of 2.3 nm CdSe NCs.....	156
Fig. 6.6: Biexciton decay dynamics.....	158
Fig. 6.7: Multiexciton decay dynamics.....	158
Fig. 6.8: Plot of energy splitting, Δ , against NC radius.....	160
Fig. 6.9: Comparison between Δ and the $1P_{3/2}-1P_e$ energy transition.....	160
Fig.6.10: Single exciton saturation curve.....	163
Fig.6.11: Power dependence of the multiexcitonic band.....	163
Fig.6.12: PL spectra after subtraction of the single exciton contribution.....	166
Fig.6.13: Calculated single exciton contribution to the PL spectrum.....	166
Fig.6.14: Biexciton power dependence.....	167
Fig.6.15: Normalized power dependence of single, bi-, multiexciton bands.....	167
Fig.6.16: Linear emission from a NC-titania film.....	169
Fig.6.17: Bi-, and multiexciton ASE from a NC-titania film.....	169
Fig.6.18: ASE intensity versus pump power curves.....	170
Fig.6.19: Bi-, and multiexciton ASE from 5.3 nm CdSe/ZnS in titania.....	170
Fig.6.20: Bi-, and multiexciton ASE from 4.2 nm CdSe/ZnS in titania.....	173
Fig.6.21: ASE intensity versus pump power curves.....	174
Fig.6.22: VSL measurements.....	176
Fig.6.23: Modal gain profile of a CdSe/ZnS-titania film.....	176
Fig.6.24: Biexciton lasing from a NC-titania DFB.....	178
Fig.6.25: Multiexciton lasing from a NC-titania DFB.....	178
Fig. 7.1: AFM and SEM images of mesoporous silica films.....	185
Fig. 7.2: Emission spectra of PbSe NC-silica films.....	187

Chapter 1

Introduction

1.1 A brief introduction to semiconductor nanocrystals

Although the initial motivation to study semiconductor nanocrystals (NCs) was to investigate and understand the evolution of bulk structural and electronic properties from the molecular scale in the early 1980's,¹ NCs have since become ubiquitous in a large and diverse number of disciplines, from synthetic chemistry²⁻⁴ and optical physics⁵⁻⁷ to biological imaging.⁸⁻¹¹ Independent research groups dedicated to NC research have, in the past two decades, made remarkable progress in enabling both fundamental scientific discoveries as well as potentially impacting technological applications such as light emitting diodes (LEDs)^{12,13} and solar cells.¹⁴

What then, are semiconductor NCs? They are essentially molecular clusters of inorganic material measuring on the order of 1 - 10 nm across in diameter. These fragments of semiconductor material, comprising of hundreds to thousands of atoms, represent an intermediate size-scale that lies in between the regimes of bulk and molecular systems.¹⁵⁻¹⁷ As the physical dimensions of these clusters become comparable to the bulk exciton Bohr radius ($\sim 56 \text{ \AA}$ in the case of CdSe), quantum confinement effects become significant and their electronic energy levels are discrete in all three dimensions. Figure 1.1 illustrates the evolution of electronic states in a semiconductor as its dimensions decrease in size. Thus while in the case of a bulk semiconductor the

density of states is essentially continuous, the density of states in a quantum well (whose carriers experience confinement in one dimension) and quantum wire (whose carriers experience confinement in two dimensions) show progressively sharper and more distinct transitions. This trend culminates in the discrete, atomic-like density of states of a nanocrystal (whose carriers experience confinement in all three dimensions), which represents the pinnacle of quantum confinement.

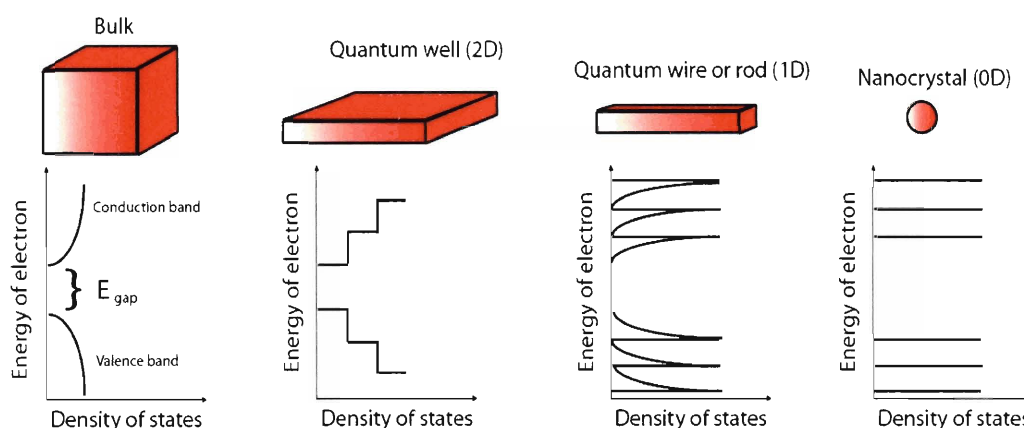


Figure 1.1 Illustration of the effects of quantum confinement as the physical dimensions of the semiconductor decrease. The density of states near the edges of the conduction and valence bands are shown. It is readily seen that the energy levels progressively become more discrete going from a bulk solid to a NC, which exhibits an atom-like electronic structure. This is perhaps why semiconductor NCs have sometimes been termed “artificial atoms”.

1.1.1 Electronic structure and optical properties

As shown above, the effect of quantum confinement reduces the electronic structure in a semiconductor NC to a few discrete optical transitions, which can be probed and characterized by spectroscopy. Although a wide variety of semiconductor NCs are known (InP, InAs, CdS, PbSe, etc.), we limit our description to a qualitative picture of the electronic structure of CdSe NCs, which is the main NC material that will be discussed in this thesis. A more quantitative and detailed theoretical account may be

found in reference [18]. Perhaps the most dramatic consequence of quantum confinement in NCs is the blue-shifting of their band-edge emission or absorption with decreasing size, as illustrated in Figure 1.2. Thus different-sized CdSe NCs can emit from 450 nm to 660 nm, covering most of the visible spectrum. A particle in a sphere model in which the carriers are confined to a potential that is infinite at the boundaries may be used to qualitatively understand this. Solving for the energy of the first excited state gives

$$E_{1s} = \hbar^2 / 8m_{eff}a^2 \quad (1.1)$$

where the effective mass, m_{eff} takes into account the interaction with the lattice, and a is the radius of the sphere. It is readily seen that the energy shifts to the blue with decreasing size according to $1/a^2$. It should be noted that while this simple effective mass model provides an intuitive description of the size-dependence of the band-edge optical transitions in CdSe NCs, it does not explain the observed luminescence Stokes shifts, long emission lifetimes and its strong magnetic field dependence. Refinements to this model to explain these phenomena take into account the electron-hole exchange interaction and nanocrystal shape asymmetry, and are detailed elsewhere.¹⁹

Besides illustrating the size-dependence of the band-edge transitions in CdSe NCs, the absorbance data in Figure 1.2 also highlights two important aspects of their optical properties. The first is their nearly continuous absorption profile at energies higher than their band-edge transition, which corresponds to the first pronounced peak from the red side of the absorption spectrum. This allows different-sized NCs to be simultaneously excited with a single light source. The second important aspect highlighted by their absorption profile is the presence of prominent features and pronounced peaks. These features are attributed to the different electronic transitions

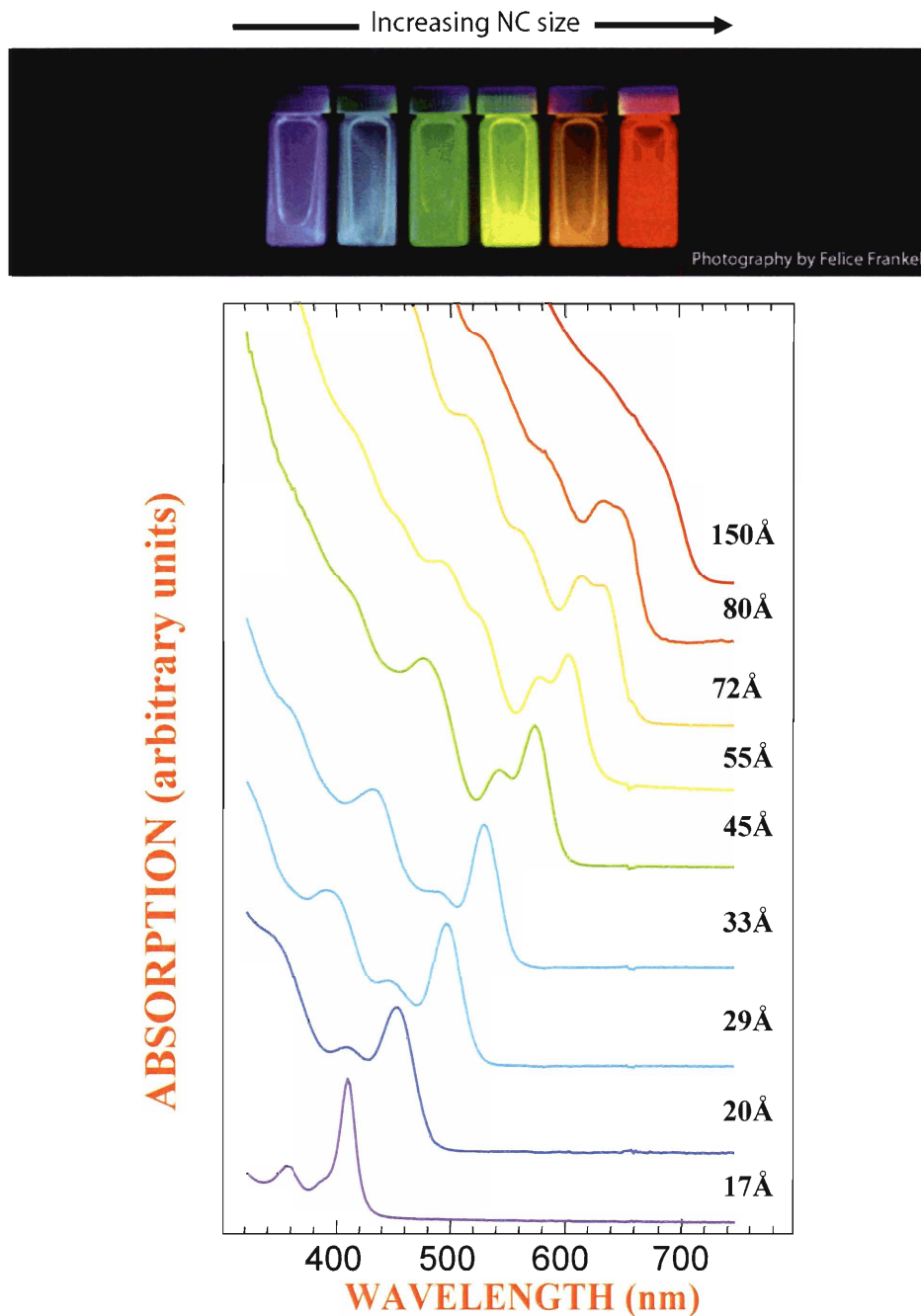


Figure 1.2 The size-dependent optical properties of CdSe NCs. Top: Photograph (courtesy of Felice Frankel) of CdSe NCs in hexane excited with a single light source, affording a wide range of colors in the visible by tuning the size of the NCs. Bottom: The linear absorption spectra of CdSe NCs, showing the prominent peaks blue-shift as the size of the NC decreases. Figure extracted from C. B. Murray, Ph.D. Dissertation, MIT, 1995.

within the NC. The investigation and assignment of these transitions using photoluminescence excitation techniques have been reported²⁰, and Figure 1.3 provides a diagrammatic representation of the first few energy transitions in a CdSe NC.

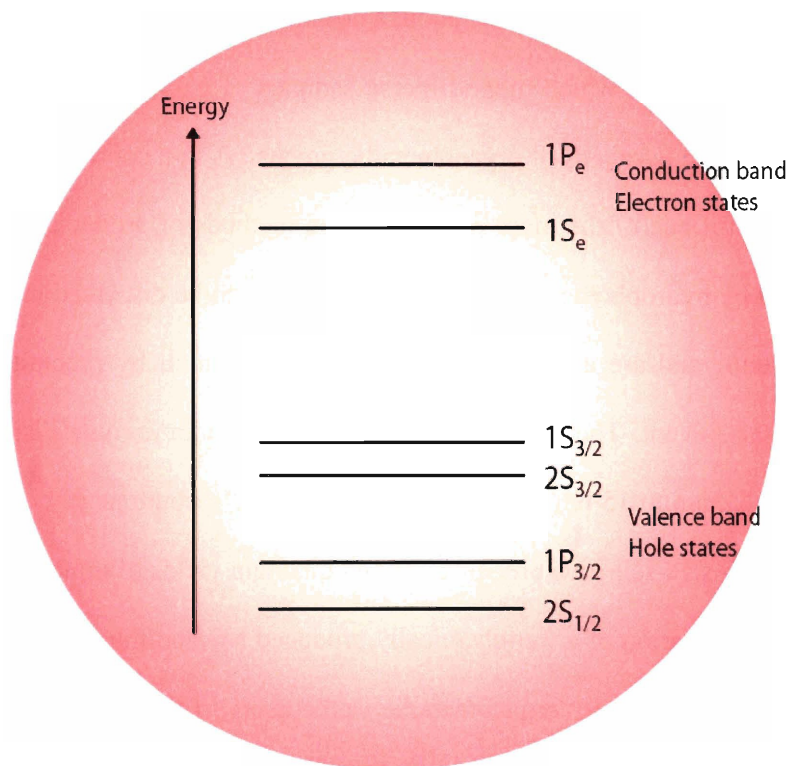


Figure 1.3 A schematic of the electronic structure of CdSe denoting the first few energy transitions. Note that the energy levels are not drawn to scale. The fine structure of the $1S_{3/2}$ and $1S_e$ states, which is discussed in reference [19], is not reflected.

1.1.2 Synthesis

Although semiconductor NCs have been prepared and optically studied in glass matrices as early as the 1980's,²¹ their immobilization in glass presented limited utility by way of applications. This was overcome about a decade later through the seminal work of Murray et. al. in 1993, in which monodisperse samples of CdS, CdTe and CdSe NCs were produced via the pyrolysis of organometallic precursors in a coordinating solvent,²² and is currently still one of the most widely adopted methods of producing NCs. These NCs are capped by hydrophobic ligands which allow them to be dispersed in a variety of non-polar solvents, and are also easily processed from solution by precipitating in an appropriate polar solvent. The CdSe NCs made via this synthetic route displayed size-tunability from 1.2 nm to 15 nm in diameter, narrow size-distributions of < 5% (RMS in diameter) by using size-selective precipitation and quantum yields of up to ~10%. Figure 1.4 provides an illustration of a wet-chemically produced NC and the experimental setup for its synthesis. Briefly, organometallic precursors (dimethyl cadmium and trioctylphosphine selenide) are mixed with trioctylphosphine and loaded into a syringe and injected rapidly into a coordinating solvent (in this case trioctylphosphine oxide) at elevated temperatures. This results in the pyrolysis of the organometallic precursors which spontaneously nucleate and grow into spherical clusters in the nanometer size range. Figure 1.5 is a transmission electron microscope (TEM) image of as-synthesized CdSe NCs, showing the uniformity of the size distributions that can be achieved by this method.

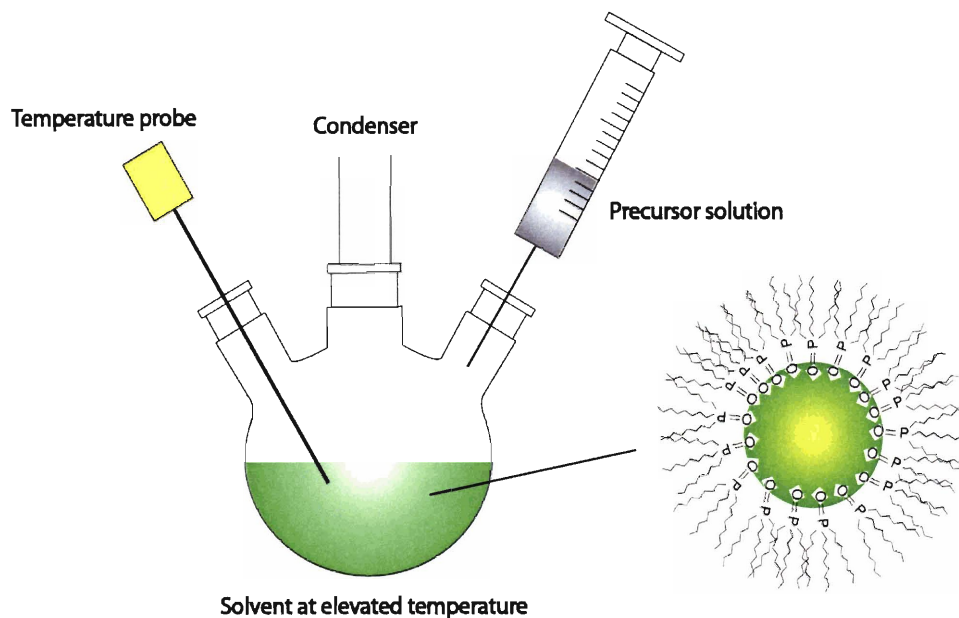


Figure 1.4 Illustration of a wet-chemically synthesized CdSe NC. An organometallic precursor solution containing cadmium and selenium is rapidly injected into a solvent at an elevated temperature, resulting in the nucleation and growth of CdSe NCs. The NCs are stabilized in the solvent by organic capping groups, which in this case are primarily trioctylphosphine and trioctylphosphine oxide.

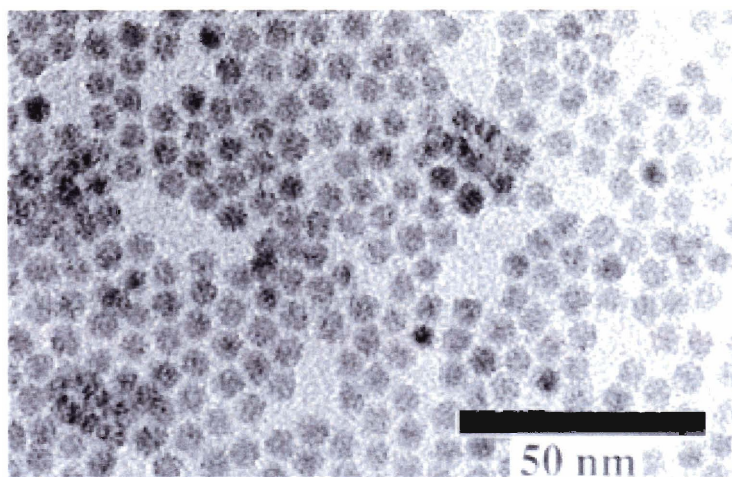


Figure 1.5 TEM image of CdSe NCs beginning to hexagonally close-pack. The image is taken from C. B. Murray, Ph.D. dissertation, Massachusetts Institute of Technology, 1995.

Recent developments in the wet-chemical synthesis of CdSe NCs have obviated the use of highly toxic and pyrophoric organometallic cadmium precursors in favor of cadmium salts such as cadmium oxide²³ and cadmium hydroxide.²⁴ These newly developed methods boast enhanced quantum yields and narrow size-distributions without size-selective precipitation, making CdSe NCs more attractive for applications. One such method, employing cadmium acetylacetonate (Cd(acac)₂) as the cadmium precursor,^{25,26} was used to synthesize most of the core CdSe NCs that are presented in this thesis. Its description will be afforded in a later chapter.

1.1.3 Surface passivation

Crystal defects and lack of capping ligands provide sites for non-radiative recombination in NCs, lowering their quantum yield. As mentioned in the previous section, as-synthesized CdSe NCs produced using the method of Murray employed trioctylphosphine (TOP) and trioctylphosphine oxide (TOPO) as capping ligands, resulting in quantum yields of up to 10%.²² It was later found that having amines as capping ligands played a pivotal role in affording better passivation of the CdSe NC surface than TOP or TOPO, yielding quantum yields of ~ 50%.^{27,28} However, as the amines are relatively labile, consecutive processing of these amine-capped CdSe NCs result in a steady decline of their quantum yield. An alternative route to increase the photoluminescence (PL) efficiency of CdSe NCs is to grow an epitaxial layer of a higher band gap material such as ZnS as a shell around the core NC. The ZnS shell not only passivates the surface of the CdSe NCs, resulting in quantum yields of up to ~ 50%,²⁸ but also serves as a protective layer against oxidation or harsh chemical processing. This

overcoating procedure presents a more robust way of increasing the quantum yields in NCs, and core-shell CdSe/ZnS NCs synthesized according to the methodology detailed in reference [28] were therefore used in most of the applications described throughout this thesis.

It should be noted that more recent developments to the inorganic passivation of CdSe NCs include epitaxially growing a shell of CdS on the CdSe core first, followed by a second shell of ZnS on CdS.³⁰ Because the CdS shell offers a relatively lower lattice mismatch with the CdSe surface (which is about 12% for ZnS on CdSe), thicker shell growth with a correspondingly smoother core-shell interface may be achieved. The second shell of ZnS on CdS serves as a wider band gap material to confine the electrons and holes in the NC core and also adds stability towards photodegradation.³⁰ These double-shell CdSe/CdS/ZnS constructs exhibit quantum efficiencies up to ~ 70%, and also possess higher absorption cross-sections than CdSe/ZnS NCs due to their significantly thicker shells. Another study reported quantum yields of up to ~ 70-85% by using a successive ion layer adsorption and reaction (SILAR) technique to grow alternating shells of CdS and ZnS on a CdSe NC, thus having control over the composition of the heterogeneous shell structure.³¹ These ongoing developments to improve the optical performance of CdSe-based NCs continue to ensure their high desirability as chromophores for various applications.

1.2 An introduction to sol-gel chemistry

As Brinker and Scherer broadly define in the context of metal oxides, “A *sol* is a colloidal suspension of solid particles in a liquid” and “If one molecule reaches macroscopic dimensions so that it extends throughout the solution, the substance is said to be a *gel*”.³² Thus sol-gel science is the study of colloidal particulates or macroscopically large molecules of metal oxides formed from the hydrolysis and subsequent condensation of metal alkoxides or salts. These studies have led to commercially important developments in ceramics such as ultra-fine powders, monoliths, thin film coatings and aerogels.³³ Because of their low absorption in the visible range, relatively high refractive index and flexibility of being shaped into various geometries, sol-gel derived metal oxides such as silica and titania make excellent materials for optical applications. For example, morphologically smooth silica films have been exploited as optical waveguides,³⁴ while monodisperse silica microspheres have been utilized for photonic applications.³⁵ It became obvious that sol-gel derived structures would make an excellent host matrix for optically active materials, and much effort has been made in doping sol-gel structures with semiconductor NCs for both applications and fundamental study. While this may seem ironic, given that NCs have been produced in glass matrices over two decades ago,²¹ the inherent flexibility of sol-gel chemistry to control the composition and morphology of metal oxides down to nanometer length scales presents sufficient impetus to warrant these endeavors. The ensuing sections will motivate and highlight past efforts in doping sol-gel derived microcavities with semiconductor nanocrystals.

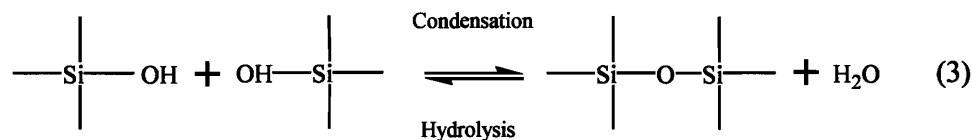
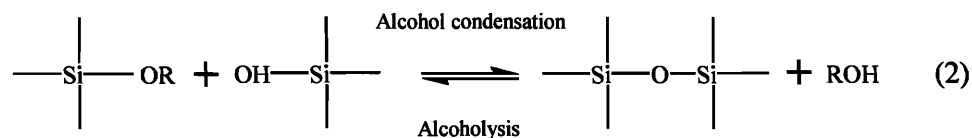
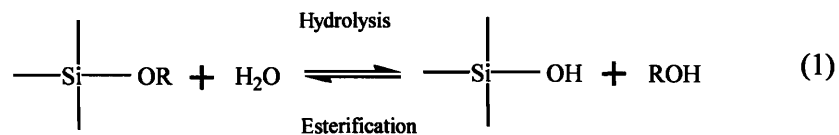
1.3 Silica microspheres

1.3.1 Motivation

The encapsulation of chromophores within a chemically inert and optically transparent microcavity has numerous advantages. Chief amongst these are: (1) the host cavity serves as a protection against the external environment, isolating the chromophores from chemical degradation; (2) in the absence of self-quenching, multiple chromophores may be packed into a single microcavity to increase its overall brightness; (3) the cavity size may be tuned to suit applications or facilitate fundamental studies which require specific size ranges. In this respect, sol-gel derived silica microspheres make excellent choices given their chemical stability in most solvents, their optical clarity and the flexibility of derivatizing their surface with different chemical functionality. It is no wonder then that organic dye-doped silica microspheres have been exploited for a myriad of uses such as flow cytometry⁴⁰ and endocytosis visualization,⁴¹ to name a few.

1.3.2 Synthesis

Perhaps the most well-known method for making silica microspheres is that of Stöber, whose landmark paper in 1968 demonstrated the controlled growth of monodisperse silica microspheres in the size range of 50 nm to 2 μm in diameter.³⁶ More commonly known as the Stöber process, the method involves the hydrolysis and subsequent condensation of a silicon alkoxide such as tetraethylorthosilica (TEOS) in a basic solution of ethanol and water. The process may be summarized as follows



Hydrolysis of the silicon alkoxide moiety, as reflected in Reaction (1), is the first step towards the formation of the silica matrix. In precursors such as TEOS, the presence of water alone is not sufficient to induce any appreciable forward reaction, and a small amount of ammonium hydroxide is used to catalyze the hydrolysis reaction in the Stöber process. In fact, the pH of the solvent environment plays an important role in the nucleation and growth kinetics of the silica monomers,³² influencing both size distribution and final particle sizes attained. In the Stöber process, the base-catalyzed hydrolysis of TEOS generally produces monodisperse microspheres in the sub-micrometer range,³⁷ whereas in the acid-catalyzed hydrolysis of TEOS, large particles (up to tens of microns in diameter) with size distributions that are difficult to control are

formed.^{38,39} Reactions (2) and (3) describe the condensation processes that facilitate the bridging of the silica network. It is seen from Reaction (2) that the alcohol solvent system can also play a role in the formation and cleaving of Si-O-Si bonds, which ultimately affects the sizes and size distributions of particles derived.³⁶ Figure 1.6 shows scanning electron microscope (SEM) images of large-area close-packing of the Stöber spheres on a silicon substrate, illustrating their monodispersity. Figure 1.7 depicts the range of sizes and size distributions of silica microspheres obtained by varying the concentration of ammonia. The trend in size obtained as a function of the concentration of ammonia is consistent with those reported in reference [37]. Low size-dispersity maintained over a range of submicron diameters is evident. Larger sizes may be obtained by increasing the concentration of TEOS. The relatively simple chemistry and exquisite control over the monodispersity and size of these silica microspheres via the Stöber process certainly make them ideal as optical microcavities for semiconductor nanocrystals.

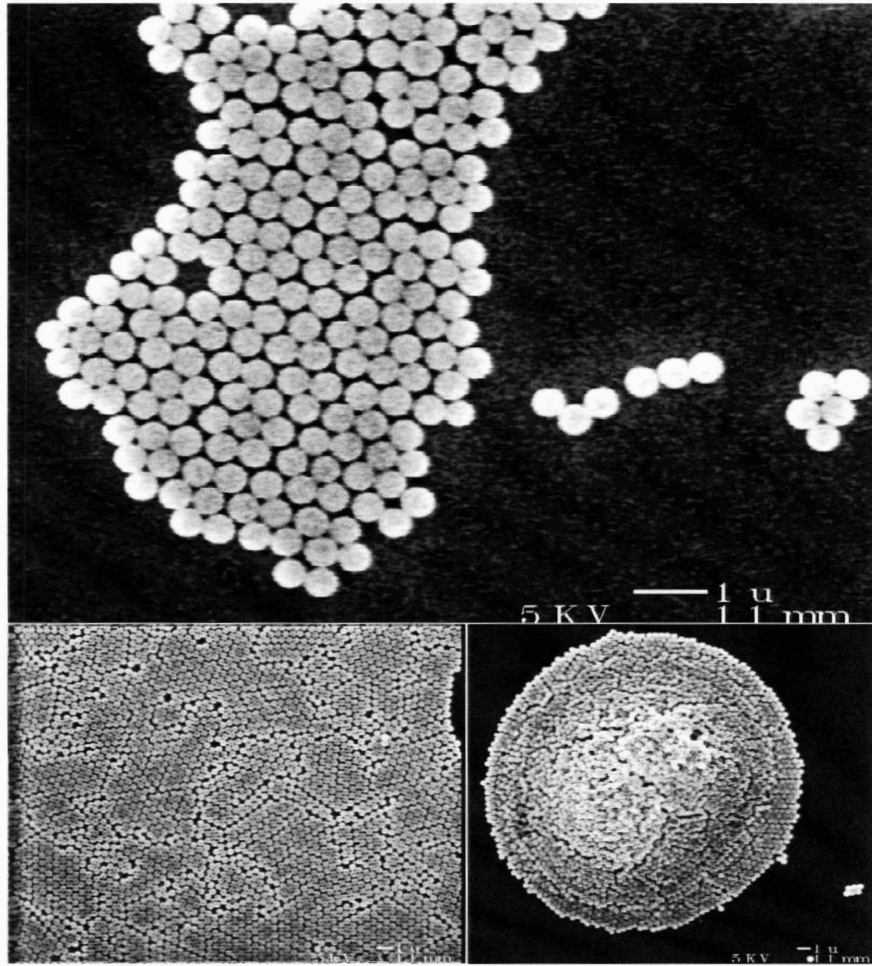


Figure 1.6 SEM images of ~ 420 nm diameter silica microspheres synthesized via the Stöber process. Owing to the monodispersity of the sample, close-packing over large areas is evident, and assembly into rational 3D structures should be readily achievable.

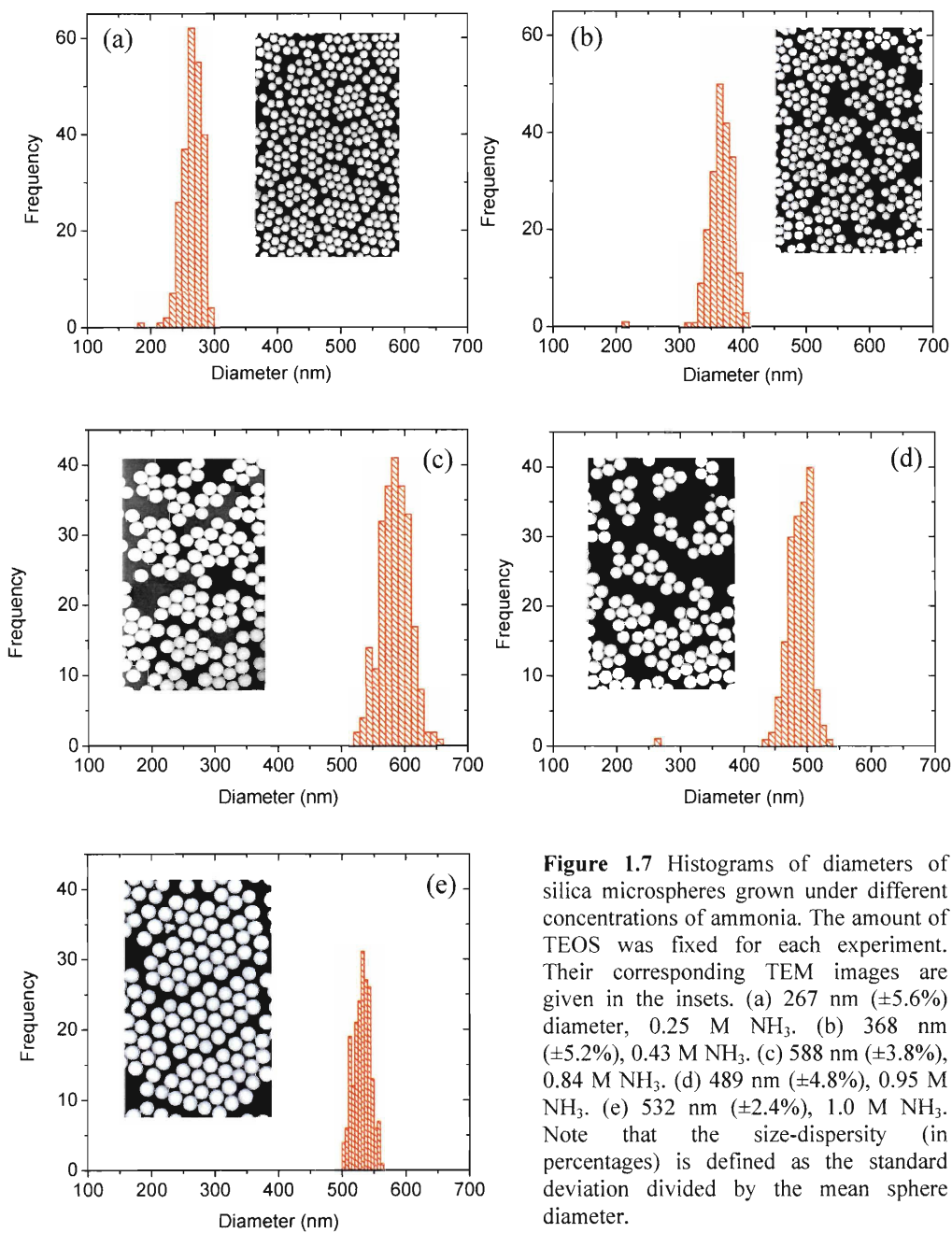


Figure 1.7 Histograms of diameters of silica microspheres grown under different concentrations of ammonia. The amount of TEOS was fixed for each experiment. Their corresponding TEM images are given in the insets. (a) 267 nm ($\pm 5.6\%$) diameter, 0.25 M NH_3 . (b) 368 nm ($\pm 5.2\%$), 0.43 M NH_3 . (c) 588 nm ($\pm 3.8\%$), 0.84 M NH_3 . (d) 489 nm ($\pm 4.8\%$), 0.95 M NH_3 . (e) 532 nm ($\pm 2.4\%$), 1.0 M NH_3 . Note that the size-dispersity (in percentages) is defined as the standard deviation divided by the mean sphere diameter.

1.3.3 The challenge of doping silica microspheres with NCs

While efforts to chemically dope microspheres with chromophores such as organic dyes^{40,42} and lanthanides⁴³ have generally been relatively straightforward and successful, many attempts utilizing various strategies to introduce semiconductor NCs into microspheres gave rather unsatisfactory results,⁴⁴⁻⁴⁸ and these will be described in more detail in the next chapter. Given the good control over the synthesis of microspheres via sol-gel processes, as well as the established procedures to produce high quality semiconductor NCs, chemically incorporating NCs into microspheres should be very feasible. Are there intrinsic reasons as to why the previous reported attempts should not work? What surface chemistry do we need to functionalize the NCs with to make them compatible with the sol-gel process? Efforts to dope high quality NCs into monodisperse microspheres have even led to alternative strategies such as confining hydrophobic NCs in commercially available mesoporous microspheres coated with hydrophobic ligands via Van der Waals interactions.⁴⁹ Submerging these microspheres into a non-polar solvent, however, results in the release of the NCs. A more robust method is clearly needed. Furthermore, another major obstacle is the difficulty of characterizing the doping concentration, spatial distribution and quantum yield of NCs within the sphere. For example, although light scattering techniques may be used to determine the increase in the refractive index of the doped microsphere in order to extract the concentration of NCs, a simple Mie theory calculation on a homogeneous sphere⁵⁰ would indicate that substantial increases in the refractive index would be needed to discern between scattering profiles. Coupled with the inhomogeneity of sphere sizes in an ensemble sample, employing such a technique would be impractical. Thus chemically

doping high quality NCs into monodisperse spherical cavities to produce well-characterized NC-microsphere composites presents a significant challenge that will be addressed in this thesis.

1.4 Titania thin films

1.4.1 Motivation: NCs as gain media

As a semiconductor becomes more and more dimensionally confined, its density of states becomes more discrete and the energy levels are spaced further apart, as described earlier. In the case of strongly confined systems such as NCs, the spacing between the electronic states is much greater than the thermal energy, preventing thermal depopulation of the first few excited states. Unlike in the case of bulk semiconductors, this should result in a temperature insensitive lasing threshold,^{51,52} thus circumventing one of the major drawbacks of bulk semiconductor lasers. The concentration of oscillator strength into a discrete, delta function-like density of electronic states should also result in the narrowing of the gain profile and increases in peak gain compared to a bulk semiconductor. This theoretical prediction is illustrated in Figure 1.8, which shows calculated peak gain values of progressively confined structures reproduced from reference [52]. It is clearly seen that the narrowest and highest peak gain profiles would be found in zero-dimensional semiconductors such as NCs. These theoretically predicted benefits, along with the ease of emission wavelength tunability, prompted numerous efforts to utilize NCs as gain media.^{53,54}

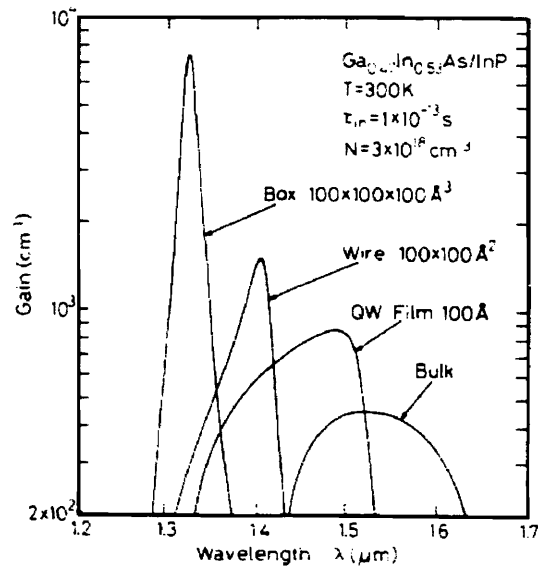


Figure 1.8 Calculated gain values for a $\text{Ga}_{0.47}\text{In}_{0.53}\text{As}/\text{InP}$ system as its physical dimensions are reduced and it becomes progressively quantum confined. The quantum box, which has the smallest dimensions, exhibits the narrowest gain profile and highest peak gain.

Stimulated emission in colloidal semiconductor NCs, however, was not demonstrated until the year 2000, in a close-packed film of CdSe NCs at low temperature.⁵⁵ The elusiveness of this achievement in the efforts of earlier investigators was attributed to an underestimation of the intrinsic non-radiative processes that occur in such strongly confined semiconductors. This point will be clarified following an explanation on the condition for optical gain: as a CdSe NC absorbs a photon, an electron-hole pair, or single exciton, is created. The electron is promoted to the doubly degenerate $1S_e$ electron state, leaving a hole behind in the $1S_{3/2}$ state. This condition is insufficient for optical gain to occur since an incoming photon resonant with the lasing transition can either be absorbed to create an additional exciton or stimulate emission

from the existing single exciton to leave behind a ground state NC. Since the probability of both these processes are on average, equal, this results in a transparency condition with no net photon amplification. If, however, the NC absorbs two photons and creates two electron-hole pairs, or a biexciton, then an incoming photon resonant with the lasing transition can only stimulate emission from the biexciton state to give a single exciton state. This is known as a gain condition and results in the net amplification of photons. A summary of these different conditions is depicted in Figure 1.9.

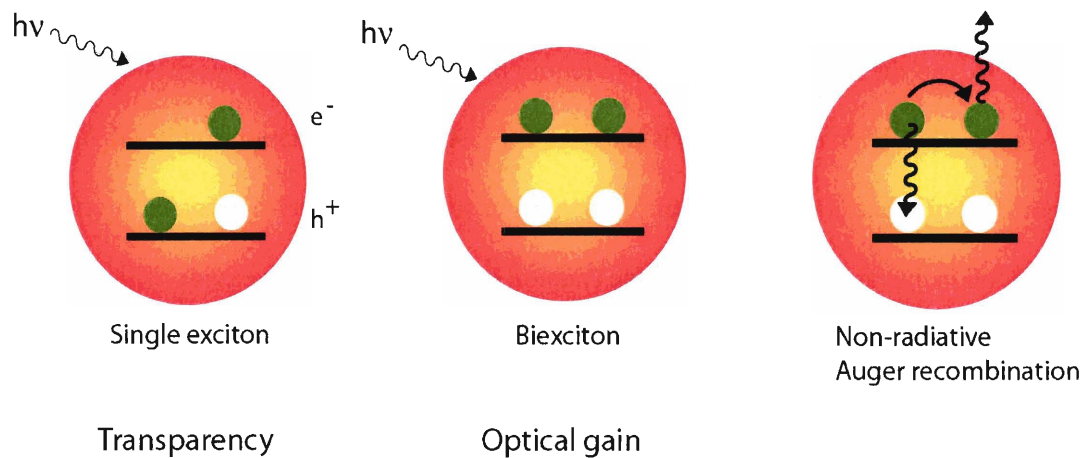


Figure 1.9 Absorption of a photon in an NC at ground state results in the creation of a single exciton, and in the context of light amplification in NCs this is known as the transparency condition. Creation of a biexciton (2 excitons) presents a gain condition, since incoming photons resonant with the lasing transition can only stimulate emission from the NC. However, the coulombic interaction between the 2 excitons results in a fast non-radiative relaxation process known as the Auger process.

The creation of the biexciton in a strongly confined system such as a NC, however, results in a strong coulombic interaction between the two excitons. This causes the non-radiative recombination of one of the excitons and the energy is transferred to the other exciton, thus effectively annihilating the gain condition. This non-radiative relaxation process, known as the Auger recombination process, is extremely fast, taking place at timescales on the order of $\sim 10 - 100$ ps.⁵⁶ A more lengthy discussion of the Auger process in NCs is given in reference [57]. With such an efficient non-radiative process that is intrinsic in NCs, it comes as no surprise that stimulated emission in NCs eluded many early investigators. An appreciation of the fast Auger relaxation timescales in NCs led to the realization that two requirements must be met before stimulated emission can be observed. The first is the need for fast, pulsed excitation sources that can generate a sufficient population of biexcitons faster than their Auger-dominated lifetime. The second is the need for a high volume fraction of NCs within a waveguide. This stems from the fact that the buildup time needs to be faster than the gain relaxation in order to observe stimulate emission. Since the gain relaxation is extremely fast due to Auger processes, the spacing between NCs needs to be close in order to ensure sufficient amplification of photons within the fast biexciton lifetime.⁵⁵ These two requirements were found to be satisfied by using a frequency-doubled, regeneratively amplified Ti:Sapph excitation source with a 100 fs pulse duration at a repetition rate of 1 kHz in conjunction with a close-packed film of CdSe NCs. The volume fraction of these films were as high as $\sim 20\%$, more than sufficient to observe stimulated emission.⁵⁵ Figure 1.10 summarizes the main results from the seminal work of reference [55].

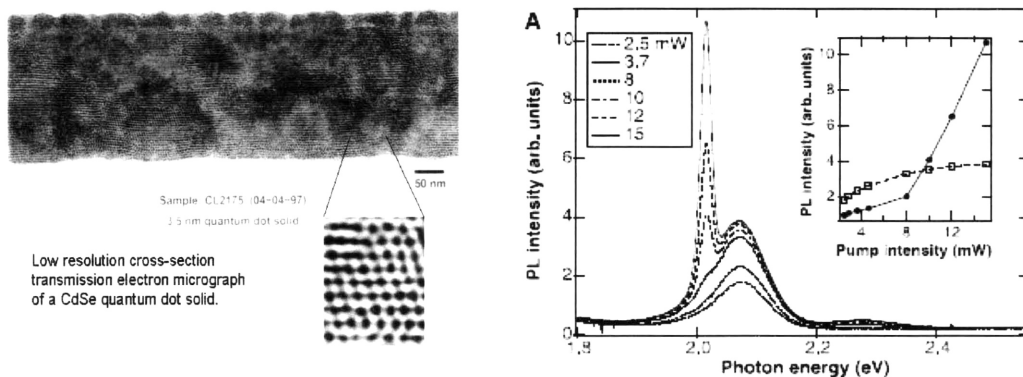


Figure 1.10 The achievement of amplified spontaneous emission (ASE) from close-packed films of CdSe (left image) at 80 K was the first demonstration of stimulated emission from colloidal semiconductor NCs. The emergence of the narrow peak on the lower energy side of the band-edge fluorescence (right image), with a corresponding threshold, signifies the development of ASE.

1.4.2 The need for sol-gel derived films

Although close-packed films possess a high volume fraction of NCs, they were thermally unstable to the intense excitation needed to obtain stimulated emission, and required low temperature conditions. This prompted the development of sol-gel derived titania films incorporating CdSe NCs in volume fractions sufficient to exhibit ASE. The key to this process was the judicious functionalization of the NC surface with ligands that made them compatible with the sol-gel process. These morphologically smooth NC-titania composite films not only possessed a relatively high refractive index ($n \sim 1.8$), making them excellent waveguides, but were also thermally resilient and could achieve ASE at room temperature.⁵⁸ This important achievement opened up the possibility of employing semiconductor NCs as robust gain media, presenting a stable platform in which to study the nonlinear optical behavior of NCs.⁵⁹

1.4.3 Further development and challenges

With the advent of thermally robust NC-titania composites, further investigation on the use of NCs as gain media may be classified into two diverging paths. The first path attempts to introduce optical feedback into the NC-titania microcavity in order to achieve emission wavelength-tunable lasing. Indeed, the utility of NC-based lasers depends strongly upon the facility of fabricating efficient optical feedback microcavity structures. Supposing that a facile procedure to produce cost-effective NC-laser microcavity structures is developed, how and why would they be useful for applications? The second path probes the fundamental optical physics of the lasing transitions. We are able to observe stimulated emission from the $1S_{3/2}$ - $1S_e$ transition in NC-titania films because the buildup time is faster than the relaxation of the biexciton to a single exciton. Would we be able to observe stimulated emission from higher transitions involving multiexcitonic (such as triexcitons, defined as 3 e-h pairs) states if we have a sufficiently fast buildup time? Assuming that this is possible, would it be stable enough that can we characterize and study its nonlinear properties (eg. modal gain, lasing threshold, etc.)? These two paths undoubtedly present numerous questions and challenges within the context of synthetic chemistry to optical physics, and efforts to address them will be elaborated in detail later on in this thesis.

1.5 Thesis overview

This thesis describes efforts to incorporate highly fluorescent semiconductor nanocrystals into various sol-gel derived microcavities. Much chemistry was developed in order to derive both novel optical physics and applications from these NC-doped microcavities. Chapter 2 details the successful incorporation of core-shell CdSe/ZnS NCs into silica or titania shells on monodisperse silica microspheres of various sub-micron diameters. These well-characterized NC-microsphere composites subsequently illustrate their utility in an in-vivo imaging experiment in the blood vessels of the brain of a mouse. Chapter 3 traces the development of NC-based lasers and is divided into two parts: the first describes soft-lithographically embossed distributed feedback (DFB) NC lasers and their flexibility in producing hierarchical structures that show simultaneous lasing at two different wavelengths. The second part focuses on deriving whispering gallery mode lasing from NC-titania films supported on large commercially available silica microsphere templates. Hundreds of these NC-microsphere resonators may be formed from a single spin-coat process, showing photostable lasing over millions of shots at room temperature. It is then shown in Chapter 4 that while titania matrices are thermally resilient, they do not offer chemical stability and structurally degrade in the presence of polar solvents. Silica is shown to be a good alternative host matrix, facilitating lasing in the presence of water and ethanol. These NC-silica composite lasers offer the possibility of being integrated with microfluidics and utilized as potential optical chemosensors. Chapter 5 introduces the possibility of extending the spectral window of NC-based lasers by using materials other than CdSe. Through the development of judicious surface chemistry, core-shell CdS/ZnS NCs are incorporated into silica matrices, showing ASE

and lasing at a large range of blue wavelengths. The optical physics of core-shell CdSe/ZnS NCs in titania matrices is probed in Chapter 6, which describes efforts in characterizing fluorescence and stimulated emission from multiexcitonic states. It is found from transient photoluminescence techniques that this fluorescence originates from a triexciton (3 electron-hole pair) state, at the $1P_{3/2}-1P_e$ transition. The NC-titania film is then embossed with a DFB structure to afford room temperature simultaneous lasing from both biexcitonic and multiexcitonic transitions. Finally, Chapter 7 offers a short overall conclusion to the thesis and a note on the future outlook of these endeavors.

1.6 References

1. R. Rossetti, S. Nakahara, L. E. Brus, *J. Chem. Phys.* **1983**, *79*, 1086
2. C. B. Murray, C. R. Kagan, M. G. Bawendi, *Annu. Rev. Mater. Sci.* **2000**, *30*, 545
3. Z. A. Peng, X. Peng, *J. Am. Chem. Soc.* **2002**, *124*, 3343
4. C. B. Murray, S. Sun, W. Gaschler, H. Doyle, T. A. Betley, C. R. Kagan, *IBM J. Res. & Dev.* **2001**, *45*, 47
5. V. I. Klimov, *J. Phys. Chem. B* **2000**, *104*, 6112
6. S. Empedocles, M. Bawendi, *Acc. Chem. Res.* **1999**, *32*, 389
7. M. Nirmal, L. Brus, *Acc. Chem. Res.* **1999**, *32*, 407
8. B. Dubertret, P. Skourides, D. J. Norris, V. Noireaux, A. H. Brivanlou, A. Libchaber, *Science* **2002**, *298*, 1759
9. X. Michalet, F. F. Pinaud, L. A. Bentolia, J. M. Tsay, S. Doose, J. J. Li, G. Sundaresan, A. M. Wu, S. S. Gambhir, S. Weiss, *Science* **2005**, *307*, 538
10. J. P. Zimmer, S. -W. Kim, S. Ohnishi, E. Tanaka, J. V. Frangioni, M. G. Bawendi, *J. Am. Chem. Soc.* **2006**, *128*, 2526
11. A. Fu, W. Gu, C. Larabell, A. P. Alivisatos, *Curr. Opin. Neurobiol.* **2005**, *15*, 568
12. S. Coe, W. -K. Woo, M. G. Bawendi, V. Bulovic, *Nature* **2002**, *420*, 800
13. J. S. Steckel, J. P. Zimmer, S. Coe-Sullivan, N. E. Stott, V. Bulovic, M. G. Bawendi, *Angew. Chem. Int. Ed.* **2004**, *43*, 2154
14. I. Gur, N. A. Fromer, M. L. Geier, A. P. Alivisatos, *Science* **2005**, *310*, 462
15. A. P. Alivisatos, *J. Phys. Chem.* **1996**, *100*, 13226
16. M. G. Bawendi, M. L. Steigerwald, L. E. Brus, *Annu. Rev. Phys. Chem.* **1990**, *41*, 477

17. L. E. Brus, *Appl. Phys. A* **1991**, *53*, 465
18. Al. L. Efros, M. Rosen, *Annu. Rev. Mater. Sci.* **2000**, *30*, 475
19. M. Nirmal, D. J. Norris, M. Kuno, M. G. Bawendi, *Phys. Rev. Lett.* **1995**, *75*, 3728
20. D. J. Norris, M. G. Bawendi, *Phys. Rev. B* **1996**, *53*, 16338
21. A. Ekimov, *J. Lumin.* **1996**, *70*, 1
22. C. B. Murray, D. J. Norris, M. G. Bawendi, *J. Am. Chem. Soc.* **1993**, *115*, 8706
23. Z. A. Peng, X. Peng, *J. Am. Chem. Soc.* **2001**, *123*, 183
24. B. K. H. Yen, N. E. Stott, K. F. Jensen, M. G. Bawendi, *Adv. Mater.* **2003**, *15*, 1858
25. B. R. Fisher, H. -J. Eisler, N. E. Stott, M. G. Bawendi, *J. Phys. Chem. B* **2004**, *108*, 143
26. N. E. Stott, Ph.D. Dissertation, Massachusetts Institute of Technology, **2004**
27. D. V. Talapin, A. L. Rogach, A. Kornowski, M. Haase, H. Weller, *Nano Lett.* **2001**, *1*, 207
28. L. Qu, X. Peng, *J. Am. Chem. Soc.* **2002**, *124*, 2049
29. B. O. Dabbousi, J. Rodriguez-Viejo, F. V. Mikulec, J. R. Heine, H. Mattousi, R. Ober, K. F. Jensen, M. G. Bawendi, *J. Phys. Chem. B* **1997**, *101*, 9463
30. D. V. Talapin, I. Mekis, S. Götzinger, A. Kornowski, O. Benson, H. Weller, *J. Phys. Chem. B* **2004**, *108*, 18826
31. R. Xie, U. Kolb, J. Li, T. Basché, A. Mews, *J. Am. Chem. Soc.* **2005**, *127*, 7480
32. C. J. Brinker, G. W. Scherer, *Sol-Gel Science: The Physics and Chemistry of Sol-Gel Processing*, Academic, Boston, MA **1990**

33. D. R. Uhlmann, G. Teowee, J. Boulton, *J. Sol-gel Sci. Technol.* **1997**, *8*, 1083
34. P. Yang, G. Wirnsberger, H. C. Huang, S. R. Cordero, M. D. McGehee, B. Scott, T. Deng, G. M. Whitesides, B. F. Chmelka, S. K. Buratto, G. D. Stucky, *Science* **2000**, *287*, 465
35. P. J. Jiang, G. N. Ostojic, R. Narat, D. M. Mittleman, V. L. Colvin, *Adv. Mater.* **2001**, *13*, 389
36. W. Stöber, A. Fink, E. Bohn, *J. Colloid Interface Sci.* **1968**, *26*, 62
37. G. H. Bogush, M. A. Tracy, C. F. Zukoski, *J. Non-Cryst. Solids* **1988**, *104*, 95
38. B. Karmakar, G. De, D. Ganguli, *J. Non-Cryst. Solids* **2000**, *272*, 119
39. T. Kawaguchi, K. Ono, *J. Non-Cryst. Solids* **1990**, *121*, 383
40. M. Bele, O. Siiman, E. Matijević, *J. Colloid Interf. Sci.* **2002**, *254*, 274
41. J. Rejman, V. Oberle, I. S. Zuhorn, D. Hoekstra, *Biochem. J.* **2004**, *377*, 159
42. A. van Blaaderen, A. Vrij, *Langmuir* **1992**, *8*, 2921
43. C. E. Moran, G. D. Hale, N. J. Halas, *Langmuir* **2001**, *17*, 8376
44. Y. Lin, J. Zhang, E. H. Sargent, E. Kumacheva, *Appl. Phys. Lett.* **2002**, *81*, 3134
45. N. A. Dhas, A. Zaban, A. Gedanken, *Chem. Mater.* **1999**, *11*, 806
46. M. A. Correa-Duarte, M. Giersig, L. M. Liz-Marzán, *Chem. Phys. Lett.* **1998**, *286*, 497
47. A. L. Rogach, D. Nagesha, J. W. Ostrander, M. Giersig, N. A. Kotov, *Chem. Mater.* **2000**, *12*, 2676
48. J. N. Cha, M. H. Bartl, M. S. Wong, A. Popitsch, T. J. Deming, G. D. Stucky, *Nano Lett.* **2003**, *3*, 907
49. X. Gao, S. Nie, *J. Phys. Chem. B* **2003**, *107*, 11575

50. C. F. Bohren, D. R. Huffman, *Absorption and Scattering of Light by Small Particles*, Wiley, New York 1998
51. Y. Arakawa, H. Sakaki, *Appl. Phys. Lett.* **1982**, *40*, 939
52. M. Asada, Y. Miyamoto, Y. Suematsu, *IEEE J. Quant. Elec.* **1986**, *QE-22*, 1915
53. F. Gindele, R. Westphalig, U. Woggon, L. Spanhel, V. Ptatschek, *Appl. Phys. Lett.* **1997**, *71*, 2181
54. J. Butty, Y. Z. Hu, N. Peyghambarian, Y. H. Kao, J. D. Mackenzie, *Appl. Phys. Lett.* **1995**, *67*, 2672
55. V. I. Klimov, A. A. Mikhailovsky, S. Xu, A. Malko, J. A. Hollingsworth, C. A. Leatherdale, H. -J. Eisler, M. G. Bawendi, *Science* **2000**, *290*, 314
56. V. I. Klimov, A. A. Mikhailovsky, D. W. Branch, C. A. Leatherdale, M. G. Bawendi, *Science* **2000**, *287*, 1011
57. A. Efros, *Los Alamos Natl. Lab. Prepr. Arch., Condens. Matter* **2002**
58. V. C. Sundar, H. -J. Eisler, M. G. Bawendi, *Adv. Mater.* **2002**, *14*, 739
59. M. A. Petruska, A. V. Malko, P. M. Voyles, V. I. Klimov, *Adv. Mater.* **2003**, *15*, 610

Chapter 2

Incorporation of NCs into Core-Shell Silica Microspheres*

2.1 Introduction

Microspheres containing chromophores have been utilized in an extensive variety of applications, including photonic crystals^{1,2}, biological labeling^{3,4}, and flow visualization in microfluidic channels⁵. In many of these applications, both the photostability of the chromophores as well as the monodispersity of the microspheres are of primary importance. The high photostability, good fluorescence efficiency and wide emission tunability of colloiddally synthesized semiconductor nanocrystals (NCs) make them excellent choices as chromophores. Indeed, recent advances in the synthesis of CdSe/ZnS and CdS/ZnS core-shell NCs have resulted in narrow fluorescence linewidths (FWHM < 30 nm) and quantum yields as high as 50%. Unlike organic dyes, the nearly continuous absorption spectrum of NCs, ranging from their bandgap emission wavelength to the ultraviolet (UV), allows different color-emitting nanocrystals to be simultaneously excited with a single light source. This salient feature of semiconductor NCs is particularly attractive for applications involving many-color multiplexing⁵. There is thus a great impetus to synthesize well-characterized NC-microsphere composites of tunable size and emission wavelength.

Previous attempts to introduce fluorescent semiconductor NCs into microspheres often involved either synthesizing the nanocrystals *in situ* using the microsphere as a host matrix^{1,6}, or using mercaptosiloxane functionalized nanocrystals as “seeds” for growing microspheres^{7,8,9}. This, however, usually produced either relatively low quality

* Many of the key results of this chapter have appeared in print (Y. Chan et. al. *Adv. Mater.* **2004**, *16*, 2092)

nanocrystals or microspheres of significant polydispersity. Significantly broadened and deep trap emission can also result from the silication process⁸. Nie *et al.* employed a different strategy to impregnate relatively monodisperse mesoporous polystyrene¹⁰ and silica¹¹ microspheres with high quality CdSe/ZnS core-shell NCs. In the case of polystyrene, this was achieved through hydrophobic interactions between the polystyrene and the hydrophobic ligands on the NC surface. For silica the method was similar, except the surface pores were first coated with small hydrophobic molecules. However, because the NCs are not chemically bound to the internal surface of the sphere, submerging the microspheres in non-polar solvents causes the NCs to leach out¹¹. This would be unsuitable in a flow visualization experiment, for example, where the velocity profiles of fluorescent microspheres in a non-polar solvent are to be determined. Moreover, the pore sizes of the mesoporous microspheres are on the order of tens of nanometers. This sets a lower limit of approximately a micron to the range of possible microsphere sizes.

It should be noted that since the paper publication of this chapter, many efforts have been made in encapsulating colloidal NCs into silica spheres. Of these, more noteworthy attempts include using a reverse microemulsion technique^{12,13,14}, where an aqueous micro-droplet containing NCs is immersed in a hydrophobic environment. Addition of a suitable hydrophilic silica precursor to the emulsion results in the formation of monodisperse silica spheres embedded with high quality NCs. Although the size-tunability of the NC-silica sphere composites derived using reverse microemulsion appears to be limited, the technique's ability to access the < 100 nm range (diameter) makes it notable.

This chapter describes a facile and robust procedure for incorporating colloiddally synthesized core-shell CdSe/ZnS and CdS/ZnS NCs into a silica or titania shell grown on preformed silica microspheres via a modified Stöber process, obtaining different color-emitting NCs in a wide range of sub-micron diameter microsphere sizes. These NC-

microsphere composites may be dispersed in a variety of polar and non-polar solvents. Repeated sonication and washes in these solvents did not result in any evident loss of NCs. Indeed, these microsphere composites uniquely combine a number of desirable features. They exhibit inherent size monodispersity due to the separate microsphere core synthesis. The independent synthesis of high-quality NCs allows the maintenance of narrow emission profiles. Access to the submicrometer range permits applications in photonics and biological imaging that would otherwise be very difficult or impossible to realize. This will become more apparent in a subsequent sub-chapter illustrating the utility of these NC-microsphere composites with in-vivo imaging of blood vessels in the brain of a mouse. The resolvable emission of different-sized microspheres becomes crucial when tracking the flow profile of blood, important for studies of ischemia¹⁵ and drug delivery¹⁶.

2.2 Strategy for incorporating NCs into microspheres

Initial strategy

It was established in Chapter 1 that the Stöber process could produce monodisperse silica microspheres through the condensation of tetraethoxysilane (TEOS) in a base-catalyzed solution of ethanol and a stoichiometric amount of water. One seemingly plausible route towards the incorporation of CdSe/ZnS NCs into microspheres would be to first render the hydrophobic NCs dispersible in ethanol by cap-exchanging the native tri-n-octylphosphine oxide (TOPO) ligands on their surface with 5-amino-1-pentanol (AP). The amino group binds to the NC surface while the hydroxyl group permits dispersion in ethanol. Nucleation and growth of the silica microspheres would subsequently take place in the presence of NCs well-dispersed in ethanol. Chemical incorporation of the NCs into the silica matrix should then be viable through the co-condensation of hydroxy groups attached to the NC surface with TEOS. An illustration of the process is given in Figure 2.1.

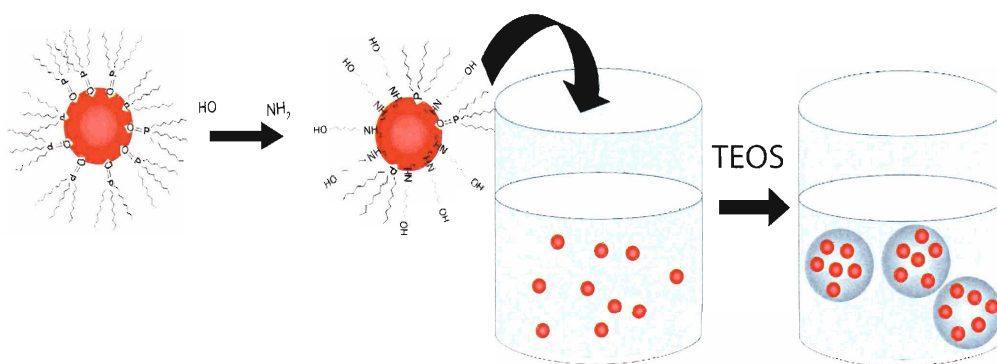


Figure 2.1 Schematic of a seemingly plausible incorporation process. The NCs are cap-exchanged with AP and dispersed in ethanol. Subsequent nucleation and growth of Stöber spheres in a homogeneous solution of CdSe/ZnS NCs should allow for their incorporation into the silica matrix.

The results of the procedure following the strategy outlined in Fig. 2.1 are summarized in Fig. 2.2. It is readily seen from the fluorescence microscope images that there is little correspondence between the dark image (no excitation) on the left and the fluorescence image (UV excitation) on the right. Much of the fluorescence appears to come from randomly distributed particles or large aggregates of clusters. Characterization from scanning electron microscopy (SEM) reveals that the large clusters are not aggregates of microspheres, but rather large particulates. Elemental mapping via Energy Dispersive X-ray (EDX) analysis concludes that the CdSe/ZnS NCs are in fact localized in either the large particulates or misshapen microspheres (circled in red in the bottom right SEM image) and are almost entirely absent from any of the regular microspheres.

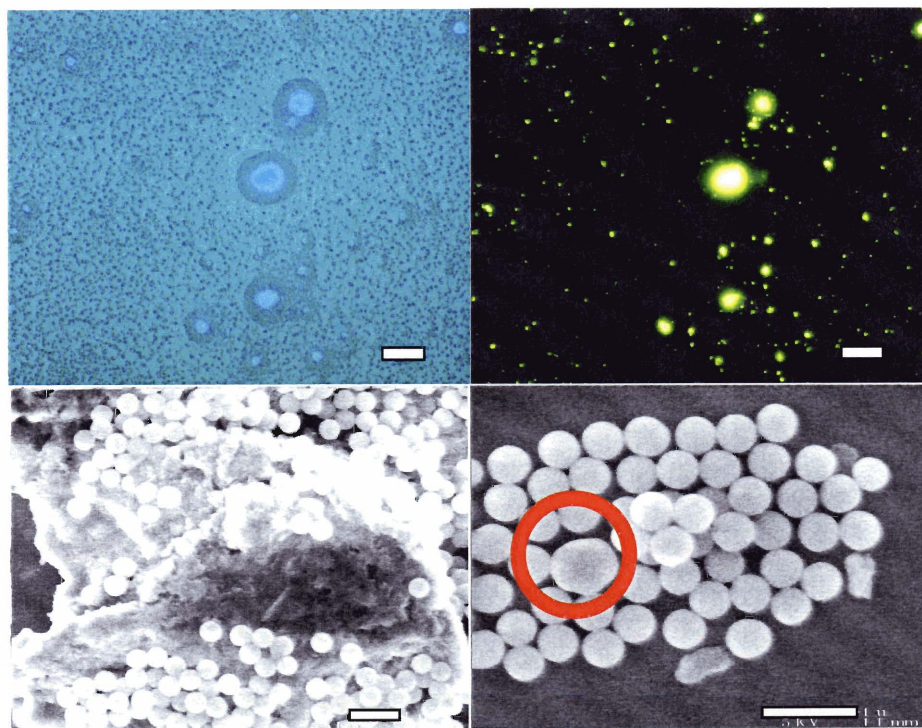


Figure 2.2 Fluorescence microscope images (top left and right image) of silica microspheres formed in the presence of CdSe/NCs. The scale bar is 5 μm . Their corresponding SEM images (bottom left and right image) show the presence of large particulates and misshapen microspheres, where the NCs are mainly localized in. The scale bar for both SEM images is 1 μm .

The failure of the method outlined in Fig. 2.1 to incorporate CdSe/ZnS NCs uniformly into monodisperse silica microspheres may be rationalized by analyzing the SEM images and their corresponding data from EDX. The fact that most of the NCs are found in irregularly-shaped particulates suggests that the NCs at least possess the appropriate functional groups on their surface to interface with the silica network. This was confirmed by the fact that the supernatant of the growth process did not contain any appreciable amount of NCs freely dispersed in solution. The presence of these large-sized particulates of various distorted geometries implies that the kinetics of nucleation and subsequent growth of Stöber microspheres are significantly perturbed by the presence of NCs, ultimately leading to the observed unsuccessful attempts at incorporation. It is perhaps reasonable to assume that, given the slower kinetics of silica growth compared to nucleation, it would be more viable to incorporate the NCs under growth conditions.

An improved strategy

Analogous to the method of Vrij and co-workers¹⁷, a more feasible strategy to incorporate NCs involves growing a shell of silica in the presence of properly derivatized NCs onto a pre-formed silica microsphere. The core silica microspheres are synthesized using previously established techniques.^{18,19} To incorporate the NCs into the microsphere shell in large quantities, it is necessary to first ensure that the ligands on the NCs impart both ethanol solubility and chemical compatibility with the silica matrix. This is achieved by cap-exchanging the native tri-n-octylphosphine oxide (TOPO) ligands on the NC surface with 5-amino-1-pentanol (AP) and 3-aminopropyltrimethoxysilane (APS). The AP imparts ethanol solubility to the NCs while the alkoxysilane moiety of APS

presumably allows the formation of siloxane bonds with the silica host matrix. The properly cap-exchanged NCs are then dispersed in a mixture of ethanol, TEOS, and bare silica microspheres. Addition of water and ammonium hydroxide to this mixture at elevated temperatures causes rapid hydrolysis of the siloxane precursor, which subsequently condenses to form a thin shell of silica around the microsphere. A summary of the reaction scheme is given in Figure 2.3. The incorporation of CdSe/ZnS NCs into microspheres via this coating procedure will subsequently be discussed throughout the rest of this chapter.

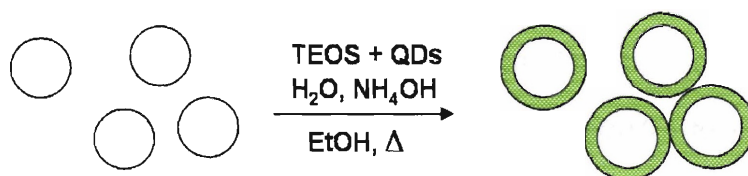


Figure 2.3 Reaction scheme depicting the incorporation of NCs into silica microspheres during shell growth rather than nucleation conditions.

2.3 Experimental

2.3.1 Silica overcoated microspheres

The CdSe and CdS NCs were synthesized according to a recently published procedure^{20,21} and then overcoated with a thin shell of ZnS using previously reported techniques^{21,22}. The resulting CdSe/ZnS core-shell NCs dispersed in butanol/hexane were then precipitated from solution using excess methanol. Repeating this dispersion/precipitation cycle about three times removes most of their native trioctylphosphine (TOPO) caps, leaving a powder which was dried under vacuum and brought into a nitrogen-atmosphere box for subsequent cap-exchange with AP and APS. As an example, ~ 135 mg of CdSe/ZnS NCs (about 4.0 nm in diameter) was mixed with 1000 mg of anhydrous ethanol and 150 mg of APS, forming a suspension of NCs. Addition of 60 mg of AP resulted in a clear solution which was subsequently heated at ~ 40 °C for about 30 minutes to ensure cap-exchange with AP and APS. Addition of 10 µL of this NC solution to 30 mg bare silica microspheres (see below) and 16 mg hydroxypropyl cellulose (avg. $M_w = 370,000$) dispersed in 10 mL of vigorously stirring ethanol was followed by the addition of 50 µL H₂O, 50 µL NH₄OH (28% in H₂O) and 0.15 mL tetraethoxysilane. The mixture was then immersed in an oil bath at 75 °C for 4 hours while stirring. The silica/silica-NCs microspheres were then isolated by 3-4 cycles of centrifugation to precipitate followed by re-dispersal in ethanol.

2.3.2 Titania overcoated microspheres

Addition of 10 µL of the NC solution in ethanol described above to 30 mg bare silica microspheres (see below) and 16 mg hydroxypropyl cellulose in 10 mL of stirring

ethanol was followed by the addition of 54 μL H_2O and 0.1 mL tetrabutylorthotitanate. The mixture was then immersed in an oil bath at 75 $^\circ\text{C}$ for 4 hours while maintaining stirring. The silica/titania-NC microspheres were then isolated by 3-4 cycles of centrifugation to precipitate followed by re-dispersal in ethanol.

2.3.3 Bare silica microspheres

Various sizes (\sim 130-900 nm in diameter) were synthesized by variants of the well known Stöber process^{18,19}. For 130 nm spheres, for example, into a solution of 0.55 mL tetraethoxysilane in 10 mL ethanol, 1 mL H_2O and 0.2 mL NH_4OH (28% in H_2O) were rapidly injected under vigorous stirring. Stirring was continued for 3 or more hours. The resulting microspheres were then isolated from excess reagents by 3 cycles of centrifugation followed by re-dispersal in ethanol.

2.3.4 Sample preparation and characterization

The coated microspheres were collected by centrifugation from the growth solution and washed three times with ethanol. Samples were prepared by drop-casting the washed microspheres from ethanol solutions (at a concentration of approximately 3 mg of coated microspheres in 3 mL of ethanol) onto silicon substrates, carbon films supported by 400 mesh copper grids (Ted Pella), and glass microscope slides for wavelength dispersive spectroscopy (WDS), transmission electron microscopy (TEM), and optical microscopy, respectively. The WDS measurements were performed on a JEOL SEM 733 electron microscope operated at 15 kV. The TEM images were obtained using a JEOL 2000FX microscope operated at 200 kV. For the fluorescence microscopy, a Nikon

Eclipse ME600 epifluorescence optical microscope equipped with a Nikon DXM1200 digital camera was employed.

2.4 Results

2.4.1 On the coating process

While the coating process is a relatively straightforward one, it is important to note that its success rests heavily upon having the right surface chemistry on the NCs. Growing a shell of silica in the presence of CdSe/ZnS NCs capped only with AP results in poor incorporation of the NCs within the silica shell. Cap-exchanging solely with APS, however, affords only partial solubility in ethanol. This results in the formation of agglomerates of NCs and agglomerates of silica, giving patchy microsphere surfaces. Thus the presence of both AP and APS is crucial to incorporate CdSe/ZnS NCs into the silica shell in large quantities. The coating process did not appear to be perturbed within the range of concentrations of NCs used (1×10^{-4} mmol L⁻¹ to 8×10^{-4} mmol L⁻¹), but it is likely that extremely high concentrations of NCs would result in agglomeration of NCs and crosslinking of spheres due to the large excess of APS in solution.

Extension of the incorporation methodology to other semiconductor NCs was not vigorously pursued in this work, with the exception of CdS/ZnS NCs. Because the synthesis of CdS/ZnS NCs differs significantly from that of CdSe/ZnS NCs, the surface chemistry of CdS/ZnS NCs is expectedly dissimilar to that of CdSe/ZnS NCs. The limited solubility of AP-exchanged CdS/ZnS NCs in ethanol, however, still permits the coating process to be used, though with lower loading fractions than in the case of CdSe/ZnS NCs. Although a different choice of surface ligands is most likely needed when attempting to incorporate other types of NCs such as PbSe, Fe₂O₃ etc. into silica microspheres using this coating process, the key considerations are ethanol solubility and a siloxane precursor with a functional group that has a good affinity for the NC surface.

2.4.2 Characterization by transmission electron microscopy

The results of the coating procedure are shown in figure 2.4, which shows a TEM image of a typical distribution of silica microspheres with CdSe/ZnS NCs localized in the shells. The inset shows a microsphere from the same distribution imaged at a higher magnification, highlighting the smooth morphology of these silica/silica-NC core-shell microspheres. The size distributions of samples were quantified using the following procedure: the diameters of a large number of spheres (typically ~ 200 spheres) were obtained from scanned TEM images processed using ImageJ (freeware, Version 1.30, July 2003, Wayne Rasband, National Institutes of Health) and tabulated. The size distribution, defined as the standard deviation divided by the mean sphere diameter, was subsequently evaluated as such for all samples reported. Figure 2.5 shows the size distribution of the sample from Figure 2.4, along with the size distribution of the starting cores, illustrating that the size distribution of coated microspheres does not significantly differ from the original cores. It should be noted that the shell thickness cannot be obtained by simply taking the difference in mean diameters between the coated and bare spheres because shrinking of the cores can occur as a result of continued condensation of unreacted Si-OH groups when the spheres are re-dispersed in a basic solution²³ for coating.

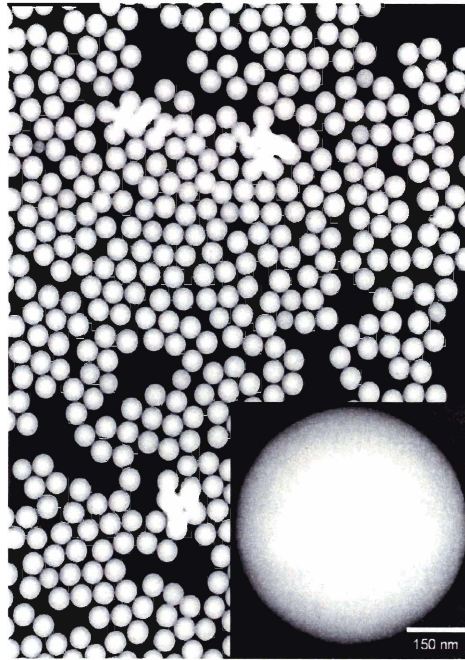


Figure 2.4 TEM image of overcoated microspheres with a mean diameter of 609 nm. The inset is an image of a microsphere from the same sample taken at a higher magnification, showing the smooth morphology of the overcoated sphere.

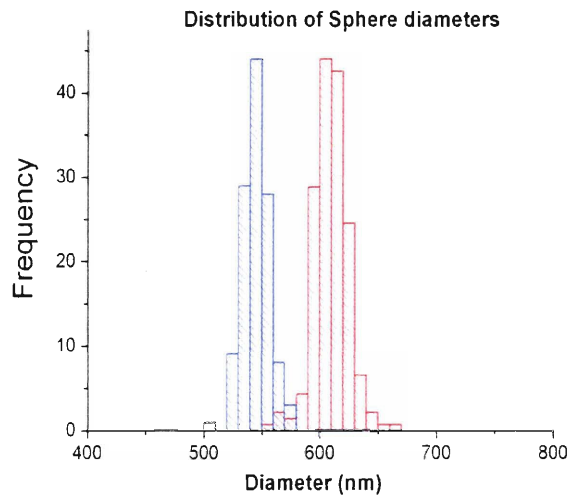


Figure 2.5 Histogram showing the distribution of diameters of spheres before (blue, mean diameter = 545 nm) and after (red, mean diameter = 609 nm) overcoating. Their respective size dispersities are 2.0% and 2.5% respectively, suggesting that the overcoating process does not significantly increase the size dispersity of the original cores.

2.4.3 Characterization by fluorescence microscopy

The as-synthesized NC-microsphere composites were characterized using fluorescence microscopy, which provides a direct method of visualizing the efficacy of the coating method. Samples were washed and sonicated multiple times to ensure there are no NCs which bind non-specifically to the surface of the microsphere. Figure 2.6 shows a typical fluorescence microscope image of a sample of coated silica microspheres. The diameter of these microspheres are about 295 nm ($\pm 4.1\%$), from TEM and ImageJ analysis. A one to one correspondence between the dark image on the left and the fluorescence image on the right is evident, suggesting uniform incorporation of the NCs into the silica shells of these microspheres.

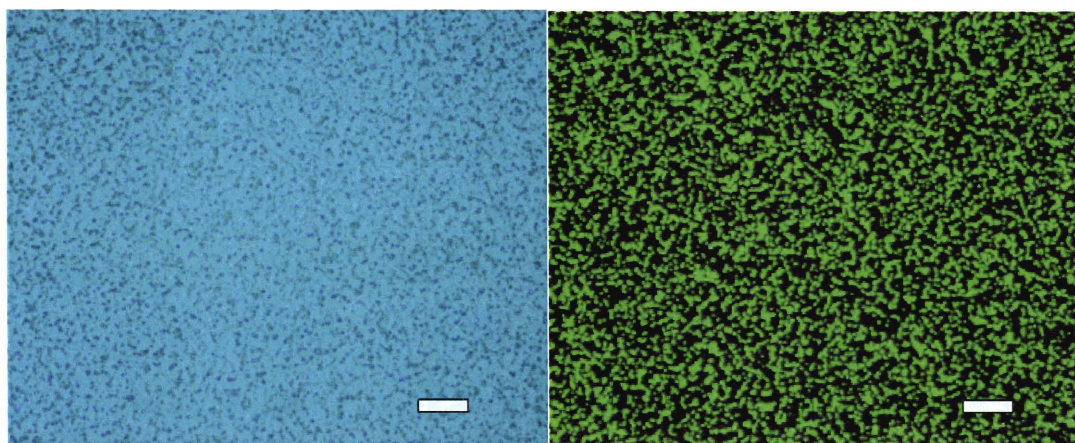


Figure 2.6 Fluorescence microscope images of 295 nm diameter NC-silica microsphere composites taken using a 100X objective. There is a clear correspondence between the dark image (left) and fluorescence image (right). The scale bar on both images is 5 μm .

Owing to the size monodispersity of the sample, close-packing of microspheres is made possible and is well-illustrated in Figure 2.7. The uniformity of NC incorporation may be attributed to the fact that the NCs are introduced under silica shell growth rather than silica nucleation conditions. The slower kinetics of silica growth permits greater control of NC incorporation and preserves the size monodispersity of the final microsphere composites. Figure 2.8 summarizes the effectiveness of the coating process, which allows for the incorporation of different color-light-emitting NCs into silica microspheres of diameters ranging from 154 nm to 954 nm after coating.

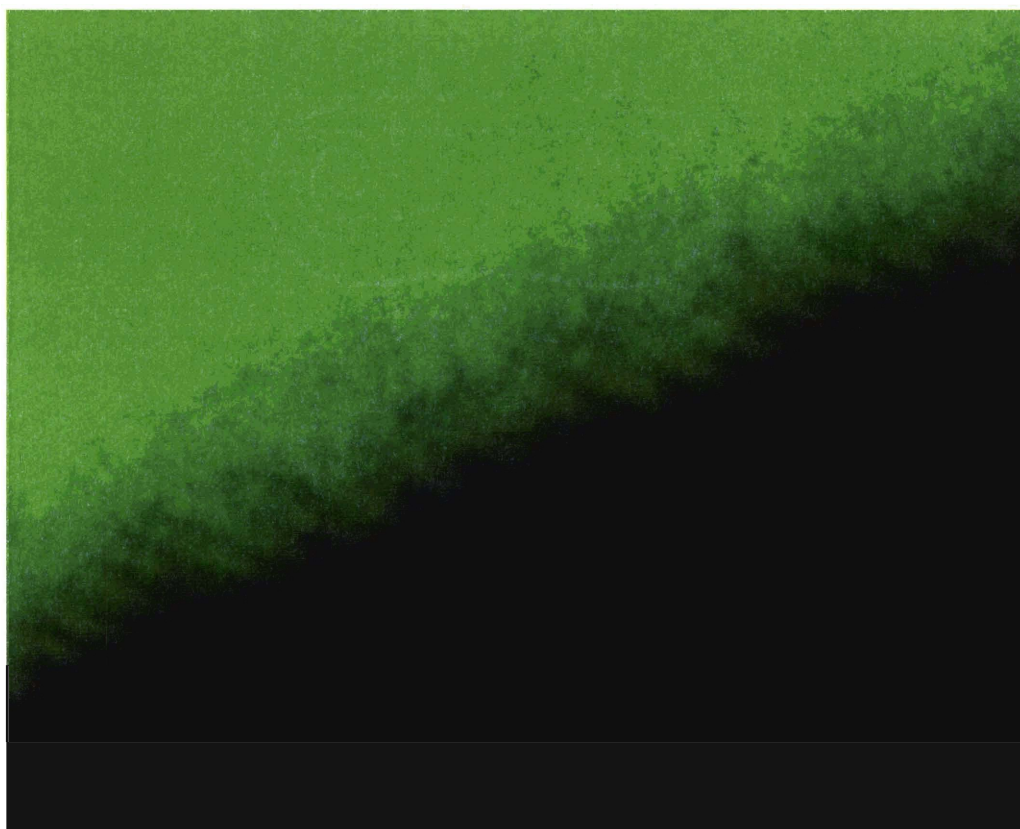


Figure 2.7 Fluorescence microscope image showing densely packed, multiple layers of coated silica microspheres. The spheres are approximately ~ 600 nm in size.

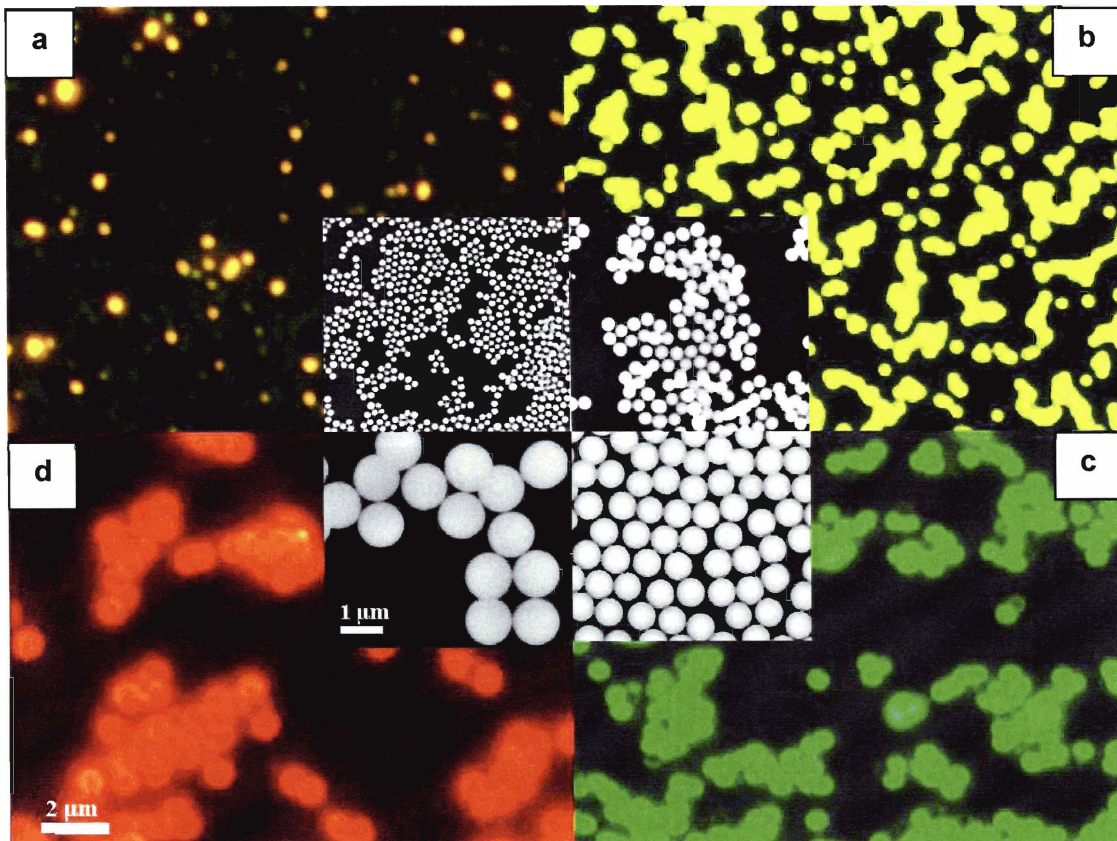


Figure 2.8 a) 154 nm ($\pm 6.6\%$) diameter coated microspheres with 604 nm-emitting NCs. b) 295 nm ($\pm 4.1\%$) diameter microspheres with emission at 580 nm. c) 609 nm ($\pm 6.9\%$) diameter microspheres with emission at 531 nm. d) 954 nm ($\pm 2.4\%$) diameter microspheres with emission at 625 nm.

2.4.4 Characterizing emission, loading fraction and quantum yield

The emission spectra of coated microspheres in an index matched liquid are shown in Figure 2.9. It is readily seen that the narrow emission profiles of the NCs are preserved. With the use of both CdS/ZnS and CdSe/ZnS NCs, emission from these NC-microsphere composites is tunable over the entire visible range. From Figure 2.10 it is further evident that the incorporation process did not result in significant broadening or deep-trap emission from the NCs, in contrast with previous efforts reported in the literature⁷. The photostability of the NCs (~ 3.8 nm diameter) in the silica microspheres

was evaluated using a 514 nm excitation source from a CW Ar⁺ laser focused through a 0.95 NA air objective at an intensity of 80 W/cm². No appreciable decrease in the fluorescence intensity was seen over a period of 20 minutes, suggesting that little, if any, photobleaching occurred.

The loading of CdSe/ZnS NCs into the silica shell was estimated by first acquiring the absorption spectrum of a known weight of overcoated microspheres, which yielded the total number of NCs and microspheres, respectively.²⁴ The microspheres were immersed in a refractive index matching liquid, comprised of a mixture of ethanol (n=1.36) and toluene (n=1.49), in order to minimize effects from light scattering by the microspheres. The reported¹⁷ density of Stöber silica microspheres is 2.03 g/cm³, with a corresponding index of refraction of 1.46. This is in agreement with the determined refractive index of our spheres. Use of this reported density allowed us to quantify the number of NCs per microsphere. As an example, the 295 nm microspheres in Fig. 2b contained ~1200 NCs per microsphere (~0.3% volume fraction). Knowing the number density of NCs in spheres also enabled us to determine* the quantum yield (QY) *within the sphere*, and quantum yields as high as 13% were obtained[†].

* The QY was determined as follows: the optical densities of the index matched coated spheres in a toluene/ethanol mixture and an appropriate reference dye in methanol were closely matched at the wavelength of excitation. To ensure that no reabsorption of the dye emission occurs, the optical densities were always maintained at a value below 0.1 at the excitation wavelength. The photoluminescence spectra of both the sample of coated spheres and the reference dye were acquired using a SPEX Fluorolog 1680 spectrometer. Comparison of their corresponding integrated emission allowed the QY of the sample to be determined.

† Although the QYs of as-synthesized core-shell CdSe/ZnS NCs used were as high as 38%, subsequent loss of the original surface ligands due to cap-exchange with AP and APS can lead to diminished QYs. Furthermore, the decline in the QY due to processing is very dependent on the quality and thickness of the ZnS shell on the NCs, which can vary significantly from sample to sample.

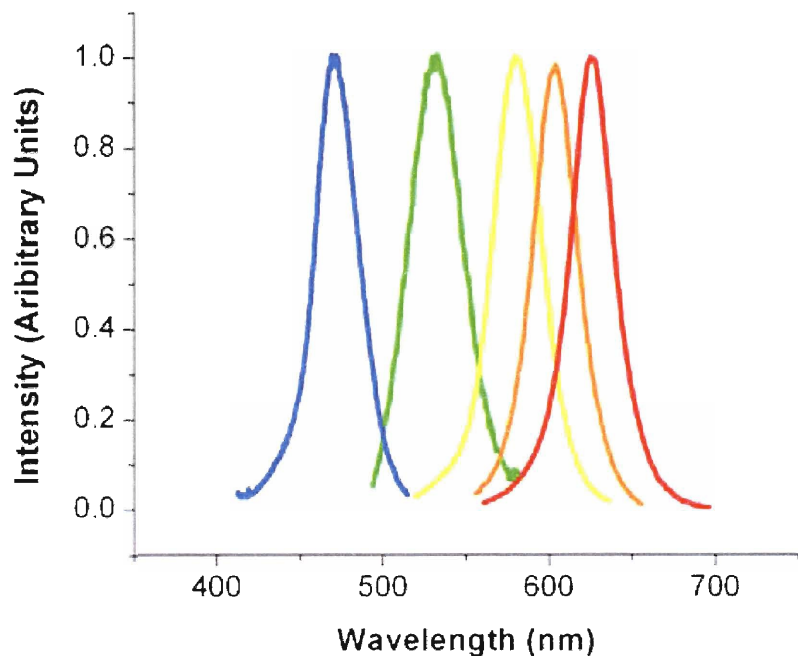


Figure 2.9 Emission spectra of CdS/ZnS and CdSe/ZnS in microspheres in an index matching liquid. The emission spectra were obtained using a Spex Fluorolog 1680 spectrometer.

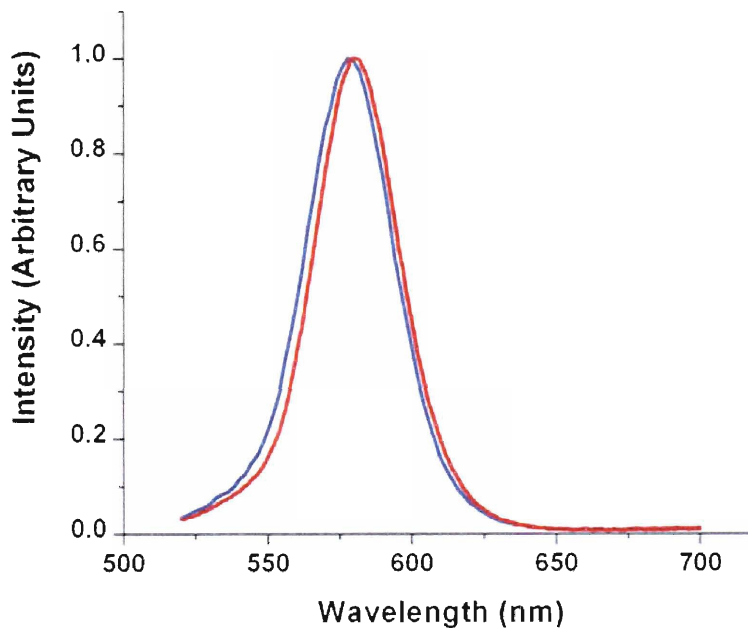


Figure 2.10 Emission spectra of 3.8 nm CdSe/ZnS NCs in hexane before incorporation (blue, peak at 578 nm) and in microspheres in an index matching liquid after coating (red, peak at 580 nm).

2.4.5 Characterization by wavelength dispersive spectroscopy

Although the spatial distribution of the NCs within the silica shell could not easily be imaged directly via TEM, wavelength dispersive spectroscopy (WDS) measurements on a number of randomly chosen individual microspheres indicate a uniform distribution of NCs from sphere to sphere, with an average Se to Si elemental mass ratio of $0.026 \pm 13\%$.^{*} This result suggests that the NCs are not aggregated, and likely are evenly distributed throughout the shell. This is also supported by the observation of only a slight 2 nm red-shift in the emission spectrum of incorporated NCs, as seen in Figure 2.10.

2.4.6 Extension of the coating procedure to titania

The methodology for incorporating NCs into silica shells of microspheres can easily be adapted to titania, and a core silica microsphere may be coated with an amorphous titania shell containing CdSe/ZnS NCs via a slight modification to the procedure for coating with silica. Fluorescence microscopy and TEM images of the silica/titania-NC microsphere composites are given in Figure 2.11 and 2.12 respectively. Unlike in the case of the silica-coated microspheres, the difference in composition between the titania shell and the silica core gives enough contrast in the TEM image to directly determine the shell thickness. The refractive index contrast between the NC-doped titania shell and air potentially could permit their use as photonic materials. WDS measurements confirm the uniformity of the distribution of NCs from sphere to sphere, with a Se to Ti elemental mass ratio of $0.019 \pm 11\%$.

^{*} The standard deviation is more significant than the absolute value of the ratio due to the curvature of the microsphere, which may introduce inherent systematic error into the WDS measurement.

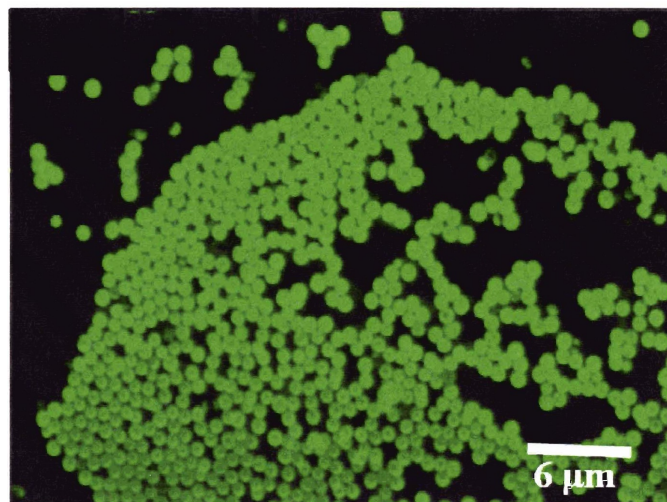


Figure 2.11 Fluorescence microscope image of the titania coated spheres.

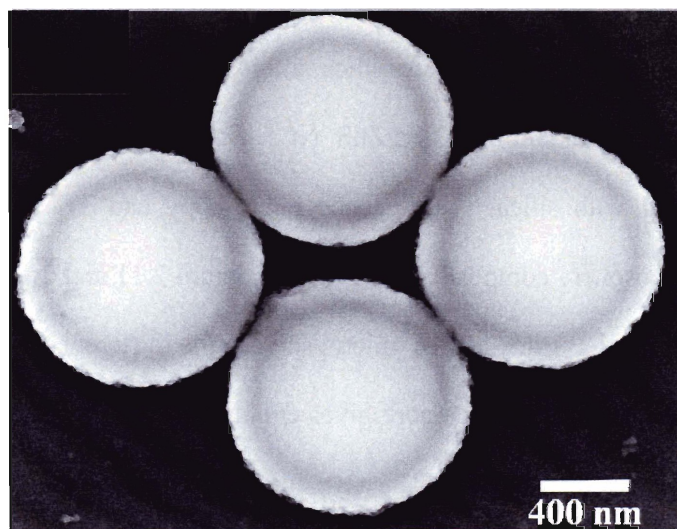


Figure 2.12 Corresponding TEM image of the silica/titania-NC microspheres shown in figure 2.11. The shell thickness is ~ 60 nm.

2.5 Application to *in-vivo* imaging

The utility of these NC-microsphere composites in biological applications is illustrated with *in-vivo* imaging. Microspheres of two distinct diameters were labeled with NCs of different emission wavelengths, and administered via carotid-artery injection²⁵ to a mouse bearing a cranial window and expressing the green fluorescent protein (GFP) in vascular endothelial cells (Tie2-GFP mouse).²⁶ Imaging was performed on the circulating microspheres, coated with polyethylene glycol to lengthen residence times in the vessels, via multiphoton microscopy (MPM) using 800 nm light delivered through a 20 X, 0.9 NA water-immersion lens.²⁷ Using MPM intravitaly, circulating microspheres could be tracked, as shown in Figure 2.13. The ability to track distinct microspheres of multiple well-defined sizes and colors simultaneously provides crucial information regarding flow characteristics in blood vessels, which can in turn guide drug delivery strategies.¹⁶ The high monodispersity allows for similar-sized spheres (400 and 500 nm diameters, for example) having different emission wavelengths to be utilized and reliably distinguished in biological experiments in which submicrometer sizes are important.²⁸ Moreover, the favorable optical properties of high quality NCs – simultaneous excitation of differently colored NCs, narrow emission profiles, and high photostability – can be harnessed for biological imaging applications inaccessible to organic dye-doped submicrometer spheres.

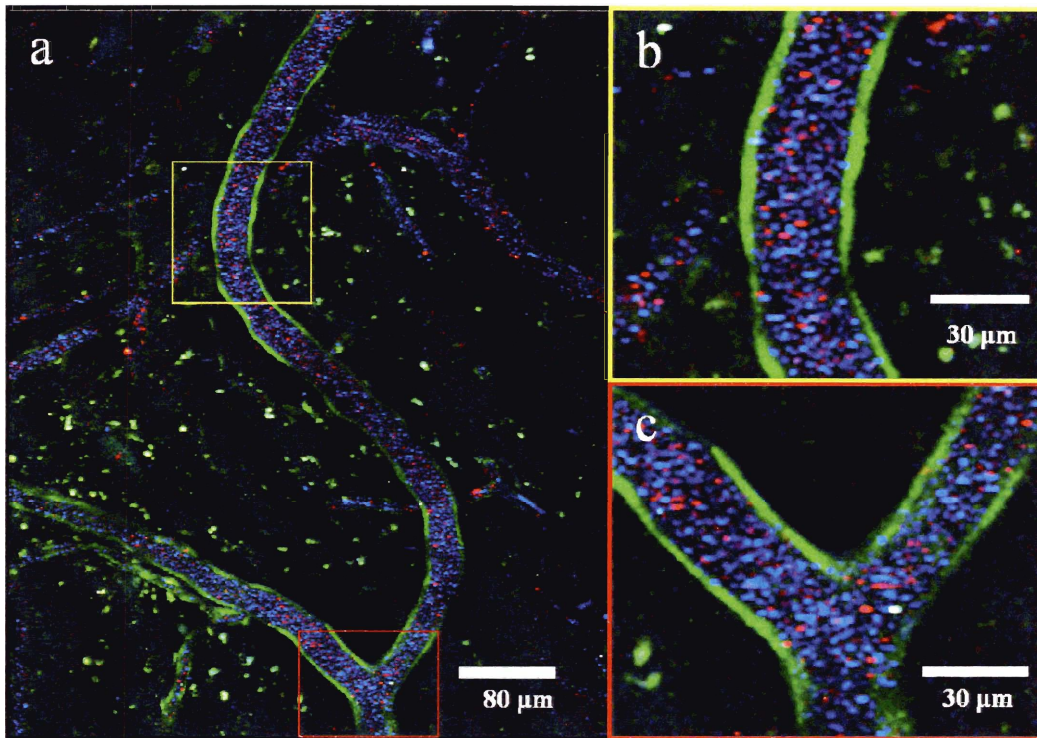


Figure 2.13 a) Image of the blood vessels in the brain of a Tie2-GFP mouse using intravital MPM. Blue-light-emitting microspheres (mean diameter 100 nm) and red-light-emitting microspheres (mean diameter 500 nm) are shown circulating within the blood vessels lined with GFP-expressing endothelial cells (green). More blue-light-emission is seen because a much higher concentration of blue microspheres was injected. Selected areas enlarged in (b) and (c).

2.6 Conclusions

In summary this chapter traces the development of a simple and effective procedure for incorporating various NCs into a silica or titania shell around silica microspheres of various diameters. Because the coated spheres have smooth surfaces, the number density of NCs per microsphere may be increased by a series of successive coatings without a significant loss of monodispersity or distortion of its spherical shape. The high monodispersity of the microspheres suggests that assembling rational three-

dimensional structures using these spheres is possible, which may have implications in studies of photonic crystals^{29,30}. The inherent stability of the spheres in aqueous solvents, as well as their photostability, brightness, and spectral resolution, allow them to be used in biological applications where the size of the chromophore is key. Examples include size-dependent endocytosis in non-phagocytic B16 cells³¹ and flow profiles in blood^{15,16}. Although the incorporation strategy highlighted in this chapter has only been demonstrated with CdSe/ZnS and CdS/ZnS NCs, it may be extended to other systems of NCs, such as PbSe, CdTe or even Fe₂O₃. These NC-microsphere composites would not only be operable at a broader range of wavelengths, from the visible to the infrared, but also possess magnetic properties as well. Such composites would undoubtedly find much utility in a whole array of applications.

2.9 References

1. Y. Lin, J. Zhang, E. H. Sargent, E. Kumacheva, *Appl. Phys. Lett.* **2002**, *81*, 3134
2. D. Wang, A. L. Rogach, F. Caruso, *Chem. Mater.* **2003**, *15*, 2724
3. X. Gao, W. Chan, S. Nie, *J. Biomed. Opt.* **2002**, *7*, 532
4. M. Han, X. Gao, J. Z. Su, S. Nie, *Nat. Biotechnol.* **2001**, *19*, 631
5. B. Dubertret, P. Skourides, D. J. Norris, V. Noireaux, A. H. Brivanlou, A. Libchaber, *Science* **2002**, *298*, 1759
6. N. A. Dhas, A. Zaban, A. Gedanken, *Chem. Mater.* **1999**, *11*, 806
7. M. A. Correa-Duarte, M. Giersig, L. M. Liz-Marzán, *Chem. Phys. Lett.* **1998**, *286*, 497
8. A. L. Rogach, D. Nagesha, J. W. Ostrander, M. Giersig, N. A. Kotov, *Chem. Mater.* **2000**, *12*, 2676.
9. J. N. Cha, M. H. Bartl, M. S. Wong, A. Popitsch, T. J. Deming, G. D. Stucky, *Nano Lett.* **2003**, *3*, 907
10. X. Gao, S. Nie, *Anal. Chem.* **2004**, *76*, 2406
11. X. Gao, S. Nie, *J. Phys. Chem. B* **2003**, *107*, 11575
12. J. Kim, J. E. Lee, J. Lee, J. H. Yu, B. C. Kim, K. An, Y. Hwang, C. -H. Shin, J. – G. Park, J. Kim, T. Hyeon, *J. Am. Chem. Soc.* **2006**, *128*, 688
13. Y. Yang, M. Gao, *Adv. Mater.* **2005**, *17*, 2354
14. S. T. Selvan, T. T. Tan, J. Y. Ying, *Adv. Mater.* **2005**, *17*, 1620
15. S. L. Hale, M. T. Vivaldi, R. A. Kloner, *Am. J. Physiol. Heart. Circ. Physiol.* **1986**, *251*, H863
16. R. K. Jain, *Nat. Med.* **1998**, *4*, 655

17. A. van Blaaderen, A. Vrij, *Langmuir* **1992**, *8*, 2921
18. G. H. Bogush, M. A. Tracy, C. F. Zukoski IV, *J. Non-Cryst. Solids* **1988**, *104*, 95
19. W. Stöber, A. Fink, E. Bohn, *J. Colloid Interface Sci.*, **1968**, *26*, 62
20. B. R. Fisher, H. -J. Eisler, N. E. Stott, M. G. Bawendi, *J. Phys. Chem. B* **2004**, *108*, 143
21. J. S. Steckel, J. P. Zimmer, S. Coe-Sullivan, N. E. Stott, V. Bulovic, M. G. Bawendi, *Angew. Chem. Int. Ed.* **2004**, *43*, 2154
22. B. O. Dabbousi, J. Rodriguez-Viejo, F. V. Mikulec, J. R. Heine, H. Mattoussi, R. Ober, K. F. Jensen, M. G. Bawendi, *J. Phys. Chem. B* **1997**, *101*, 9463
23. C. J. Brinker, G. W. Scherer, *Sol-gel Science: The Physics and Chemistry of Sol-gel Processing*, Academic, Boston, MA **1990**
24. C. A. Leatherdale, W. -K. Woo, F. V. Mikulec, M. G. Bawendi, *J. Phys. Chem. B* **2002**, *106*, 7619
25. R. J. Melder, H. A. Salehi, R. K. Jain, *Microvasc. Res.* **1995**, *50*, 35
26. T. Motoike, S. Loughna, E. Perens, B. L. Roman, W. Liao, T. C. Chau, C. D. Richardson, T. Kawate, J. Kuno, B. M. Weinstein, D. Y. Stainier, T. N. Sato, *Genesis* **2000**, *28*, 75
27. E. B. Brown, R. B. Campbell, Y. Tsuzuki, L. Xu, P. Carmeliet, D. Fukumura, R. K. Jain, *Nat. Med.* **2001**, *7*, 864
28. S. K. Hobbs, W. L. Monsky, F. Yuan, W. G. Roberts, L. Griffith, V. P. Torchilin, R. K. Jain, *Proc. Natl. Acad. Sci.* **1998**, *95*, 4607
29. S. H. Im, Y. T. Lim, D. J. Suh, O. O. Park, *Adv. Mater.* **2002**, *14*, 1367

30. P. J. Jiang, G. N. Ostojic, R. Narat, D. M. Mittleman, V. L. Colvin, *Adv. Mater.*

2001, *13*, 389

31. J. Rejman, V. Oberle, I. S. Zuhorn, D. Hoekstra, *Biochem. J.* **2004**, *377*, 159

Chapter 3

On the Development of CdSe/ZnS Nanocrystal Lasers

3.1 Chapter overview

In Chapter 1 we were introduced to the motivation behind numerous efforts over the past decade towards achieving lasing in chemically-synthesized semiconductor nanocrystals (NCs). While many of these attempts managed to establish the presence of optical gain, exhibition of stimulated emission from these strongly confined, zero-dimensional semiconductors remained elusive. The demonstration of amplified spontaneous emission (ASE) from a close-packed film of CdSe NCs¹ marked a milestone in the widespread pursuit of NC-based gain media, showing for the first time the feasibility of producing a laser whose amplification derives from these emission-tunable chromophores. However, as mentioned in Chapter 1, the close-packed films were not thermally stable towards the intense optical excitation from a pulsed laser system needed to generate optical gain, owing to the fact that the NCs are primarily held together by weak Van der Waals interactions. This restricted the optical pumping of these films to low temperature conditions, thus severely limiting their use as gain media.

The inherent drawbacks of close-packed films of NCs as gain media prompted the development of CdSe NCs incorporated in high loading fractions into a sol-gel derived titania matrix^{2,3}. These NC-titania composite films were not only structurally and thermally stable towards the intense optical excitation required to produce optical gain, their smooth surface morphology and relatively high refractive index made them

excellent waveguides, facilitating the achievement of ASE at room temperature. The straightforward but efficient process of spin-coating the NC-titania sol followed by subsequent annealing at elevated temperatures also allowed for the production of more complicated waveguide structures, such as the sequential build-up of two different layers of NC-titania that exhibit ASE simultaneously at two distinct wavelengths.² This flexibility associated with the physical deposition of the CdSe NC-titania sol was subsequently exploited to produce distributed feedback (DFB) lasing via a patterned silicon grating with the active NC-titania layer on top,⁴ as well as whispering gallery mode (WGM) lasing via a glass capillary tube with the NC-titania composite localized around its inner walls.³

This chapter elaborates on the continued development of CdSe NC-based lasers since their inception, delineating the invention of novel fabrication methods for producing various titania-based feedback structures. The description of the fabrication of optical microcavities derived from titania is divided into two distinct parts: the first focuses on soft-lithographically embossed DFB structures and the second on NC-microsphere resonator composites. Room temperature lasing is shown to follow from optically pumping these feedback structures, which are produced via relatively inexpensive and facile processes. Newer and arguably improved methods of synthesizing core CdSe, core-shell CdSe/ZnS and CdSe/CdZnS NCs also presented opportunities to improve the performance of the NC-titania composites. The ensuing challenges faced in making core-shell CdSe/ZnS NCs produced by these different methods (thus having different surface chemistries) compatible with the incorporation process into sol-gel derived titania are described in Appendix A at the end of this chapter.

3.2 Soft-Lithographically Embossed Distributed-Feedback NC Lasers^{*}

3.2.1 Motivation

The flexibility of employing various physical techniques such as spin-coating, dip-coating or drop-casting to deposit the NC-titania sol onto planar substrates facilitated the construction of NC-titania DFB structures in which the NC-titania film rests on top of a lithographically patterned silicon substrate. These composite structures showed the first evidence of lasing at room temperature from strongly quantum-confined colloidal CdSe NCs, displaying color tunability through the use of different-sized NCs.⁴ Advances in pattern transfer techniques via soft-lithography⁵, however, presented new strategies for introducing feedback to the NC-titania films. One such strategy was to directly imprint the NC-titania film with a DFB structure using a patterned stamp, similar to imprint lithography, in which grating structures are transferred above the glass-transition temperature of the composite.⁶ There are some inherent advantages to this. Firstly, multiple-wavelength lasing, which is desirable for applications such as wavelength division multiplexing,⁷ can be achieved from the successive build-up of different color-emitting NC-titania layers since each active NC-titania layer can be embossed with a grating of appropriate periodicity according to the Bragg condition.⁸ This leads to a hierarchical structure that can lase simultaneously at different wavelengths. Secondly, the embossing of these films is carried out with a re-usable poly(dimethylsiloxane) (PDMS) stamp, thus obviating the need for costly lithographically patterned substrates. The subsequent sections describe the fabrication, physical and optical characterization of these soft-lithographically produced NC-based DFB lasers.

^{*} Some of the key results of this section have appeared in print (V. C. Sundar et. al. *Adv. Mater.* **2004**, *16*, 2137)

3.2.2 Experimental

Incorporation into titania:

As-synthesized CdSe/ZnS core-shell NCs (see Appendix A) were processed following three cycles of precipitation in methanol and re-dispersal in hexane/butanol to ensure the removal of excess surface ligands. The NCs are then dried under vacuum and brought into a nitrogen-atmosphere glovebox. Addition of ethanol to the dried powder of NCs results in a cloudy suspension which clears upon the addition of 5-amino-1-pentanol (AP) (95%, Sigma). This is followed by the addition of *tris*-hydroxypropylphosphine (THPP) and titanium (IV) butoxide (TBOT), resulting in a relatively viscous sol. As an example, to 100 mg of CdSe/ZnS NCs, 640 mg of EtOH is added, followed by 90 mg of AP (50% wt/wt in EtOH). This should give a clear solution of NCs in EtOH. Additional amounts of AP may be added if the NCs are not well-dispersed in EtOH. To this clear solution of NCs in EtOH, 36 mg of THPP is added, followed by 60 mg of TBOT. The mixture is then stirred under mild heating on a hot plate for about 2 hours at ~ 60 °C. This yields a clear but viscous NC-titania sol that is spin-coated onto a glass substrate. The thickness of the resulting film is dependent on the spin speed and the relative amounts of THPP, TBOT and EtOH added. For example, a larger amount of THPP and TBOT relative to EtOH at a given spin speed affords thicker films.

Embossing of NC-titania films:

The PDMS stamps bearing a grating pattern are made by casting Sylgard 184 (1:10 wt./wt., crosslinker/base) against a silicon DFB grating of a known periodicity. To

ensure the clean release of the PDMS mold the silicon DFB is first exposed to 1-2 drops of tridecafluoro-1,1,2,2-tetrahydrooctyl-1-trichlorosilane before coming into contact with the PDMS. The stamp is then cured either at room temperature for about 24 hours or at $\sim 60\text{ }^{\circ}\text{C}$ in an oven for about 6 hours. This results in the transfer of the grating pattern onto the PDMS mold, which is then carefully peeled off the Si grating. These PDMS gratings are then brought into contact with a NC-titania sol that has been spin coated onto a glass slide, and the entire construct is brought onto a hot plate to anneal at $200\text{ }^{\circ}\text{C}$ for 2 min. A pressure of $\sim 9.8\text{ KN/m}^2$ is applied to the stamp during this time, pressing it against the underlying NC-titania sol. Subsequent removal of the PDMS stamp revealed a NC-titania film with the DFB structure imprinted on it. The PDMS stamp is then washed with ethanol and firmly pressed against a piece of scotch-tape in order to remove any dust or debris, ready for re-use. These PDMS gratings can generally be used about 4 times on average before incurring significant degradation of the grating features.

The multi-layered structures were prepared as follows: First, the active layer of NC-titania sol is spin-coated and embossed upon annealing. This is then followed by the spin-coating of a neat titania layer which is subsequently annealed. A second layer of NC-titania is then spin-coated on top of the neat titania layer and embossed upon annealing. Thus the sequential build-up of these hierarchical structures proceeds through the deposition of alternating layers of NC-titania and neat titania. The entire process is depicted in Figure 3.1.

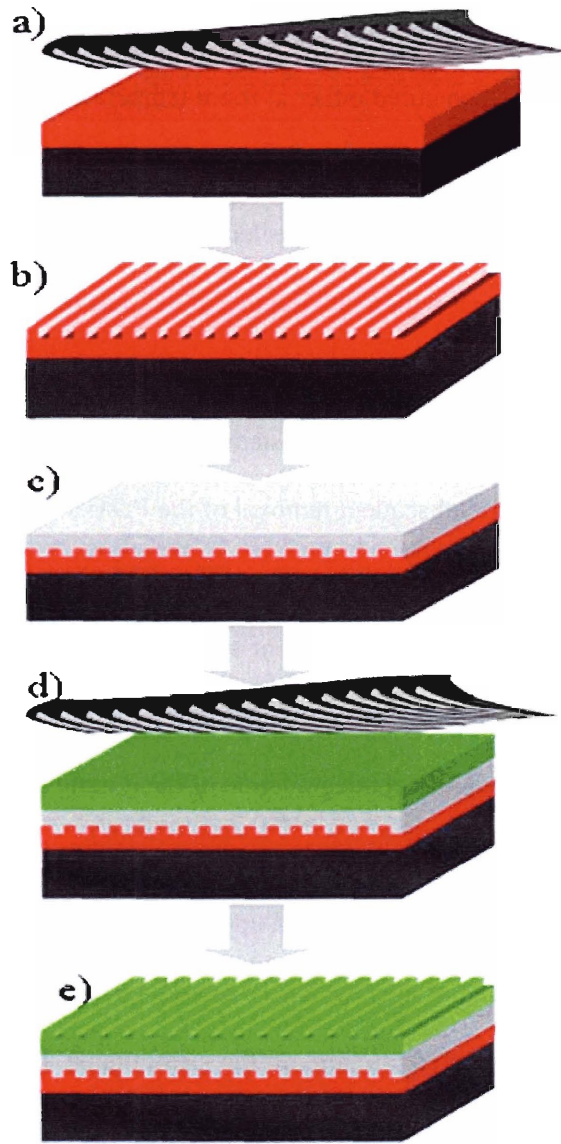


Figure 3.1 Illustration of the embossing procedure. Steps (a) through (e) depict the different stages in producing a multi-layer NC-titania structure that should be capable of lasing at multiple wavelengths. The active NC-titania layers are denoted in color while the separating neat titania layer is denoted in gray.

3.2.3 Characterization by Atomic Force Microscopy

Surface characterization of the embossed NC-titania films proceeded via Atomic Force Microscopy (AFM), which afforded information on both the surface morphology and modulation depth of the patterned film. Figure 3.2 shows an AFM image of a typical CdSe/ZnS NC-titania film embossed with a PDMS stamp. The inset is a cross-sectional analysis of the film, depicted by the white dashed line. A modulation depth of ~ 45 nm is seen, consistent with the original grating pitch of 50 nm. The uniformity of the surface corrugations suggests good fidelity of pattern transfer.

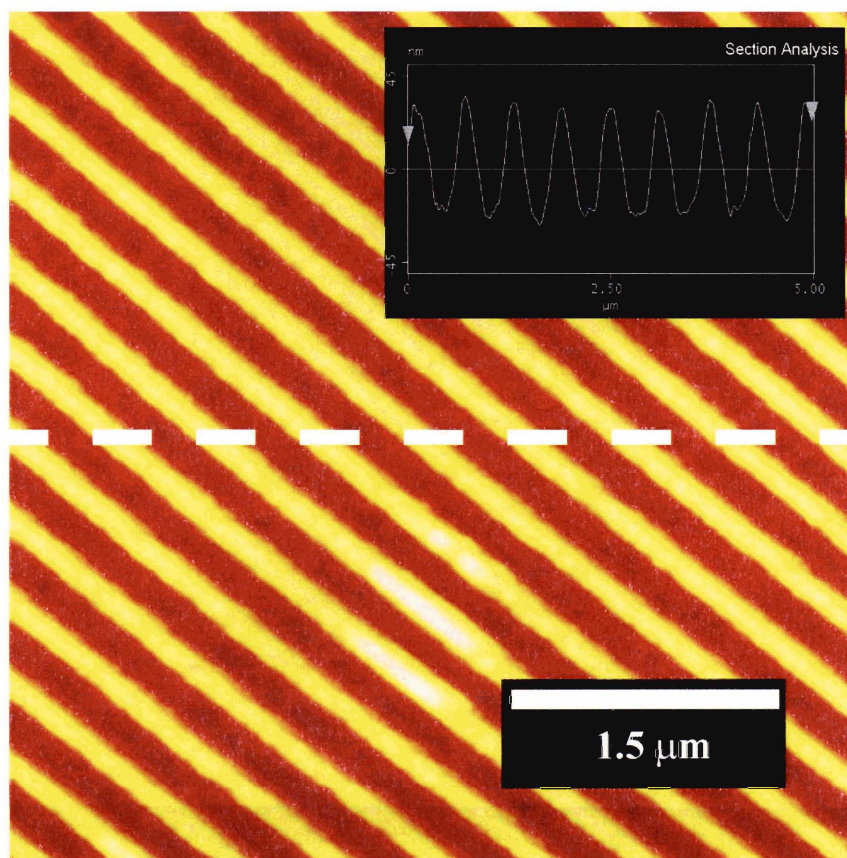


Figure 3.2 AFM image of a typical single NC-titania film embossed with a PDMS stamp bearing a grating pattern with a periodicity of 360 nm. The inset is a cross-section analysis following the linescan across the film depicted by the bold white dashed line.

For the hierarchical multi-layered structures, AFM characterization of the bottom and top layer (a total of 3 layers) is given in Figure 3.3. It is evident that the buffer layer of neat titania affords a relatively good platform in which to spin-coat the top active NC-titania layer since the fidelity of the pattern transfer is comparable to that of the bottom layer.

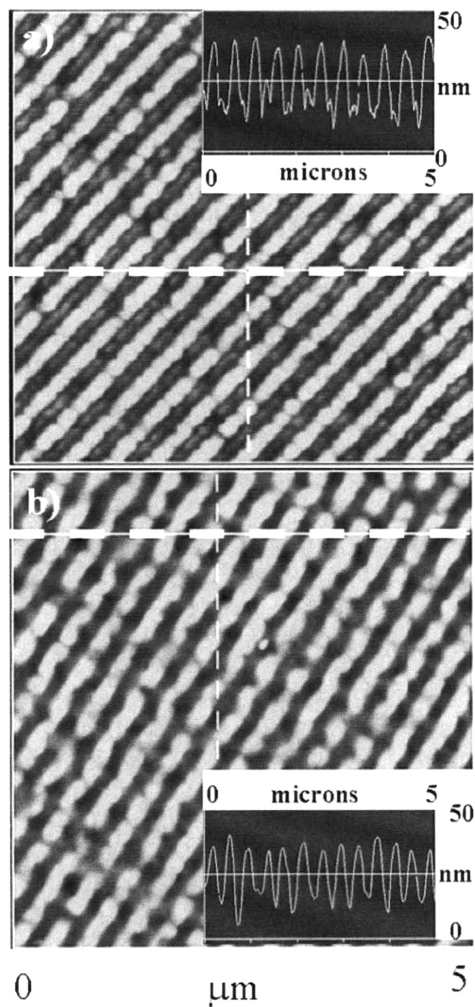


Figure 3.3 AFM images of (a) the bottom NC-titania film embossed with a PDMS stamp bearing a grating pattern with a periodicity of 350 nm, and (b) the top NC-titania layer embossed with a grating pattern with a periodicity of 330 nm. The modulation height (~ 25 nm) is similar in both cases.

3.2.4 Optical characterization

The embossed NC-titania DFB films were optically pumped using a frequency-doubled, regeneratively amplified Ti:Sapph with a repetition rate of 1 kHz and a pulse width of 100 fs. The excitation light was focused with a cylindrical lens on the front face of the film. The emission from the film is then coupled into a spectrometer with an attached nitrogen-cooled CCD camera. Above threshold, the emergence of a peak on the lower energy side of the band-edge emission featuring a dramatically reduced linewidth is readily observed. This demarcates the onset of lasing. Figure 3.4 shows the room temperature lasing spectrum of a CdSe/ZnS NC-titania film embossed with a 360 nm periodicity grating. The quality factor of the cavity is ~ 450 (approximated by $\lambda/\Delta\lambda$ at the lasing transition), which is most likely limited by the fidelity of the pattern transfer and the surface roughness of the titania film. The threshold for lasing at room temperature is ~ 300 nJ / pulse over an excitation area of 5×10^{-5} cm², comparable to that of a NC-titania film on a silicon DFB grating.⁴ Figure 3.5 shows simultaneous lasing at two distinct wavelengths from a multi-layered NC-titania DFB structure. Due to a slight mismatch in the refractive indices of the composite film and the lower grating, lasing at both wavelengths was emitted at different output angles. This mismatch may be reduced by changing the NC size, the refractive index of the film or the grating periodicity⁸ of the individual layers to produce multi-wavelength lasing in a more collinear fashion.

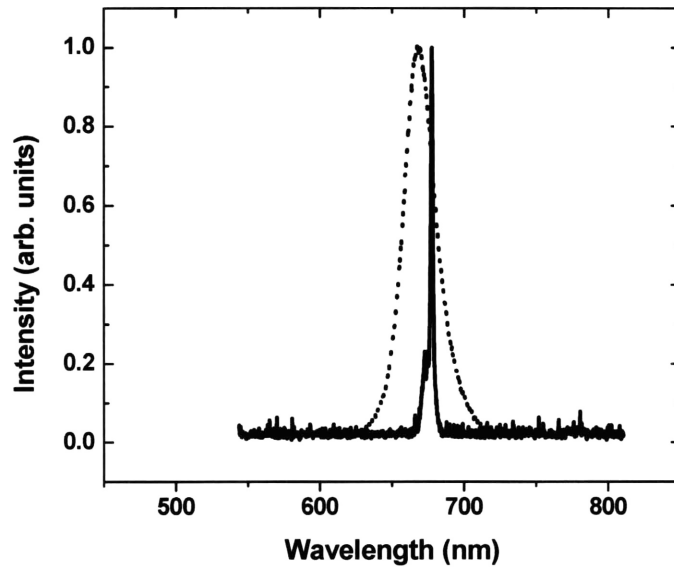


Figure 3.4 Emission spectra from a NC-titania film embossed with a 360 nm periodicity grating, optically pumped with a regeneratively amplified frequency-doubled Ti:Sapph source. A dramatic change in the linewidth, from ~25 nm to ~1.5 nm is seen above threshold, depicting the onset of lasing.

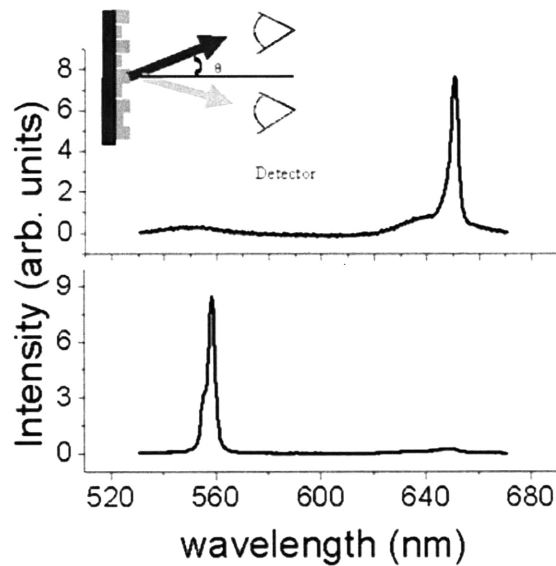


Figure 3.5 Lasing spectra from a multi-layered NC-titania film. Simultaneous lasing is seen at two distinct wavelengths, corresponding to two different active NC-titania layers comprising of 3.3 nm and 2.0 nm CdSe NCs. As a result of a slight mismatch in the Bragg condition, the lasing output from the film was detected at different angles.

3.2.5 Conclusions

Room-temperature lasing from embossed NC-titania DFB structures was presented in this part of the chapter. Of particular importance is the grating pattern transfer from the PDMS stamp to the pre-polymerized NC-titania sol. The permeability of ethanol through the PDMS stamp aided in this pattern transfer since annealing of the titania sol at elevated temperatures to complete condensation causes rapid evaporation of the ethanol. The facility of the embossing procedure provides impetus for fabricating these NC-based lasers via soft-lithography, and the re-usability of the PDMS stamp provides a relatively cost-effective route towards the production of these devices. Moreover, the inherent flexibility of the technique allows for the sequential build-up of more complicated heterostructures, facilitating multi-layered NC-titania devices that exhibit simultaneous lasing at spectrally distinct wavelengths. These composite resonators represent a step forward in the evolution of NC-based lasers, where the gain media and feedback structure are easily handled.

3.3 Semiconductor NC/Microsphere Resonator Composites *

3.3.1 Introduction

The use of circular cavities for optical studies is attractive due to their whispering-gallery-modes (WGM), which are formed from the total internal reflection of light at the dielectric interface along the circumference of a sphere.⁹ The quality (Q) factor of these modes (calculated as $\lambda/\Delta\lambda$, where λ and $\Delta\lambda$ are the wavelength and full width at half maximum of the laser emission) can be extremely high ($> 10^8$) because of the strong confinement of photons within the modal volume,^{10,11} thus making spherical microcavities attractive resonators for laser devices.¹² Incorporating a gain material within the resonant modal volume of an optical microcavity can pose significant fabrication challenges, however. In this respect, colloidal semiconductor NCs are particularly desirable for use as a gain material as their surfaces may be chemically functionalized to support adhesion onto the exterior of a microcavity, such as a silica or polystyrene microsphere. Such functionalization allows for NC incorporation into a titania sol, which imparts more mechanical and chemical stability^{2,3} than devices fabricated using close-packed NC films¹³, as mentioned earlier in the chapter.

Numerous studies have been undertaken on coupled NC/dielectric micrometer-sized cavities to investigate a variety of optical phenomena, from enhanced spontaneous emission to lasing.^{3,14-20} These reports of lasing using NCs as gain material, however, either employed polydisperse and poor-quality microsphere templates, expensive lithographically prepared substrates, or a fiber-optic or microcapillary tube, which resulted in the formation of only a single cavity. In this section it is introduced a facile

* Much of this work has appeared in print (P. T. Snee et. al. *Adv. Mater.* **2005**, *17*, 1131)

method of incorporating colloiddally synthesized CdSe/CdZnS NCs onto the surface of monodisperse, micrometer-sized silica or polystyrene microspheres by depositing a NC-titania sol onto a microsphere substrate, producing hundreds of uniform spherical resonators in a single spin-coating process. Stable room-temperature WGM lasing was observed when individual microspheres were optically pumped. Single-mode versus multimode lasing can be selectively achieved by adjusting the size of the microsphere template, the spectral position of the gain of the NC sample, and the pump power of the laser. This work presents a simple route to studying the optical behavior of NCs coupled to lasing microcavities, and although only lasing at optical frequencies using core-shell CdSe/CdZnS NCs is described, the techniques reported here may be extended to other systems, such as infrared-emitting PbSe NCs which have recently been demonstrated to exhibit optical gain.²¹

3.3.2 Experimental

Synthesis of core-shell CdSe/CdZnS NCs

See Appendix A for details.

Fabrication of NC titania-microsphere composite resonators

The NC titania-microsphere composite resonators were prepared under inert atmospheric conditions via a typical procedure presented here. First, 50 mg of CdSe/CdZnS NCs were precipitated and re-dispersed three times from a butanol/hexane solution using methanol to remove excess capping groups. Next, 67 mg of 5-amino-1-pentanol (50% wt/wt in ethanol) was added, followed by 200 mg of ethanol. After mixing for several minutes, an additional portion of 8 mg tris-hydroxypropylphosphine was added, followed by 120 mg of ethanol. The capped solution was rapidly heated to reflux temperature while stirring, and then cooled before the addition of 30 mg of titanium (IV) butoxide. The sample was then allowed to pre-polymerize at 60 °C for 2 hr. After cooling the sample, the sol was diluted by a factor of 2 with anhydrous ethanol and filtered. Approximately 1 mg of microspheres was added per 200 μ L of filtered sol, which was then spin-cast onto a microscope coverslip at 4000 rpm. The sample was then annealed at 200 °C for 2 min and allowed to cool under an inert atmosphere.

Sample Characterization

The NC titania-microsphere composites were analyzed using a Nikon Eclipse ME600 fluorescence microscope for optical and fluorescence characterization. Scanning electron microscopy (SEM) images were obtained using a JEOL 6320 FV operating at 1.0 keV on 100 Å carbon-coated samples. The spectroscopic ellipsometry measurements

were made on samples spin-coated on a silicon wafer using a Sopra GES 5 ellipsometer at incidence angles of 65°, 67° and 69°. The laser spectroscopic measurements were made with a home-built fluorescent microscope coupled to a modified SPEX 270M and a Princeton Instruments LN/CCD-512TKB1 camera. Our spectral resolution was measured to be 0.4 nm at FWHM. The excitation source was based upon a Coherent Mira 900 Ti:Sapphire oscillator coupled to a BMI Alpha-1000 regenerative amplifier to generate 100 fs, 400 nm pulses of light. The power of the beam was measured before it reached the microscope objective. As a result, the threshold power for lasing in the microsphere composites was likely less than reported due to pump losses in the objective and at the air/glass and glass/titania interfaces. The NC loading content in the titania films was determined according to previously described methods.²

3.3.3 Materials characterization

Initial attempts on developing a NC / WGM microsphere resonator were based on the construction of an evanescent wave coupled structure starting with a polymer or silica sphere onto which CdSe NC's are deposited using a layer-by-layer wet chemical procedure.^{17,22} Unfortunately, this method did not allow for the reliable incorporation of the high loading fraction of NCs that is necessary for light amplification in a weakly coupled system.¹ This prompted the modification of a previously established method to make a NC / sol with a high volume fraction of CdSe, which is subsequently deposited onto the surface of a sample of microspheres. First, a NC-titania sol is prepared via a wet chemical method similar to our previously reported procedure.² Next, the viscous sol is diluted and mixed with the microspheres before spin casting onto a clean glass substrate

and annealed at high temperature. The disparity in the size of the resulting titania / NC film (with thicknesses of ~120-175 nm from ellipsometry) and the microsphere feedstock (>5 μm diameter) results in the physical “wetting” of the surface of the microsphere with the NC-titania composite such that the shape of the spherical template is preserved. Numerous microsphere structures are produced on a single substrate, which is a function of the loading level of the microsphere template in the diluted sol. Optical and SEM images of several of these devices are shown in Fig. 3.6. It can be seen that the surface of the microsphere core is evenly coated with the NC-titania composite, allowing for the formation of a structure with the feedback of a spherical resonator.²³ Furthermore, the size dispersity of the composites is the same as the original template.

Caution must be taken to ensure that the sol is neither diluted too much (this may reduce the volume fraction of NCs) nor too little with ethanol, which results in an overly thick NC-titania layer that envelops the microsphere template to form a hemispherical structure. This is undesirable since optical feedback in these structures is likely to take place along the widest circumference of the sphere parallel to the film surface. The loading level of the microsphere template should also not be excessive, as this would yield dimers or trimers of microspheres that are necked together to form irregularly-shaped structures. Figure 3.7 shows a close-up of the bridging film between these spheres, which often display signs of cracking that is likely due to thermal stresses induced by rapid annealing at elevated temperatures. No evidence of lasing was found in any of these joint structures.

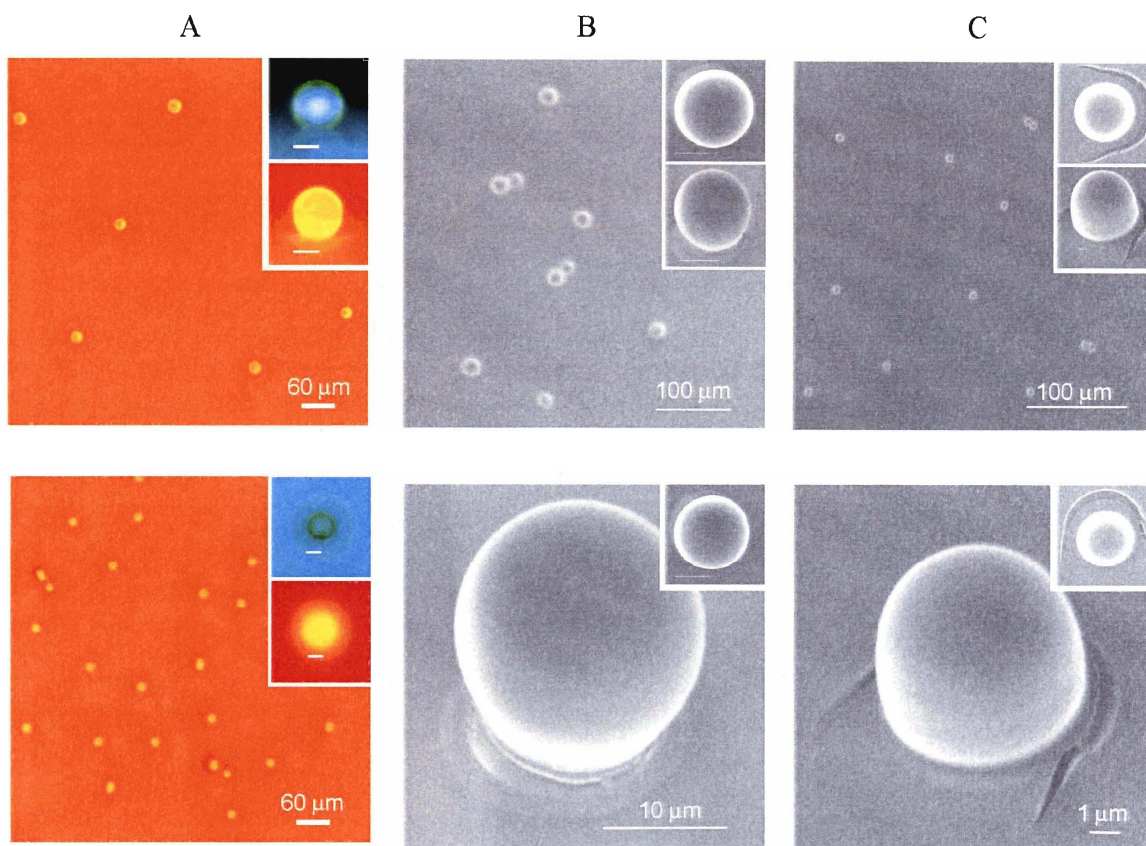


Figure 3.6 The fluorescence optical microscope and SEM images of as-synthesized NC-microsphere composites. (A) Fluorescent optical image of 20 μm , 30 μm (top) and 6.85 μm (bottom) silica microspheres coated with a CdSe/CdZnS titania film. The insets show the optical and fluorescent images of the microsphere composites. Top inset scale bar is 15 μm and bottom scale bar is 5 μm . Also shown are SEM micrographs of NC titania / 20 μm (B) and 6.85 μm (C) silica core composite samples. While the film occasionally forms cracks near the base of the structure, this does not appear to prevent the observation of laser emission from the sample. The cracks in the base of the spheres provide a visual contrast that shows the evenness of the NC / titania coating on the microsphere template. We expect that the Whispering Gallery Mode lasing occurs along the circumference of the sphere parallel to the surface as the film near the base of the microsphere has been largely perturbed.



Figure 3.7 SEM image of two joint microspheres formed as a result of close proximity with each other. This may be minimized by using a lower concentration of microsphere templates during the spin-coating process. Fracturing of the neck between the spheres may be attributed to thermal stresses induced by the rapid annealing of the NC-titania sol at elevated temperature. These misshapen structures do not show any utility as optical resonators. The scale bar is 1 μm .

3.3.4 Optical characterization

Laser emission from these structures was observed using a home-built imaging/dispersive fluorescence microscope coupled to a frequency-doubled 1 kHz Ti:sapphire regeneratively amplified laser light source for pumping the devices. The excitation laser was coupled to collect the emission from the sample. Shown in Figure 3.8 are the spectra of several individual NC/WGM resonator composites derived from a variety of different CdSe/CdZnS NC samples and microsphere templates. The spectra reveal clear threshold behavior of lasing only on the low-energy side of the NC fluorescence, consistent with the red-shifted gain profiles described in previous reports.¹⁻³ Single-mode lasing was observed by tuning the NC fluorescence emission wavelength and the diameter of the template microspheres, as seen in the single biexcitonic emission spectrum (green line) in Figure 3.8B. This results when a single WGM resonance overlaps with the narrow gain profile of the NC sample. At higher pump intensities a second set of laser-emission lines are observed in the sample, which are blue-shifted with respect to the biexciton peaks due to formation and gain from the optically allowed CdSe $1P_{3/2}-1P_e$ transition (red line in Figure 3.8B).^{24,25} This recombination occurs at a higher²⁶ energy than the $1S_{3/2}-1S_e$ transition that is responsible for biexcitonic lasing. Such multiexcitonic lasing will be described in greater detail in Chapter 6.

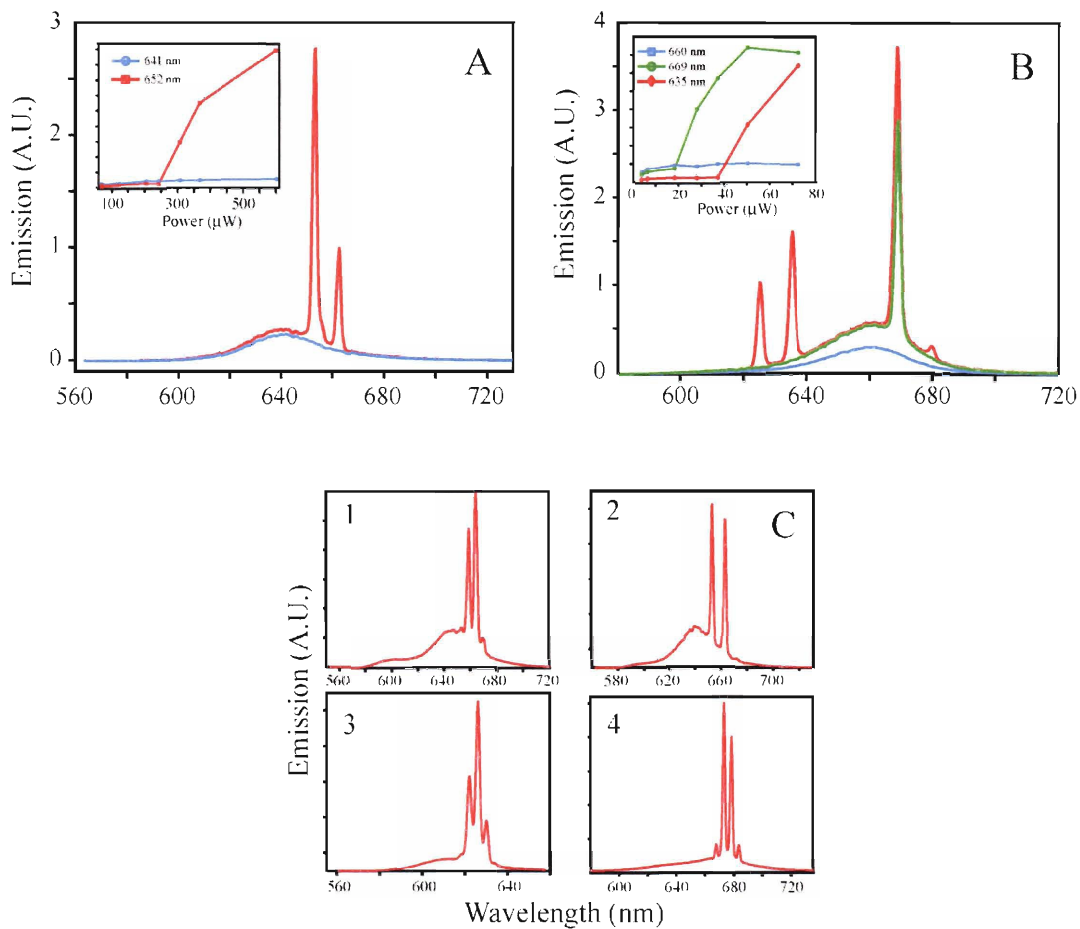


Figure 3.8 – The lasing spectra of NC-microsphere composites. **(A)** The spectra of a single 7 μm Bangs labs core microsphere below (205 μW) and above (366 μW) laser threshold. Inset shows the power dependent intensity of the fluorescence at 641 nm and the laser emission at 652 nm. Close inspection of the spectra reveal WGM mode structure coupled to the free fluorescence at low intensity excitation. **(B)** The spectra of a single 5.6 μm hollow glass Aldrich core microsphere below and above threshold. At low pump intensities single mode biexcitonic emission is observed, while at higher intensities simultaneous biexcitonic and multiexcitonic laser emission is seen. Inset shows the threshold behavior of biexcitonic and multiexcitonic lasing. Multiexcitonic lasing in CdSe NCs will be explained in detail in a later chapter. **(C)** More examples of saturated laser emission using a variety of NC samples and microsphere templates: (1) 25 μm polystyrene, (2) 6.85 μm silica, (3) and (4) 20 μm silica with different wavelength emitting CdSe/CdZnS NCs as the gain material.

3.3.5 Quality factor, threshold and stability characterization

The Q factors of these NC-microsphere composites shown in Figure 3.6c (calculated using $Q = \lambda/\Delta\lambda$ from the instrument response deconvoluted spectra) range from ~400 to 1000. In general, the FWHM of the WGM lasing was 1-2 nm, which is greater than our instrument resolution of ~0.4 nm (at FWHM). The magnitudes of the Q factors are likely a function of the quality of the microsphere template, the surface roughness of the titania sol, and losses due to self-absorption and scattering resulting from defects. The lasing thresholds of 30 individual microspheres from a single sample have been quantified, as shown in Figure 3.9. While the onset of laser emission from this set of microspheres occurs over a range of 130 to 670 μW (corresponding to flux densities of 8.1 mJ cm^{-2} to 41.8 mJ cm^{-2}), threshold behavior as low as 12 μW has been observed in other samples. The observation of these high threshold flux densities and low Q factors indicates that this chromophore/cavity is likely in the weak-coupled regime.²⁷ Overall, the most robust composites were made using a silica-microsphere feedstock, as polystyrene core samples are more easily damaged at pump powers near their laser-emission threshold. The larger 20 μm diameter silica cores formed the best cavities, while the smaller 6.85 μm silica microspheres often suffered from agglomeration of the sol at the base of the coupled structure, which reduced laser performance. The time-dependent ability of the integrated laser emission from a single NC-microsphere (20 μm diameter) silica composite is shown in Figure 3.10. It is readily seen that the decay of the integrated laser intensity tracks the loss of fluorescence over the course of $\gg 1$ hr. Compared to Rhodamine 6G dye-doped laser microspheres prepared via a previously reported method,²⁸ these NC-microsphere composites are over four decades more resilient under

optical excitation. Furthermore, the laser emission has been observed to partially recover if the bleached sample is left in the dark for several minutes, similar to previous observations made in fluorescence-quenching studies of CdSe NCs.²⁹

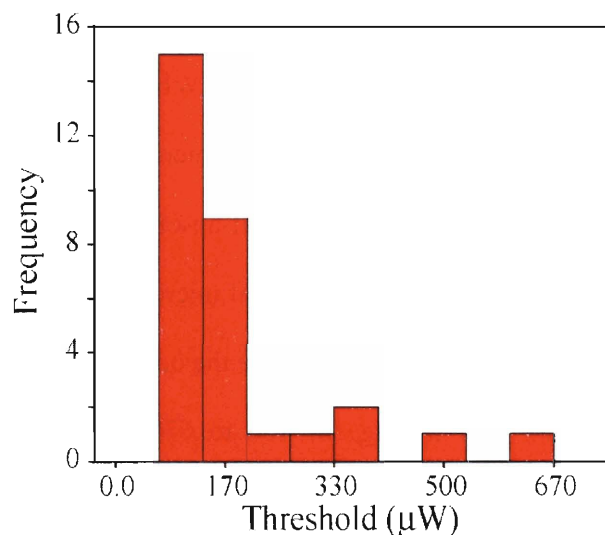


Figure 3.9 A histogram of the laser thresholds for 30 individual NC-microsphere lasers from a single sample. Thresholds as low as 12 μW have been observed for red-light-emitting CdSe/CdZnS samples on 20 μm silica spheres.

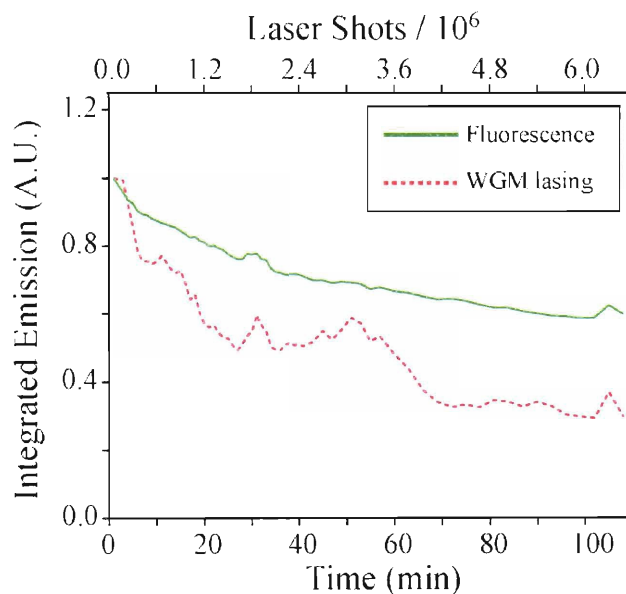


Figure 3.10 Time- and shot-dependent laser intensity of a single NC-microsphere.

3.3.6 Fitting with Mie theory

The mode frequencies observed in the lasing spectrum of a single microcavity have been compared to Mie theory calculations for coated spheres in which the shell refractive index and sphere outer diameter were used as fitting parameters to match the experimental data.³⁰ The results are shown in Figure 3.11. A good agreement between theory and experiment was obtained using reasonable parameters for the shell thickness and refractive index of the coating. As an example, for the fit presented in Figure 3.11, the known refractive index of 1.37 if the 6.84 μm diameter core sphere was used without adjustment. The best fit to the experimentally obtained lasing data was obtained with a shell refractive index of 1.846 and an outer sphere diameter of 7.746 μm . The fitted coating size is consistent with the experimentally measured diameter of $7.66 \pm 0.11 \mu\text{m}$, as determined by SEM images of similar samples and the experimental results from spectroscopic ellipsometry, which show that the index of refraction varies from 1.82 to 1.83 over the wavelength range of 600 to 700 nm. The refractive index (approximately 0.14 greater relative to a similar film without NCs) is consistent with the incorporation of a large (14.8%) volume fraction of NCs into the titania matrix. Note that the SEM results reveal that the sphere coating is thicker than the substrate film, perhaps due to the surface tension of the liquid sol surrounding the sphere core upon spin-casting. Differences in the fitted and measured values for the refractive index are likely due to the dependence of the index on the volume fraction of CdSe in the matrix, which varies from sample to sample.

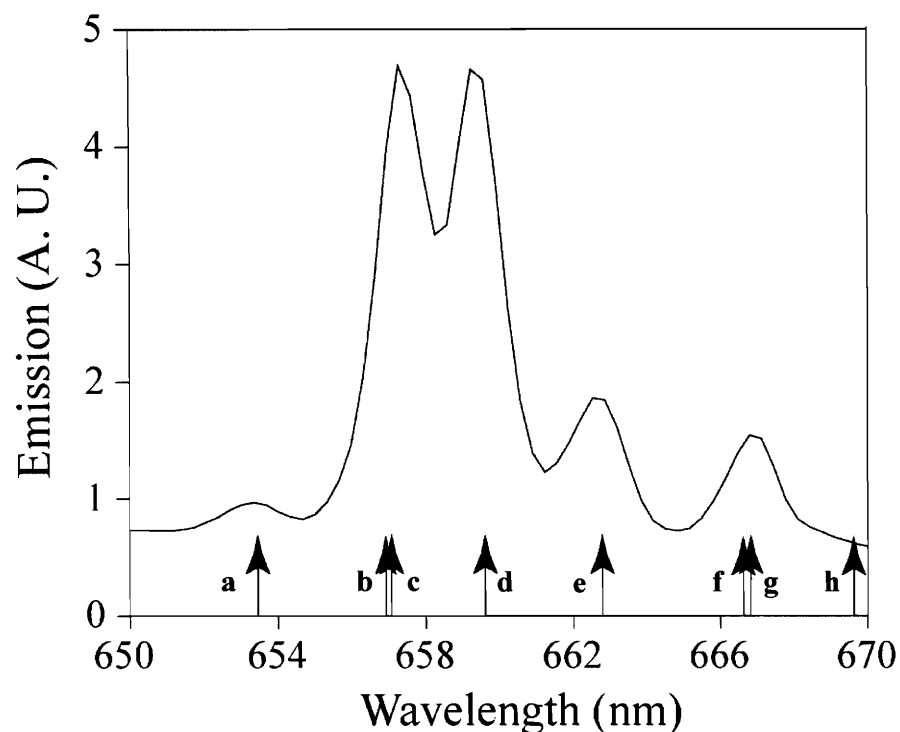


Figure 3.11 The lasing spectrum of an individual $\sim 7.5 \mu\text{m}$ microsphere. Arrows depict the calculated resonant-cavity-mode frequencies from Mie theory for a coated sphere. The mode frequencies are: a) TM_{49}^2 b) TM_{60}^1 c) TE_{52}^2 d) TE_{61}^1 e) TM_{48}^2 f) TE_{51}^2 g) TM_{59}^1 h) TE_{60}^1 . Other high angular modes are outside of the gain spectrum while low angular modes in this window have weak Mie resonances.

3.3.7 Conclusions

The NC titania-microsphere composites presented here have many advantages over previously reported microscopic material systems for laser applications. First, the inherent photostability of NCs in a titania matrix is evident by the observation of stable room-temperature lasing over a much longer period of time than can be observed using organic dyes, which are well-known to irreversibly photobleach. Furthermore, these WGM resonant-cavity structures can be introduced using a variety of commercially available microsphere templates, thus avoiding the difficult wet-chemical incorporation

of dye into a microcavity or the need for costly lithographically patterned silicon DFB gratings. The many whispering gallery modes of a large microsphere allows for multiple-wavelength laser emission to occur simultaneously, as shown by the observation of simultaneous multiexcitonic lasing. The fabrication procedure also produces large numbers of uniform optical resonators with a single spin-coating process, which may open up avenues for applications in such areas as chemical and biological sensing if the titania surface can be directly chemically functionalized. The viability of such a premise will be addressed in the following chapter.

3.4 Chapter conclusion

Many advances in the development of NC-based lasers have been made since the discovery of amplified spontaneous emission at low temperature in close-packed films of CdSe NCs. From room temperature ASE through NCs incorporated into titania matrices to DFB lasing from NC-titania films on lithographically patterned silicon substrates, NC-based gain media has progressed considerably towards being feasible for applications. The work described in this chapter has advanced this progress, presenting soft-lithographically embossed DFB NC lasers which offer multiple-wavelength lasing as well as numerous WGM NC lasers formed via a single spin-coating process. These microscale lasers not only demonstrate room temperature operability, wavelength-tunability and photostability, but are fabricated via facile and inexpensive processes. These desirable characteristics indeed assure us of the utility of these NC lasers for both fundamental study and applications.

3.5 References

1. V. I. Klimov, A. A. Mikhailovsky, Su Xu, A. Malko, J. A. Hollingsworth, C. A. Leatherdale, H. –J. Eisler, M. G. Bawendi, *Science* **2000**, *290*, 314
2. V. C. Sundar, H. –J. Eisler, M. G. Bawendi, *Adv. Mater.* **2002**, *14*, 739
3. M. A. Petruska, A. V. Malko, P. M. Voyles, V. I. Klimov, *Adv. Mater.* **2003**, *15*, 610
4. H. –J. Eisler, V. C. Sundar, M. G. Bawendi, M. Walsh, H. I. Smith, V. I. Klimov, *Appl. Phys. Lett.* **2002**, *80*, 4614
5. Y. Xia, G. M. Whitesides, *Ann. Rev. Mater. Sci.* **1998**, *28*, 153
6. S. Y. Chou, P. R. Krauss, P. J. Renstrom, *J. Vac. Sci. Technol., B* **1996**, *14*, 4129
7. R. Phelan, V. Weldon, M. Lynch, J. F. Donegan, *Electron. Lett.* **2002**, *38*, 31
8. H. Kogelnik, C. V. Shank, *Appl. Phys. Lett.* **1971**, *18*, 152
9. A. N. Oraevsky, *Quantum Electron.* **2002**, *32*, 377
10. D. K. Armani, T. J. Kippenberg, S. M. Spillane, K. J. Vahala, *Nature* **2003**, *421*, 925
11. S. M. Spillane, T. J. Kippenberg, K. J. Vahala, *Nature* **2002**, *415*, 621.
12. C. G. B. Garrett, W. Kaiser, W. L. Bond, *Phys. Rev.* **1961**, *124*, 1807
13. A. V. Malko, A. A. Mikhailovsky, M. A. Petruska, J. A. Hollingsworth, H. Htoon, M. G. Bawendi, V. I. Klimov, *Appl. Phys. Lett.* **2002**, *81*, 1303
14. M. V. Artemyev, U. Woggon, *App. Phys. Lett.* **2000**, *76*, 1353
15. M. V. Artemyev, U. Woggon, R. Wannemacher, H. Jaschinski, W. Langbein, *Nano Lett.* **2001**, *1*, 309

16. J. N. Cha, M. H. Bartl, M. S. Wong, A. Popitsch, T. J. Deming, G. D. Stucky, *Nano Lett.* **2003**, *3*, 907
17. V. I. Klimov, M. G. Bawendi, *MRS Bull.* **2001**, *26*, 998
18. X. Fan, M. C. Lonergan, Y. Zhang, H. Wang, *Phys. Rev. B.* **2001**, *64*, 115310
19. Y. P. Rakovich, L. Yang, E. M. McCabe, J. F. Donegan, T. Perova, A. Moore, N. Gaponik, A. Rogach, *Semicond. Sci. Technol.* **2003**, *18*, 914
20. M. Kazes, D. Y. Lewis, Y. Ebenstein, T. Mokari, U. Banin, *Adv. Mater.* **2002**, *14*, 317
21. R. D. Schaller, M. A. Petruska, V. I. Klimov, *J. Phys. Chem. B* **2003**, *107*, 13765
22. P. T. Snee, unpublished.
23. H.-M. Tzeng, K. F. Wall, M. B. Long, R. K. Chang, *Opt. Lett.* **1984**, *9*, 499
24. J. -M. Caruge, Y. Chan, V. Sundar, H. J. Eisler, M. G. Bawendi, *Phys. Rev. B* **2004**, *70*, 085316
25. Y. Chan, J. -M. Caruge, P. T. Snee, M. G. Bawendi, *Appl. Phys. Lett.* **2004**, *85*, 2451
26. D. J. Norris, M. G. Bawendi, *Phys. Rev. B* **1996**, *53*, 16338
27. K. J. Vahala, *Nature* **2003**, *424*, 839
28. S. Shibata, M. Yamane, K. Kamada, K. Ohta, K. Sasaki, H. Masuhara, *J. Sol-Gel Sci. Technol.* **1997**, *8*, 959
29. I. Chung, M. G. Bawendi, *Phys. Rev. B* **2004**, *70*, 165304
30. C. F. Bohren, D. R. Huffman, *Absorption and Scattering of Light by Small Particles*, Wiley, New York **1998**

31. B. R. Fisher, H. –J. Eisler N. E. Stott, M. G. Bawendi, *J. Phys. Chem. B* **2004**, *108*, 143
32. L. Qu, Z. A. Peng, X. Peng, *Nano Lett.* **2001**, *1*, 333
33. B. K. H. Yen, N. E. Stott, K. F. Jensen, M. G. Bawendi, *Adv. Mater.* **2003**, *15*, 1858
34. C. B. Murray, D. J. Norris, M. G. Bawendi, *J. Am. Chem. Soc.* **1993**, *115*, 8706
35. B. O. Dabbousi, J. Rodriguez-Viejo, F. V. Mikulec, J. R. Heine, H. Mattoussi, R. Ober, K. F. Jensen, M. G. Bawendi, *J. Phys. Chem. B* **1997**, *101*, 9463
36. N. E. Stott, Ph.D. Dissertation, Massachusetts Institute of Technology, **2004**
37. D. V. Talapin, A. L. Rogach, A. Kornowski, M. Haase, H. Weller, *Nano Lett.* **2001**, *1*, 207

Chapter Appendix A – Notes on the synthesis of core and core-shell NCs and their incorporation into titania matrices

Various methods for the synthesis of core CdSe NCs have been reported³¹⁻³³ since the seminal work of Murray et. al.,³⁴ featuring higher quantum yields, better size-distributions and less toxic precursors. The quantum yield of the bare NC may be increased further by epitaxially growing a shell of ZnS (more commonly known as overcoating) in order to passivate its surface³⁵. More recently, a cadmium precursor is intentionally added with the zinc and sulfur precursors during the overcoating process, yielding core-shell CdSe/CdZnS NCs which possess quantum yields higher than those of CdSe/ZnS NCs. It was also found that core-shell NCs are more robust than core NCs towards the incorporation process into the sol-gel derived titania matrix. For these reasons, only core-shell CdSe/ZnS and CdSe/CdZnS NCs were utilized in the fabrication of the NC-titania composites described in this chapter.

A.1 Synthesis of core CdSe NCs via the Cd(acac)₂ method

A recently developed method using Cd(acac)₂ as the cadmium precursor was adopted for the synthesis of monodisperse CdSe NCs. The intricate details of the method may be found in reference [36]. Figure 3.A.1 reproduces the optical characterization results from reference [36], summarizing the small size-dispersity and range of sizes one would expect from to achieve with this method. Sizes larger than 8 nm in diameter (or equivalently ~ 640 nm first absorbance peak) may be achieved by replacing 1,2-hexadecanediol with dodecanal as the reducing agent for Cd(acac)₂ and using TOPO of 99% purity. As an example, a solvent mixture in a 50 mL round bottom flask comprising

of trioctylphosphine oxide (TOPO) (6.25 g, 99% Strem), hexadecylamine (HDA) (5.75 g, 90% Sigma) and trioctylphosphine (TOP) (3.4 mL, 97% Strem) is degassed for 2 hours at 140 °C. In a separate 20 mL vial, cadmium 2,4-pentanedionate ($\text{Cd}(\text{acac})_2$) (317 mg or equivalently 1 mmol), TOP (7.5 mL, 97% Strem) and dodecanal (0.5 mL, Lancaster) are mixed, degassed for 1 hour at 100 °C and cooled to room temperature before TOPSe (2 mL, 1.5 M) is added. The solvent mixture is then raised to 360 °C under vigorous stirring before rapidly injecting the mixture from the 20 mL vial. The resulting solution is then allowed to cool to 80 °C. Figure 3.A.2 shows a typical absorption and emission spectrum of the CdSe NCs produced by this procedure. The resolvable features in the absorption spectrum as well as the relatively narrow FWHM of the emission (which gives an approximate idea of the size distribution) suggests that the procedure affords decent results for synthesizing large CdSe NCs.

A.2 Synthesis of core-shell CdSe/ZnS NCs

The overcoating of core CdSe NCs proceeded via previously established methods.³⁵ It is important that core CdSe NCs synthesized via the $\text{Cd}(\text{acac})_2$ method are processed via a minimum of 2 cycles of precipitation with methanol and re-dispersal with butanol/hexane. This is to ensure the removal of residual amines from the CdSe growth solution. Core-shell CdSe/ZnS NCs synthesized via this method typically possess quantum yields of ~ 20-30%.

A.3 Synthesis of core-shell CdSe/CdZnS NCs

Core/shell CdSe/CdZnS nanocrystals have been synthesized via a modification of a previously reported method.^{31,35} A bath of 3.125 g of purified TOPO, 2.875 g hexadecylamine, 0.4g n-hexylphosphonic acid, and 1.7 mL TOP is degassed at 140 °C for 1 hour. Larger CdSe core samples may be prepared by removing the phosphonic acid component. A precursor solution comprising of 1 mmol cadmium 2,4-pentanedionate and 2.2 mmol 1,2-hexadecanediol in 3 mL TOP is degassed at 100 °C for 1 hour, followed by an addition of 2 mL of 1.5 M tri-octylphosphine selenide (prepared by mixing 11.84 g selenium shot in 100 mL TOP with stirring overnight) after cooling to room temperature. The precursor solution is then rapidly injected into the bath at 360 °C and maintained at ~280 °C until the desired emission wavelength is achieved (typically 600-650 nm). The core size distribution for overcoating is narrowed via size selective precipitation after annealing overnight in growth solution at 80 °C. The cores are then dispersed in hexane and added to a degassed solution of 10g distilled TOPO and 0.4g n-hexylphosphonic acid. After removing the hexane under vacuum at 80 °C, 8mL of a TOP solution containing an 80% / 20% molar percent ratio of diethylzinc to dimethylcadmium and a 3-fold excess hexamethyldisilathiane is added at approximately 1 drop / sec using an addition funnel at a bath temperature of 145 °C. The sample is allowed to anneal in growth solution at 80 °C overnight. The quantum yield for core shell particles prepared using this method can be as high as 46%, and are typically higher than those of core-shell CdSe/ZnS NCs.

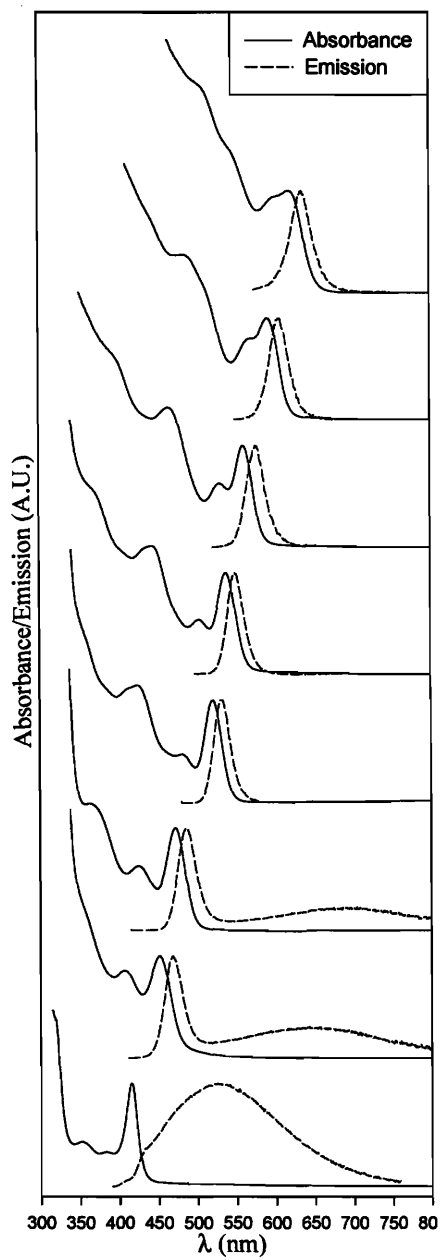


Figure 3.A.1 Room temperature absorption and emission spectra of CdSe nanocrystals ranging from 12-60Å in diameter taken from respective growth solutions without size selection. 12-24Å samples display deep-trap luminescence (Reproduced from reference [36]).

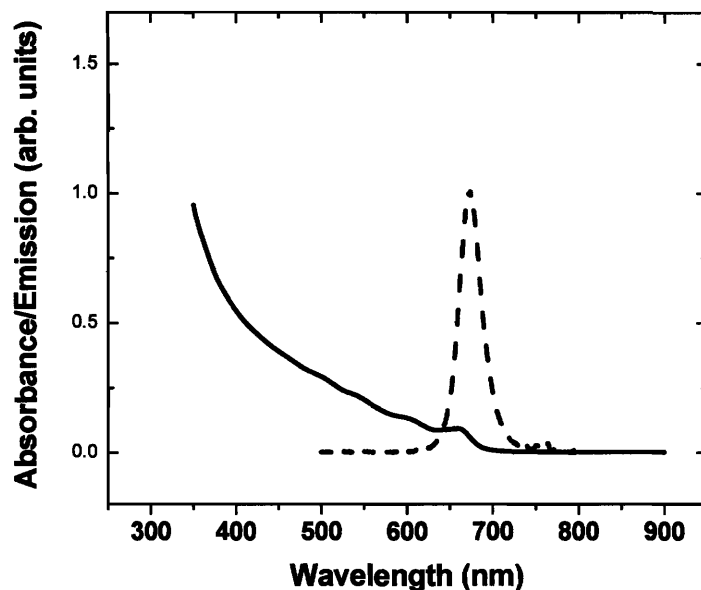


Figure 3.A.2 Room temperature absorption and emission spectra of ~13 nm diameter (first absorption feature at 662 nm) CdSe nanocrystals synthesized using a slightly modified procedure. The sample was taken from growth solution without any size selection. The emission peak is at 673 nm with a FWHM of ~ 31 nm.

A.4 A note on the incorporation of core-shell NCs into titania

Although it has been shown that overcoating CdSe with a shell of ZnS in the presence of amines can dramatically enhance the quantum yield of the resulting core-shell CdSe/ZnS NCs, incorporating NCs overcoated by this method into a titania matrix presented numerous intractable problems. Firstly, the processed core-shell NCs have significant difficulty dispersing in ethanol even after the addition of copious amounts of 5-amino-1-pentanol (AP). Secondly, the NCs which were rendered dispersible in ethanol precipitate upon the introduction of titanium (IV) butoxide (TBOT) and subsequent application of heat. This occurrence generally indicates that the incorporation procedure is unsuccessful and little can be done to salvage the reaction mixture past this point.

The exact mechanism by which NCs overcoated in the presence of amines spontaneously precipitate upon the addition of TBOT is largely unknown, although it may be speculated that the presence of tightly-bound ligands of amine salts on the surface of the NCs prevents cap-exchange with AP and dramatically reduces the solubility of the NCs in ethanol. Further loss of AP from the NC surface due to co-condensation with TBOT then causes the NCs to precipitate out of solution. Cap-exchanging with more labile ligands such as TOP before the introduction of AP required relatively aggressive conditions which exacerbated the surface of the NCs and lowered their quantum yield. Thus overcoating CdSe NCs with ZnS in the presence of amines in order to obtain higher quantum yields is redundant in the context of sol-gel processing. The advent of CdSe/CdZnS NCs, on the other hand, provides core-shell NCs with relatively high quantum yields without the need for amines during overcoating, as described in the previous section. These NCs are readily incorporated into films of titania using the same protocols as those for core-shell CdSe/ZnS NCs not overcoated in the presence of amines.

Chapter 4

A Solvent Stable Nanocrystal-Silica Composite Laser*

4.1 Chapter overview

The previous chapter described the fabrication of different titania-based optical feedback structures via facile processes. These structures facilitated the achievement of lasing from semiconductor nanocrystals (NCs), demonstrating room temperature operability, wavelength-tunability and photostability. A natural extension of these developments would be in the utility of NC lasers towards applications. Aside from the salient optical properties of NC gain media enumerated in previous chapters, two potential characteristics of NC-based, sol-gel derived optical resonators stand out: (i) The sol-gel derived host matrix should allow for functionalization with different ligands to yield a chemically dynamic surface. This may find uses in applications such as optical chemosensing where a chromophore is derivatized in such a way that its emission properties become a function of its chemical environment.¹ (ii) The micron-sized scale of the NC-based microcavities make them suitable for integration with microfluidic devices that have recently been exploited for optofluidic applications,^{2,3} providing an opportunity to have liquids interface and interact with the gain media in a controlled fashion on a very localized scale.

We discover, however, that the NC-titania matrices structurally and photophysically degrade upon exposure to polar solvents such as ethanol and water. This

* Many of the key results in this chapter have appeared in print (Y. Chan et. al. *J. Am. Chem. Soc.* **2006**, *128*, 3146)

imposes a strict restriction on their use with microfluidic systems, which often employ polydimethylsiloxane-based (PDMS) structures that are generally incompatible with non-polar solvents. This chapter describes the use of silica as an alternative host matrix to titania, incorporating NCs in volume fractions sufficient to exhibit stimulated emission. These NC-silica composites do not suffer from the vulnerabilities of titania and are subsequently shown to achieve stable lasing action in solvents such as water and ethanol. This desirable chemical stability is exploited through the use of a channel-bearing PDMS block interfaced with a NC-silica composite film, facilitating the study of amplified spontaneous emission (ASE) in NCs under the influence of a primary amine, 6-amino-1-hexanol (AH). It is subsequently found that AH increases both the single exciton and the biexciton quantum yield, resulting in an increase in the modal gain of the device.

This work presents a unique opportunity to marry the intrinsic advantages from two seemingly disparate fields. The pertinent optical properties of NCs embedded in a stable matrix of silica, along with the fine control of fluid motion at the micro-scale in a microfluidic system, offer a robust platform in which to study the nonlinear optical properties of ensembles of NCs under the influence of a chemically and physically dynamic environment.

4.2 Introduction

Colloidal semiconductor NCs incorporated into sol-gel derived titania matrices have been exploited as optical gain media, exhibiting amplified spontaneous emission that is tunable and microcavity lasing at room temperature.⁴⁻⁷ The micro-scale dimensions of these photostable NC-based lasers should make them ideal for integration with microfluidic networks, facilitating the interaction of liquids with the laser on a miniaturized scale. This would provide the potential of dynamically tuning⁸ the optical properties of the laser, enabling possible applications such as nonlinear optical chemosensing⁹ at small length scales. However, although sol-gel derived titania provides a host structure that is thermally resilient⁴ to the intense optical excitation required to achieve gain in NCs, exposure to water and short-chain alcohols results in rapid structural and photophysical degradation of the NC-titania composite, as shown in Figure 4.1. The extensive cracking observed may be attributed to a dramatic syneresis¹⁰ of the titania matrix, which incorporates unreacted titanium butoxide moieties as a result of a necessarily low annealing temperature.² This makes NC-titania matrices unsuitable as robust NC-based lasers within a microfluidic framework. Indeed, such a device requires a composite that (i) does not suffer from any significant structural and photophysical degradation when exposed to polar solvents, (ii) incorporates NCs in high volume fraction to achieve optical gain, and (iii) has the versatility to be coupled to a microcavity, facilitating room temperature lasing in the presence of solvents. This chapter details the development of a NC-silica composite that addresses all of the above requirements.

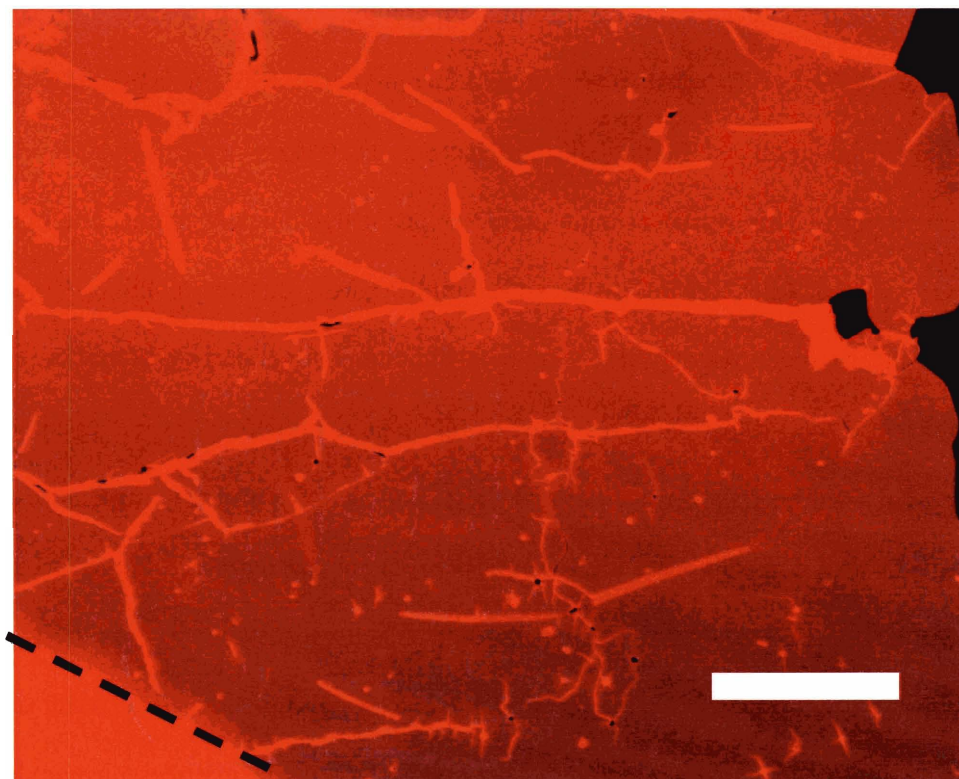


Figure 4.1 Fluorescence microscope image of a NC-titania film that has been exposed to water. The film was left to dry in air before the image was taken. The dotted line on the left separates the area on the NC-titania film that did not come into contact with water. Darkening of the areas exposed to water may be attributed to a loss of capping ligands tethering the NCs to the titania matrix as a result of its rapid collapse. The scale bar is 30 μm .

4.3 Initial attempts

It became increasingly apparent that NC-titania composites were unable to be used in any application that required exposure to moisture or non-anhydrous solvents, thus warranting the need for an alternative host matrix. Silica presented itself as a forerunning candidate for an alternative sol-gel derived matrix due to the vast literature and body of work done on its material synthesis and characterization.¹⁰ More importantly, the reactivity of common silica precursors used in sol-gel chemistry is in general lower than that of titania. As an example, under room temperature conditions, tetraethoxysilane or tetraethylorthosilicate (both abbreviated by TEOS) does not react with water on an appreciable time scale (on the order of months) without the use of base or acid catalysts whereas tetraethylorthotitanate (TEOT) reacts spontaneously with water to form titania. An initial consideration was thus to employ TEOS as the silica precursor, following a methodology similar to the modified Stöber process listed in Chapter 2 to incorporate NCs into silica shells on microspheres. Unlike the Stöber process, however, the formation of silica films requires that the hydrolysis of TEOS takes place in the presence of an aqueous acid. Thus ethanol-solubilized core-shell CdSe/ZnS NCs (through use of 5-amino-1-pentanol or AP) were mixed with a pre-hydrolyzed solution of TEOS and hydrochloric acid in ethanol. This resulted in the spontaneous formation of a monolithic gel. Although not rigorously verified, cursory examination of the homogeneously colored gel suggested that the NCs were uniformly incorporated. Recent interest in NC-doped monolithic aerogels¹¹ may serve as impetus to pursue the mesoporous analog of the NC-silica gel described above. Such mesoporous structures may be formed via the addition of

certain block co-polymers to the acid-catalyzed solution of TEOS.^{12,13} It was clear, however, that the rapid formation of the gel made coupling to a microcavity intractable.

An alternative route employing 3-aminopropyltrimethoxysilane (APS) as the silica precursor was pursued, obviating the use of an acid catalyst. Ethanol-solubilized core-shell CdSe/ZnS NCs were mixed with APS and simply spin-coated onto a glass substrate, analogous to the methodology used for producing NC-titania composites. A schematic illustrating the incorporation process is given in Figure 4.2. The process for incorporating NCs into titania is also included for comparison.

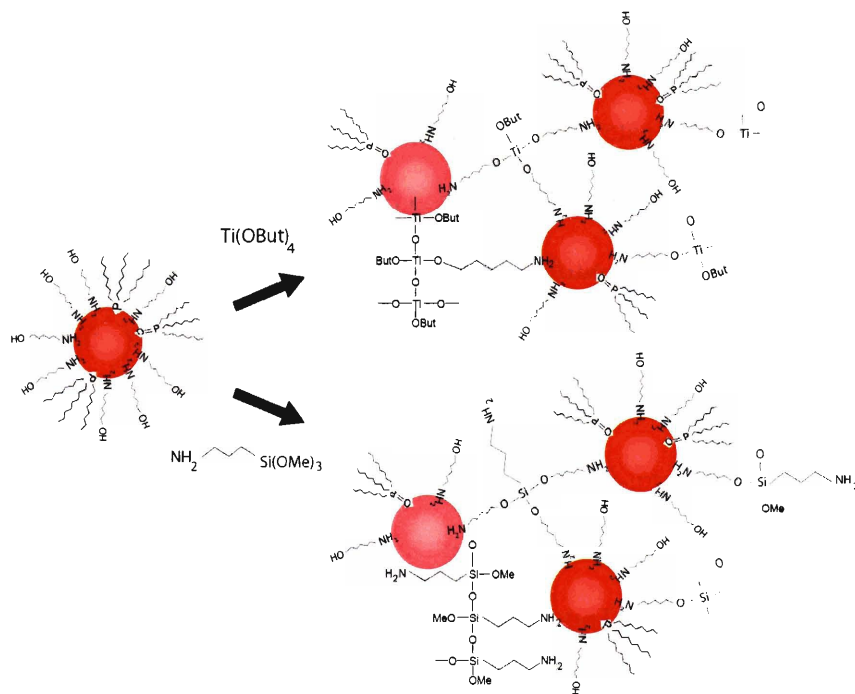


Figure 4.2 Schematic of the incorporation process for NCs into titania (top) and silica (bottom) using titanium (IV) butoxide and APS respectively. Note the presence of unreacted Ti-OBut groups which is believed to cause continued syneresis of the titania matrix.

Figure 4.3 shows a fluorescence microscope image of a film of NC-silica after spin-coating but without annealing at an elevated temperature. This afforded clear, homogeneously colored films (comparable to NC-titania composites) that seem to suggest that the NCs were uniformly incorporated into the silica matrix. Upon exposure to water, however, extensive cracking started to develop, as illustrated in Figure 4.4. This was similar to what was observed in NC-titania composites. This occurrence is not surprising, given that condensation of most of the silicon (IV) methoxide groups were unlikely to have proceeded to completion without the application of heat (annealing step). Figure 4.5 shows a NC-silica film that was annealed at $\sim 80\text{ }^{\circ}\text{C}$ for 5 minutes. This afforded a slight improvement over the films which did not receive any thermal annealing, given that only microscopic cracks were visible upon exposure to water. The increase in structural resilience towards water prompted for higher annealing temperatures, though it should be noted that too high a temperature can result in a loss of quantum yield in the NCs.¹⁴ Figure 4.6 shows a NC-silica film that was annealed at $\sim 200\text{ }^{\circ}\text{C}$ for 2 minutes. Exposure to water did not produce any noticeable cracking using the optical microscope. This remarkable preliminary result encouraged further improvements to the fabrication of NC-silica composites under the framework of using APS and annealing temperatures in excess of $150\text{ }^{\circ}\text{C}$. These developments will subsequently be described throughout the rest of this chapter.

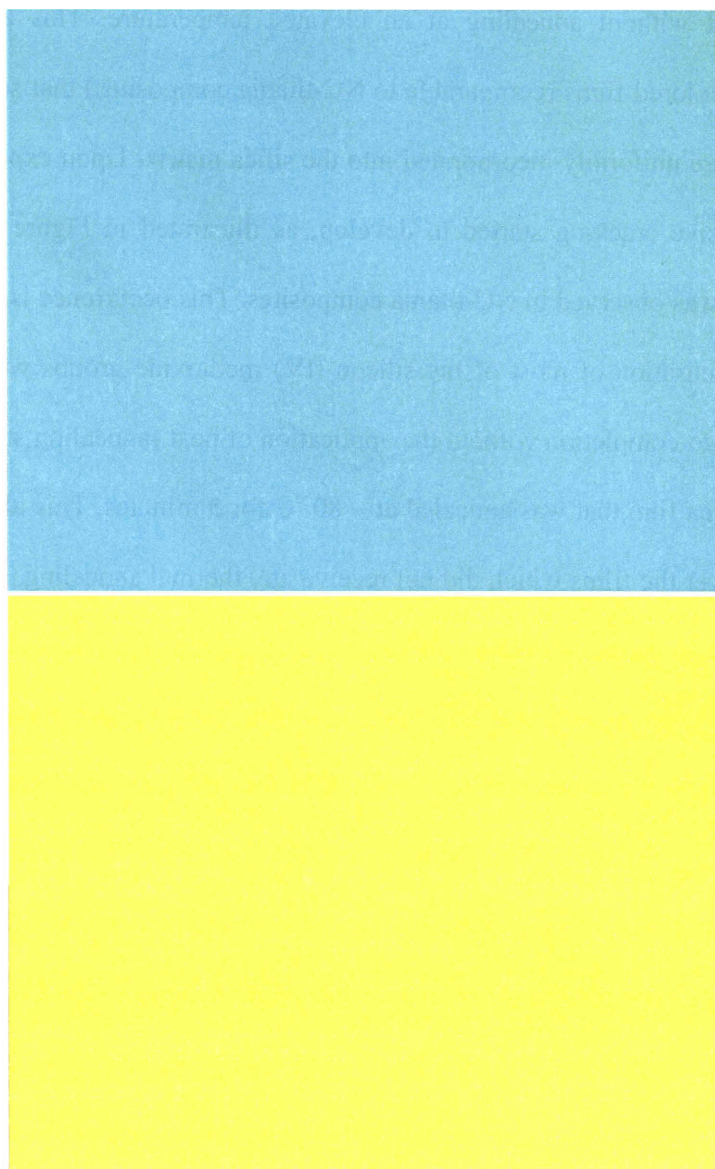


Figure 4.3 Fluorescence microscope image of a NC-silica film freshly spin-coated onto a glass substrate without thermal annealing. The dark (top) and UV (bottom) image both depict a smooth morphology, suggesting that the method is promising. The images were taken using a 20X objective.

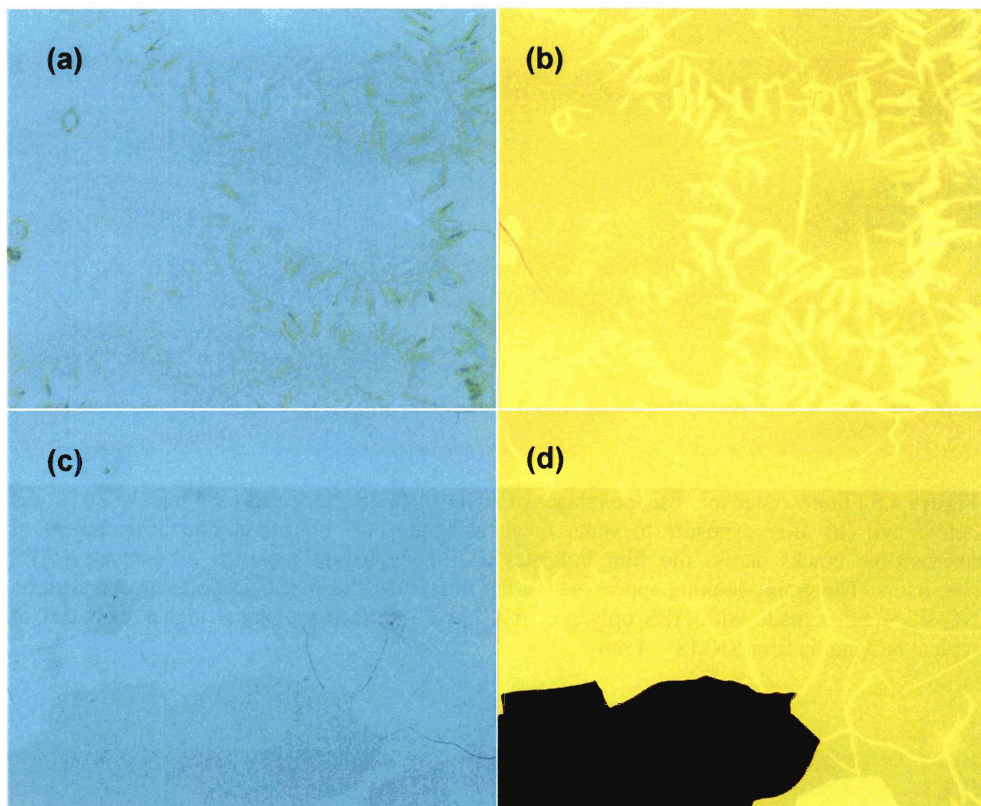


Figure 4.4 Fluorescence microscope image of a NC-silica film that was not thermally annealed and subsequently exposed to water. **(a)** and **(b)** are the respective dark and fluorescence images of one section of the film. Extensive fracturing of the film surface is evident. In some other areas, severe cracking resulted in parts of the film being lifted off the substrate, as illustrated in the dark and fluorescence images depicted by **(c)** and **(d)**. The images were taken using a 20X objective.

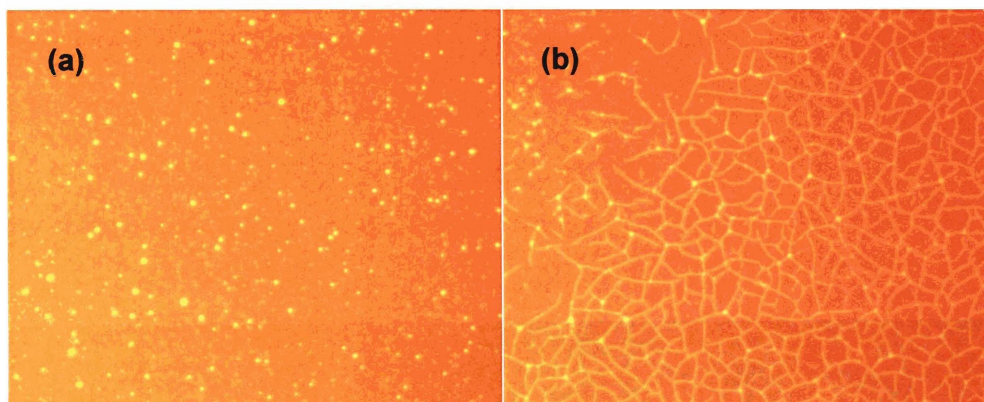


Figure 4.5 Fluorescence microscope images of a NC-silica film annealed for 5 mins at 80 °C, (a) before and (b) after exposure to water taken using a 100X objective. The development of microscopic cracks across the film indicates a still significant presence of unreacted APS precursors. The grainy-looking appearance of the film under this magnification suggests that the NC-silica films made with APS only probably have a surface roughness higher than that of typical NC-titania films (RMS ~ 4 nm).

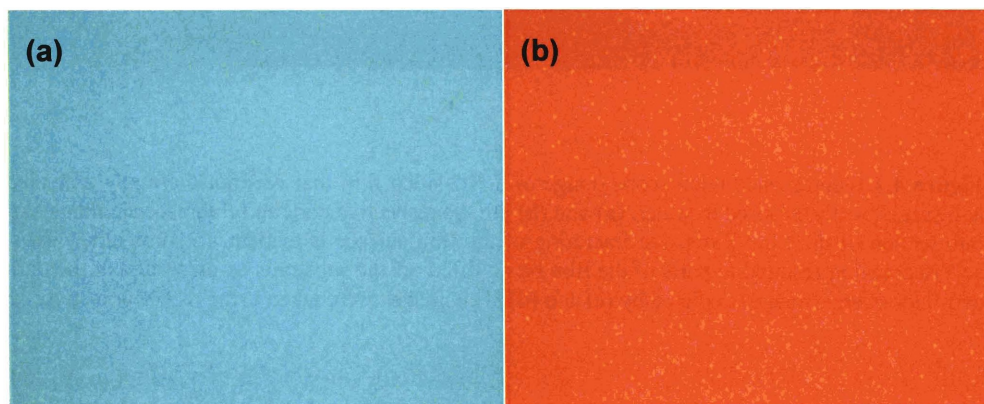


Figure 4.6 Fluorescence microscope images of a NC-silica film annealed for 2 mins at 200 °C. The left (dark) and right (fluorescence) images were taken after the film had been exposed to water. No cracking was observed, suggesting that the annealing temperature was sufficient to drive the condensation of hydrolyzed APS to completion.

4.4 Experimental

4.4.1 Preparation of NC-silica sols

Colloidal CdSe NCs and their subsequent overcoating with ZnS were synthesized according to previously reported procedures.^{15,16} The NCs were processed via repeated cycles of precipitation in methanol/butanol and dispersion in hexane before addition of the silica precursors under inert atmospheric conditions. As an example, to 105 mg of CdSe/ZnS NCs, 205 mg of 5-amino-1-pentanol (AP) (50% wt/wt in ethanol) is added, followed by 286 mg of ethanol. This afforded a clear solution of NCs in ethanol. To this solution, 10 mg of (triethoxysilyl)propyl isocyanate (TSPI) and 52 mg of aminopropyltrimethoxysilane (APS) are added, under vigorous stirring. This resulted in a relatively viscous liquid that is filtered and spin-coated onto a pre-cleaned glass substrate, giving a clear, smooth film. The thickness of the film is crudely controlled by the spin-coating speed. The film is then allowed to anneal on a hot plate at ~ 150 °C for 2 minutes.

4.4.2 Preparation of Distributed Feedback NC-silica Structures

After the pre-polymerized NC-silica sol (synthesized from procedures stated above) is spin-coated onto a glass substrate, a polydimethylsiloxane (PDMS) stamp bearing a grating pattern is placed on the film under a constant pressure of ~ 9.8 KN/m² and transferred onto a hot plate at ~ 150 °C for 2 minutes. It is important to note that the ratio of TSPI to APS should be approximately 1:5 for good pattern transfer. Higher ratios of TSPI to APS lead to an immediate detachment of the stamp from the film when pressure is applied, while lower ratios of TSPI to APS lead to a strong adherence of the

stamp to the film such that the patterned area is lifted off the glass substrate upon removing the stamp.

4.4.3 Preparation of NC-silica Microsphere Resonator Structures

The pre-polymerized NC-silica sol (synthesized from procedures stated above) is further diluted with 2X the amount of ethanol and mixed in with 20 μm diameter commercially available silica microspheres. As mentioned in Chapter 3, there is flexibility in the choice of sphere sizes, although smaller microspheres ($< 7 \mu\text{m}$ in diameter) tend to be partially buried by the film, resulting in hemispherical structures that show poor lasing performance. The resultant mixture is spin-coated at 4000 rpm onto a glass substrate and then annealed on a hot plate at $\sim 150 \text{ }^\circ\text{C}$ for 2 minutes.

4.5 Results

4.5.1 The incorporation process

Previous efforts to chemically incorporate CdSe NCs into sol-gel derived silica resulted in composites with a relatively low volume fraction of NCs,^{17,18} insufficient to exhibit ASE.¹⁹ We saw in an earlier section that the initial strategy of using APS with ethanol-solubilized NCs showed promising results. Thus the surface of core-shell CdSe/ZnS NCs were modified with AP to impart ethanol solubility before introducing APS as the silica precursor. The amino group on APS presumably binds to the NC surface, allowing the NCs to be incorporated in high volume fraction into the silica network. Due to the affinity of the amino group on APS for the NC surface, however, sole use of APS resulted in some displacement of AP, causing a slight aggregation of the

NCs in ethanol. This yielded composites with a rough surface morphology (~ 8 RMS by Atomic Force Microscopy (AFM)) and is consistent with the grainy-looking fluorescence microscope image shown in Figure 4.5.

We circumvent this complication by replacing a small amount of APS with (triethoxysilyl)propyl isocyanate (TSPI), a silica precursor reactive enough to co-condense with APS without the need for acid catalysts that are detrimental to the optical properties of NCs. Since the isocyanate group has a much lower affinity for the NC surface than primary amines, displacement of AP is minimized, rendering the NCs more dispersible in ethanol. Use of TSPI as the only silica precursor, however, resulted in very smooth films but with a low volume fraction of NCs. This is expected since TSPI, lacking a functional group with good affinity for the NCs, cannot assist in the incorporation of NCs into the silica matrix. A judicious choice of the relative amounts of APS and TSPI used afforded silica films with a high volume fraction of NCs ($\sim 12\%$) that did not structurally degrade when exposed to water, as evidenced in Figure 4.7. It was found that a lower and more desirable¹⁴ annealing temperature of $150\text{ }^{\circ}\text{C}$ was sufficient to establish a structurally stable silica network. Surface analysis of the film via AFM revealed a roughness (RMS) of ~ 1.4 nm, as depicted in Figure 4.8, and suggests a uniform dispersion of NCs within the silica matrix. These morphologically smooth NC-silica composites therefore incorporate a high volume fraction of NCs and in addition have an enhanced structural resilience over NC-titania composites that is achieved because APS and TSPI are less susceptible toward hydrolysis or alcoholysis than titanium butoxide.

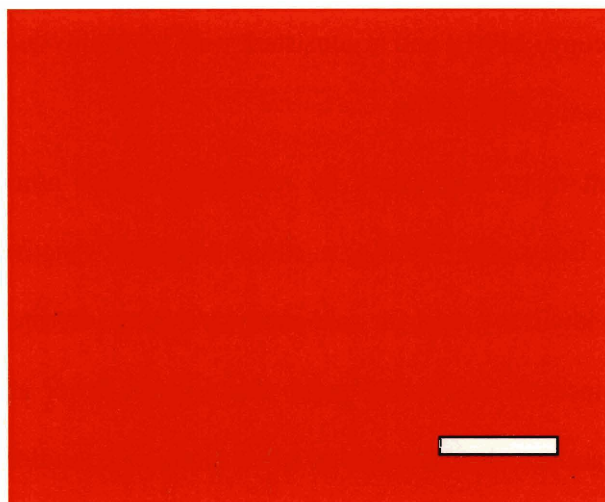


Figure 4.7 Fluorescence microscope image of a NC-silica film that has been exposed to water. The film was left to dry in air before the image was taken. These NC-silica films, made from APS and TSPI, were allowed to anneal at ~ 150 °C on a hot plate prior to exposure to water. No cracking is evident. The scale bar is $30\ \mu\text{m}$.

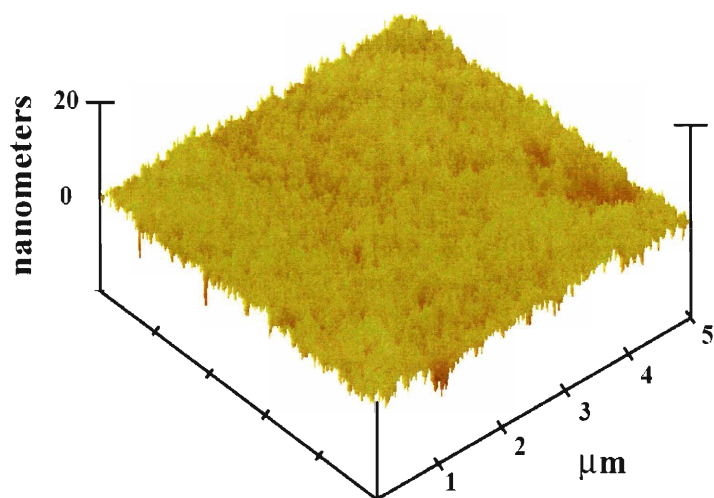


Figure 4.8 AFM image showing a $5 \times 5\ \mu\text{m}$ area of a typical NC-silica film made from APS and TSPI. The surface roughness (RMS) is $\sim 1.4\ \text{nm}$, suggesting the uniform incorporation of NCs into the silica matrix.

4.5.2 Optical characterization

The NC-silica composites readily exhibited ASE under ambient conditions using a frequency-doubled Ti:Sapphire laser with a 60-fs pulse width at 1 kHz, as illustrated in Figure 4.9. We utilize the versatility of these NC-silica composites to couple them to various feedback structures, achieving lasing at room temperature and, more importantly, while submerged in solution. Figure 4.10 shows distributed feedback (DFB) lasing in water from a NC-silica film embossed with an ~ 360 nm periodicity grating pattern via soft lithography.²⁰ The AFM image in the inset illustrates the uniformity of the periodicity and modulation depth (~ 45 nm) of these NC-silica films. Figure 4.11 shows whispering gallery mode (WGM) lasing in methanol from a NC-silica composite coated onto the surface of a 20 μm diameter microsphere via a simple spin-coating process.⁶ Lasing in the presence of water and short-chain alcohols from these composites was stable over hours ($\sim 10^6$ laser shots). The development of these robust, solvent-stable CdSe/ZnS NC-silica microcavity lasers not only allows for integration with microfluidic devices for potential applications, but also presents a platform in which to study the nonlinear optical properties of NCs as a dynamic function of their environment. We demonstrate this dynamical response by studying the effect of adding primary amines to the solution under lasing conditions, as will be described in the following section.

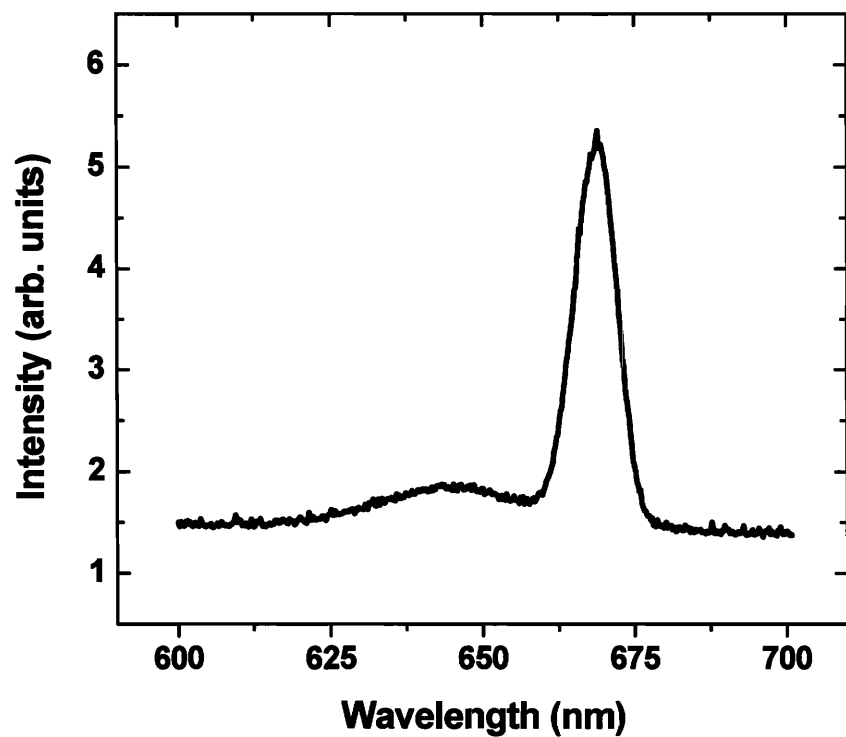


Figure 4.9 Room-temperature ASE from a typical NC-silica slabguide in air. The ASE thresholds for these composites are generally comparable to that of NC-titania, on the order of $\sim 1 \mu\text{J}$ per pulse over an excitation area of $5 \times 10^{-3} \text{ cm}^2$.

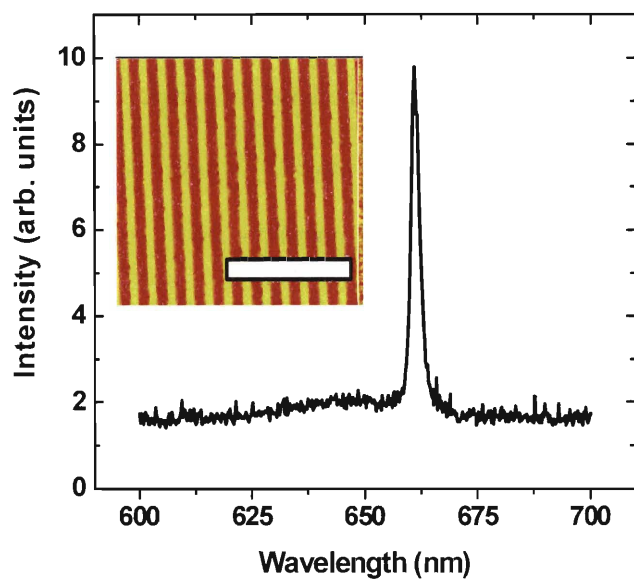


Figure 4.10 DFB lasing in water from a NC-silica film embossed with a 360 nm grating. The inset is an AFM image showing the high fidelity of pattern transfer. The scale bar is 2.5 μm .

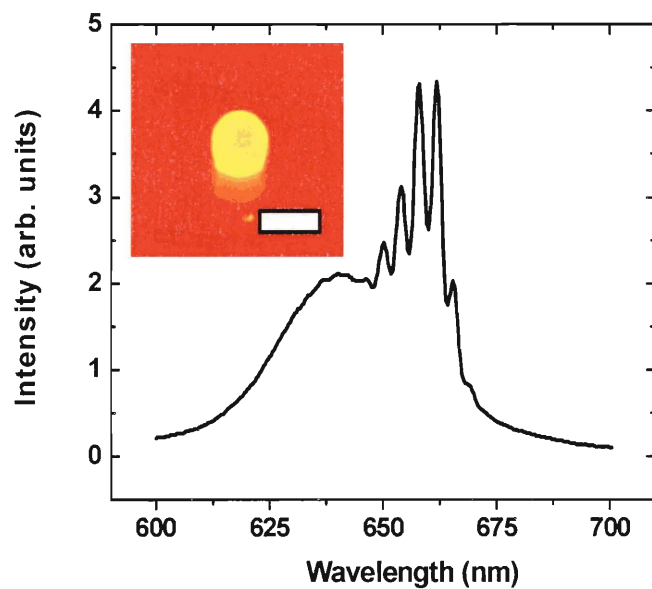


Figure 4.11 WGM lasing in methanol from a silica microsphere coated with a NC-silica composite film. The inset is a fluorescence microscope image of the construct. The scale bar is 20 μm . All ASE and lasing spectra shown were taken at room temperature.

4.5.3 Effect of amines on lasing

While amines have been shown to increase the single exciton quantum yield in CdSe NCs, it was not clear that they should have any effect on the optical gain, which is due to biexcitons.¹⁹ We utilize the porosity and solvent stability of the organoalkoxysilane-derived NC-silica films to investigate their modal gain in the presence of 6-amino-1-hexanol (AH) in water. The films are first interfaced with a block of poly(dimethylsiloxane) (PDMS) containing two isolated channels, each bearing an inlet/outlet duct to facilitate liquid flow, as illustrated in Figure 4.12. Upon exposure to AH, a dramatic increase in the single exciton intensity was found, as shown in Figure 4.13.

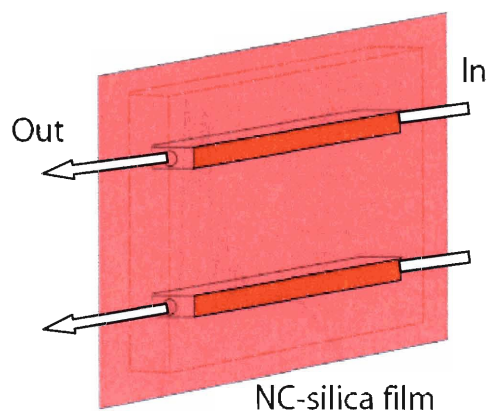


Figure 4.12 Device structure for liquid flow experiments. The NC-silica film is sandwiched between a glass substrate and a PDMS block. Capillary tubes are connected to the inlet and outlet channels to facilitate liquid flow.

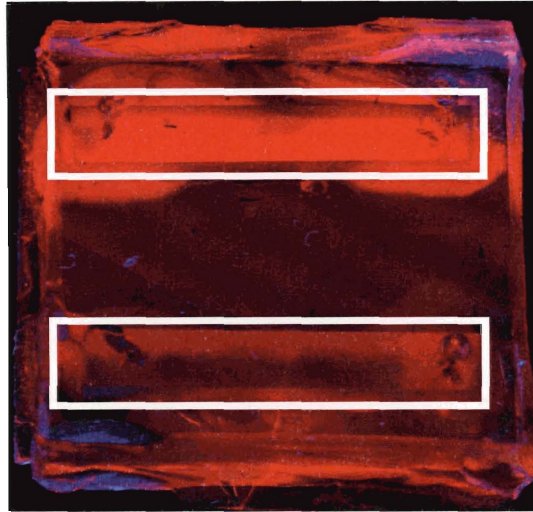


Figure 4.13 The NC-silica film excited using a UV-lamp. The upper channel was exposed to 0.1 M AH, while the lower channel was exposed to pure water.

Variable stripe length (VSL) measurements on the silica film incorporating 4.1 nm CdSe/ZnS NCs were analyzed according to a previously described procedure²¹, yielding a modal gain that increased from $\sim 32 \text{ cm}^{-1}$ in water to $\sim 62 \text{ cm}^{-1}$ in the presence of 0.1 M AH, as depicted in Figure 4.14. Care was taken to ensure that the area of excitation as well as the excitation intensity was the same in both cases. The ASE intensity is plotted as a function of stripe length and fitted according to the equation $I \propto e^{g l_a (1 - e^{-z/l_a})}$, where I , g , and z are the ASE intensity, biexciton modal gain, and stripe length, respectively, and l_a is defined as the optical gain lifetime multiplied by the speed of light in the amplifying medium. This equation is derived from the expression $\frac{dI}{dz} \propto g I e^{-z/l_a}$, where the exponentially decaying term reflects the effect of fast Auger recombination on the amplification of light traversing through the gain medium. The

saturation of the gain is thus taken into account through the parameter l_a , which for these fits gives an optical gain lifetime on the order of ~ 1 ps, consistent with previously reported values for CdSe NCs.²²

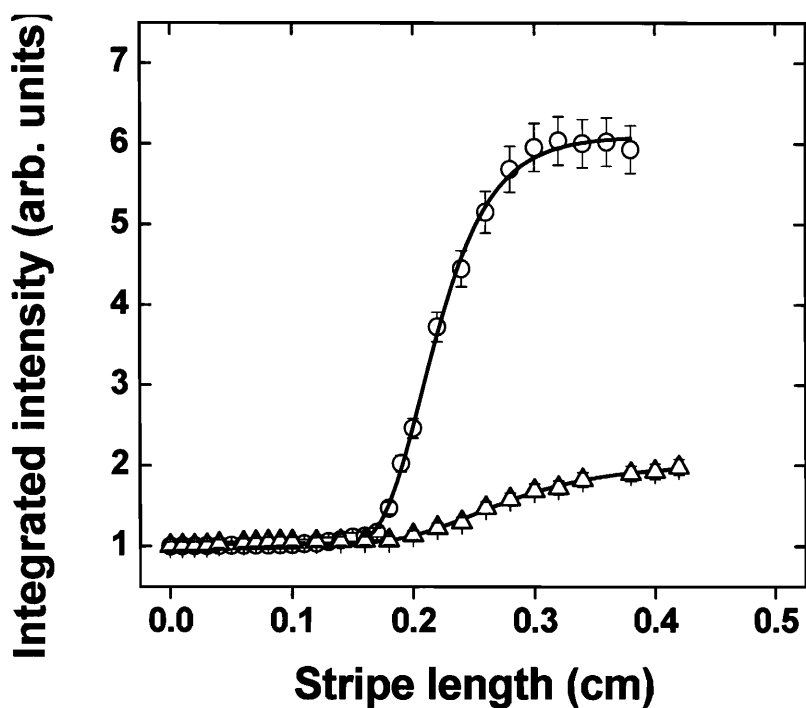


Figure 4.14 The ASE intensity plotted as a function of excitation stripe length for a NC-silica film in 6-amino-1-hexanol (open circles) and in water (open triangles). The solid lines are fits to $I \propto e^{gl_a(1-e^{-z/l_a})}$.

Streak camera measurements on the PL intensity of a similar film, shown in Figure 4.15, revealed that the biexciton quantum yield also increased upon optical excitation in the presence of AH. This suggests that AH plays a role in neutralizing charged NCs that are known to have extremely fast nonradiative relaxation pathways,²³ rendering them available for lasing. This also suggests that a charged biexciton has a nonradiative lifetime that is significantly faster than a charged exciton. The increase in the population of neutral NCs subsequently contributes to the increase in both the single and biexciton quantum yield upon optical excitation, consistent with the observed increase in modal gain. We thus see in this exemplary experiment that it is possible for certain amines to play a role in enhancing both the linear and nonlinear optical properties of NCs.

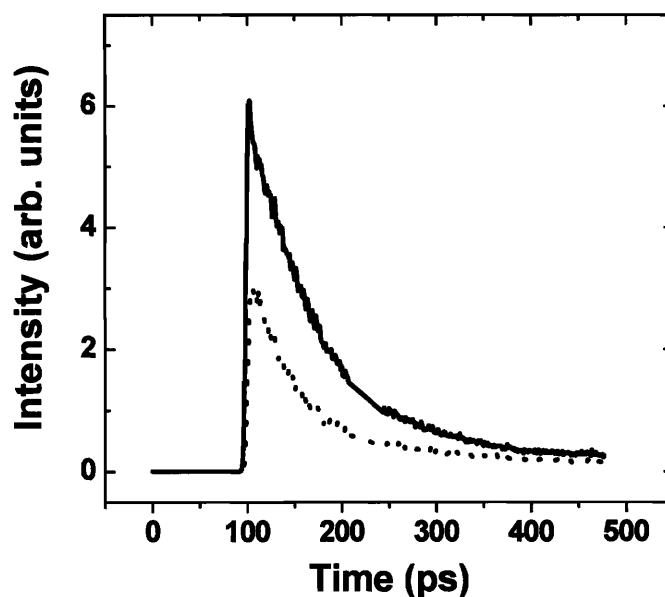


Figure 4.15 Streak camera lifetime measurements using a 1 ns time window on a NC-silica film exposed to water (dotted line) and AH (solid line). The decays are dominated by biexcitonic emission, with a lifetime of ~ 150 ps. An increase in the biexciton quantum yield from water to AH is seen by comparing the areas under their respective PL decay curves.

4.6 Conclusions

This chapter concludes with the overarching statement that we have produced a NC-silica based laser that is robust under different chemical environments, making it suitable for integration with a microfluidic network. Conclusions from the VSL and streak camera measurements on a NC-silica film interfaced with a channel-bearing PDMS block indicate that the nonlinear optical properties of the NC-silica composite can be a dynamic function of its local environment. Through these investigations, one observation that emerged was that the stimulated emission component of the PL can be more sensitive to the environment than its fluorescence counterpart, as illustrated in Figure 4.16. While optimized strategies are required to impart both specificity and sensitivity to NC-silica composites to realize this potential utility of theirs as nonlinear optical chemosensors, the preliminary results presented in this chapter suggest that such an outlook is promising.

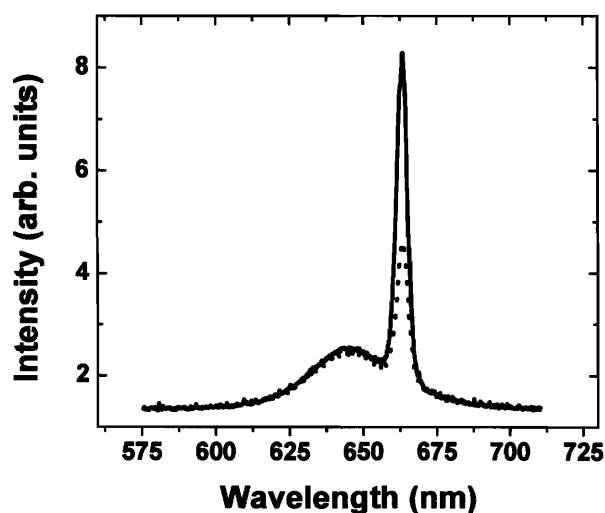


Figure 4.16 The PL spectra of a DFB NC-silica laser immersed in water before (dotted line) and after (solid line) exposure to AH. The excitation intensity, the area of excitation and the detection angle were kept constant. A significant increase in the lasing intensity and a less dramatic increase in the fluorescence intensity were observed.

4.7 References

1. C. M. Rudzinski, A. M. Young, D. G. Nocera, *J. Am. Chem. Soc.* **2002**, *124*, 1723
2. D. V. Vezenov, B. T. Mayers, D. B. Wolfe, G. M. Whitesides, *Appl. Phys. Lett.* **2005**, *86*, 041104
3. D. B. Wolfe, D. V. Vezenov, B. T. Mayers, G. M. Whitesides, *Appl. Phys. Lett.* **2005**, *87*, 181105
4. V. C. Sundar, H. -J. Eisler, M. G. Bawendi, *Adv. Mater.* **2002**, *14*, 739
5. M. A. Petruska, A. V. Malko, P. M. Volyes, V. I. Klimov, *Adv. Mater.* **2003**, *15*, 610
6. P. T. Snee, Y. Chan, D. G. Nocera, M. G. Bawendi, *Adv. Mater.* **2005**, *17*, 1131
7. H. -J. Eisler, V. C. Sundar, M. G. Bawendi, M. Walsh, H. I. Smith, *Appl. Phys. Lett.* **2002**, *80*, 4614
8. D. V. Vezenov, B. T. Mayers, R. S. Conroy, G. M. Whitesides, P. T. Snee, Y. Chan, D. G. Nocera, M. G. Bawendi, *J. Am. Chem. Soc.* **2005**, *127*, 8952
9. A. Rose, Z. Zhu, C. F. Madigan, T. M. Swager, V. Bulovic, *Nature* **2005**, *434*, 876
10. C. Brinker, G. W. Scherer, *Sol-Gel Science: The Physics and Chemistry of Sol-Gel Processing*; Academic: Boston MA, 1990
11. J. L. Mohanan, I. U. Arachchige, S. L. Brock, *Science* **2005**, *307*, 397
12. P. Yang, T. Deng, D. Zhao, P. Feng, D. Pine, B. F. Chmelka, G. M. Whitesides, G. D. Stucky, *Science* **1998**, *282*, 2244
13. D. Zhao, J. Feng, Q. Huo, N. Melosh, G. H. Fredrickson, B. F. Chmelka, G. D. Stucky, *Science* **1998**, *279*, 548

14. V. C. Sundar, Ph.D. Dissertation, Massachusetts Institute of Technology, **2002**
15. B. R. Fisher, H. –J. Eisler, N. E. Stott, M. G. Bawendi, *J. Phys. Chem. B* **2004**, *108*, 143
16. B. O. Dabbousi, J. Rodriguez-Viejo, F. V. Mikulec, J. R. Heine, H. Mattoussi, R. Ober, K. F. Jensen, M. G. Bawendi, *J. Phys. Chem. B* **1997**, *101*, 9463
17. S. T. Selvan, C. Bullen, M. Ashokkumar, P. Mulvaney, *Adv. Mater.* **2001**, *13*, 985
18. M. Epifani, G. Leo, M. Lomascolo, L. Vasanelli, *J. Sol.-Gel Sci. Technol.* **2003**, *26*, 441
19. V. I. Klimov, A. A. Mikhailovsky, S. Xu, A. Malko, J. A. Hollingsworth, C. A. Leatherdale, H. –J. Eisler, M. G. Bawendi, *Science* **2000**, *290*, 314
20. V. C. Sundar, H. –J. Eisler, T. Deng, Y. Chan, E. L. Thomas, M. G. Bawendi, *Adv. Mater.* **2004**, *16*, 2137
21. Y. Chan, J. S. Steckel, P. T. Snee, J. –M. Caruge, J. M. Hodgkiss, D. G. Nocera, M. G. Bawendi, *Appl. Phys. Lett.* **2005**, *86*, 073102
22. A. V. Malko, A. A. Mikhailovsky, M. A. Petruska, J. A. Hollingsworth, H. Htoon, M. G. Bawendi, V. I. Klimov, *Appl. Phys. Lett.* **2002**, *81*, 1303
23. A. L. Efros, D. J. Lockwood, L. Tsybeskov, *Semiconductor Nanocrystals: from Basic Principles to Applications*; Kluwer Academic: New York, 2003

Chapter 5

A Blue Nanocrystal Laser : The Case of CdS/ZnS*

5.1 Chapter Overview

This chapter details efforts in employing core-shell CdS/ZnS nanocrystals (NCs) as an alternative gain media to CdSe/ZnS in order to achieve stimulated emission and lasing at blue wavelengths. The need for a higher band-gap semiconductor despite the ability of CdSe to access most of the visible range is elaborated on, followed by a brief introduction to CdS/ZnS NCs as a choice candidate. The differences in the synthesis and consequently surface chemistry of CdS/ZnS and CdSe/ZnS NCs are then highlighted in order to illustrate the major challenges faced in incorporating the former into a sol-gel derived matrix. A significant modification of the procedure used for CdSe/ZnS NCs was subsequently effected to allow for the uniform incorporation of CdS/ZnS NCs into silica. The physical and structural characterization of these CdS/ZnS NC-silica composites is then presented, culminating in the demonstration of room temperature microcavity lasing at blue wavelengths. This work represents a successful but small part of a more general effort towards achieving stimulated emission in different semiconductor NCs, with the ultimate goal of producing NC-based micro-scale lasers emitting from visible to far infrared wavelengths.

* Much of this work has appeared in print (Y. Chan et. al. *Appl. Phys. Lett.* **2005**, *86*, 0173102)

5.2 Introduction

Semiconductor NCs are unique as optical gain media due to their size-dependent color-tunability and chemical flexibility. Previous work on CdSe NCs has shown that both amplified spontaneous emission (ASE) and lasing at room temperature can be achieved under appropriate conditions¹⁻³. Despite the fact that CdSe NCs have emission tunability over a large portion of the visible range, however, neither ASE nor lasing at blue wavelengths has been demonstrated from these NCs. This may be attributed to highly efficient non-radiative Auger relaxation processes which become dominant as the size of the nanocrystal decreases⁴. Indeed, the Auger-dominated biexciton lifetime of a blue-emitting CdSe NC is on the order of ~ 1 ps⁴, which is too short a time to build up gain within a microcavity. Recently, ASE at blue wavelengths was achieved through the use of Type-II NCs, but only at low temperature⁵. There is thus a great impetus to explore alternative nanocrystalline materials of higher band gap energies to circumvent size-dependent Auger relaxation processes and achieve room temperature stimulated emission at blue wavelengths. One material that offers such promise is CdS.

Much attention has been given to CdS NCs in view of their potential use as nonlinear optical materials, such as optical switches and amplifiers. From z-scan measurements elucidating the third and higher order nonlinearities⁶⁻⁸, to theoretical⁹ and experimental¹⁰ efforts determining optical gain, CdS NCs have been the subject of much fundamental study. Numerous efforts have therefore been dedicated to embedding these NCs in a host matrix. Many of these efforts, however, employ CdS NCs whose surfaces are not well passivated, resulting in significant deep trap emission^{7,10,11}. This leads to a broadened emission spectral profile¹¹ (FWHM > 150 nm) which can overlap with the

size-tunable band-edge emission, making it difficult to separate the emissive contribution from deep-trap states to the observed fluorescence. The spectrally broadened emission is also undesirable for optical applications that rely upon the narrow emission profiles of NCs. Thus core CdS NCs are not attractive as gain media, even though they may be shown to achieve stimulated emission (see Appendix A).

The recent development¹² of core-shell CdS/ZnS NCs present blue-emitting NCs which not only exhibit quantum efficiencies of 20% – 30%, but also display an absence of any deep trap emission. Their emission spectra from 460 – 480 nm show a narrow band edge luminescence with a full-width-at-half-maximum (FWHM) of < 28 nm. The lack of deep-trap emission, relatively high quantum efficiencies and monodispersity of these core-shell NCs make them highly desirable as NC-based gain media. We take advantage of these high-quality CdS/ZnS NCs and chemically modify them for incorporation into a sol-gel derived silica matrix.

5.3 Experimental

5.3.1 Synthesis of CdS/ZnS NCs

The synthesis of core CdS and core-shell CdS/ZnS NCs are described in great detail elsewhere¹³, and will only be highlighted briefly in this chapter to emphasize the differences in surface ligands with CdSe/ZnS NCs. Typical procedures used for core and core-shell synthesis of the CdS NCs that was used in this work are given below, and may be compared to the synthesis procedures for CdSe/ZnS NCs in Chapter 3.

Synthesis of CdS cores

A solvent solution in a round-bottomed flask comprising of oleylamine (7 mL, 98% Pfaltz & Bauer Inc.) and trioctylphosphine (TOP) (8 mL, 97% Strem) is degassed under vacuum for 1 hour at 100 °C. In a 20 mL vial cadmium acetate hydrate (461 mg, equivalent to 2 mmol) is mixed with TOP (6 mL, 97% Strem) and bis(2,4,4-trimethylpentyl)phosphinic acid (BTMPPA) (632 µL, equivalent to 2 mmol) and degassed for 1 hour at 100 °C. In a separate 20 mL vial, elemental sulfur (64 mg, equivalent to 2 mmol) and oleylamine (3 mL, 98% Pfaltz & Bauer Inc.) and degassed at room temperature for 30 minutes. The degassed solutions from both vials are subsequently cooled to room temperature, mixed and injected rapidly into the solvent solution at 340 °C. The resulting solution is then maintained at 250 °C for ~ 5 mins before cooling down to room temperature.

Overcoating the CdS cores with ZnS

The CdS cores were first precipitated out of growth solution using acetone and then re-dispersed in hexane. This was followed by 2 more cycles of precipitation using methanol/butanol and re-dispersal using hexane. The CdS cores dispersed in hexane were then injected into a degassed solvent solution (~2 hrs at 100 °C) comprising of trioctylphosphine oxide (TOPO) (12 g, 99% Strem), hexadecylamine (2 g, 98% Sigma), oleylamine (3 mL, Pfaltz and Bauer) and BTMPPA (316 µL, equivalent to 1 mmol). The hexane was pulled off at 80 °C, leaving the CdS cores well-dispersed in the solvent solution. A mixture consisting of diethylzinc (min 95%, filtered, Strem), hexamethyldisilthiane (>97%, Fluka) and TOP (97%, Strem) was added dropwise to the

solvent flask at 170 °C. The resulting solution was then allowed to stir overnight at 80 °C. Note that in a more recently modified procedure¹³, a small amount of dimethylcadmium (min 95%, filtered, Strem) is also added to the overcoating solution, resulting in (CdS)Cd_xZn_{1-x}S NCs that have quantum yields up to 50%. A summary of the absorption and emission spectra for both CdS cores and CdS/ZnS core-shell NCs is given in Figure 5.1.

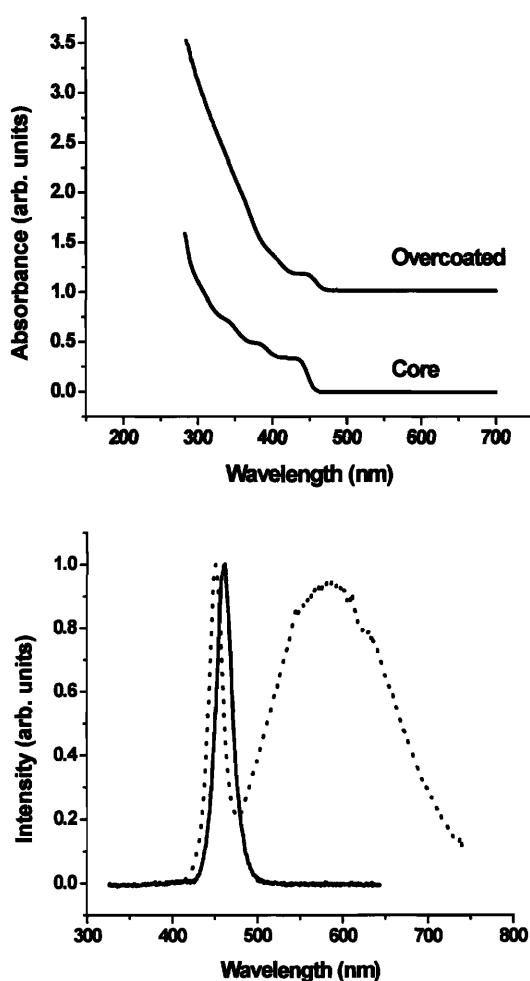


Figure 5.1 *Top:* Absorption spectra of CdS cores and overcoated CdS/ZnS core-shell NCs. *Bottom:* Corresponding emission spectra of CdS cores (dotted line) and overcoated CdS/ZnS core-shell NCs (solid line). It is readily seen that the overcoating process eliminates deep-trap emission.

5.3.2 Incorporation of CdS/ZnS into silica waveguides

As-synthesized CdS/ZnS NCs were first processed from growth solution following 3 cycles of precipitation in methanol/butanol and re-dispersal in hexane. Introduction of ethanol to a dried powder of CdS/ZnS NCs produced slurry that cleared up with a slight addition of tetrahydrofuran (THF), 5-amino-1-pentanol (AP) and oleylamine. This was followed with an addition of 3-aminotrimethoxysilane (APS) as the sol-gel precursor. As an example, to 100 mg of CdS/ZnS NCs, 313 mg of EtOH, 254 mg of AP (50% by weight), 54 mg of oleylamine and 181 mg of THF are added, affording a clear solution of NCs. To this solution 79 mg of APS is added, resulting in a slightly viscous but clear sol upon vigorous stirring for ~ 5 min. The sol is then spin coated onto a glass substrate and annealed on a hot plate for ~ 5 min at 100 °C and then for ~ 2 min at 200 °C. This yielded clear films of CdS/ZnS NC-silica composites that serve as waveguides. The thickness of the film is crudely controlled by the spin speed and ratio of ethanol to APS used.

5.3.3 Coupling the NC-silica composites to microspheres

The CdS/ZnS NCs are first ethanol solubilized according to the procedure stated above, except that the ethanol used is about 2 times the amount used in the incorporation of CdS/ZnS NCs into waveguides. The diluted sol is mixed with large (> 10 μm in diameter) commercially available silica microspheres and spin cast directly onto a glass substrate. An annealing step identical to the one described above is then effected, yielding microspheres coated with a layer of NC-silica.

5.4 Results and discussion

5.4.1 On the incorporation process

A summary of the main differences between CdS/ZnS NCs and CdSe/ZnS NCs is given below:

<p>CdS/ZnS</p> <p>Possible surface ligands:</p> <ol style="list-style-type: none">1. TOP2. Oleylamine3. BTMPPA4. TOPO5. Hexadecylamine	<p>CdSe/ZnS</p> <p>Possible surface ligands:</p> <ol style="list-style-type: none">1. TOP2. TOPO3. Hexylphosphonic acid
--	---

It is evident that the surface of CdS/ZnS is more complicated than that of CdSe/ZnS. Numerous attempts to utilize existing methods of incorporating CdSe/ZnS into titania matrices (described in Chapter 3) met with no success. In fact, the CdS/ZnS NCs are only minimally soluble in ethanol with the use of AP, therefore incorporating them into titania matrices using the methods used for CdSe/ZnS NCs was unfeasible. It became necessary to modify the recipe used to incorporate CdSe/ZnS NCs into a sol-gel derived matrix. The foremost consideration was to find a set of ligands and solvent conditions that would allow the CdS/ZnS NCs to be dispersible in ethanol. While processed CdS/ZnS NCs were easily dispersed in the presence of large amounts of tetrahydrofuran (THF), the resulting NC-film composites often displayed extremely rough surface morphology filled with micron-sized holes. This may be attributed to the fact that the annealing step at elevated temperatures ($> 150\text{ }^{\circ}\text{C}$) causes rapid evaporation of THF (boiling point $66\text{ }^{\circ}\text{C}$) from the film, leaving a significantly patchy surface.

By reducing the amount of THF and adding AP along with a small amount of oleylamine, it was found that CdS/ZnS NCs may be rendered dispersible in ethanol at relatively high concentrations. Addition of titanium (IV) butoxide to this solution, however, resulted in precipitation of the CdS/ZnS NCs, as was observed in the case of CdSe/ZnS NCs overcoated in the presence of amines. This problem was circumvented by employing a silica precursor, 3-aminopropyltrimethoxysilane (APS), which was shown in Chapter 4 to be able to host CdSe/ZnS NCs in sufficient volume fractions to achieve stimulated emission. Introduction of APS to the solution of dispersed CdS/ZnS NCs in ethanol resulted in a slightly viscous but clear sol that could be spin-coated onto a glass substrate. Annealing of the spin-coated film on a hot plate required to proceed via two separate heating steps due to the rapid evaporation of THF at high temperature causing rupturing in the film, as mentioned before. These films were thus annealed at 100 °C for about 5 min to allow most of the THF to evaporate and again at 200 °C to complete the condensation of the siloxane moiety in APS, thus bridging the silica network. Figure 5.2 shows an atomic force microscope (AFM) image of a typical CdS/ZnS NC-silica film. The smooth morphology, with a surface roughness (RMS) of ~ 4.6 nm, as well as the optical clarity of the film, suggests that the NCs are uniformly dispersed within the silica matrix.

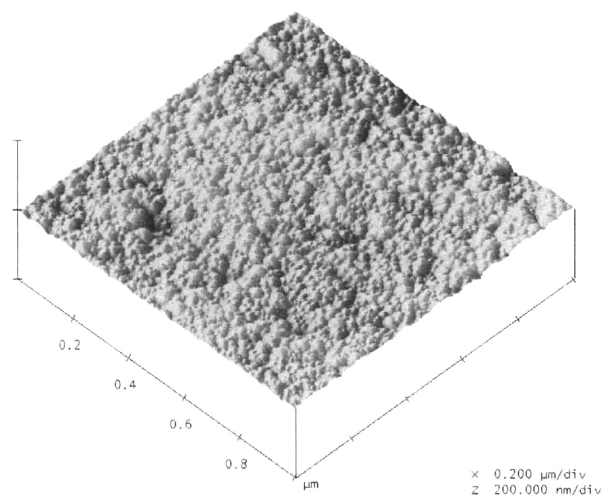


Figure 5.2 AFM image of a typical CdS/ZnS NC-silica film over a $1\ \mu\text{m} \times 1\ \mu\text{m}$ area. The surface roughness (RMS) is $\sim 4.6\ \text{nm}$, consistent with the smooth surface morphology depicted in the image.

5.4.2 Tunable ASE at room temperature

Since the CdS/ZnS NCs were independently synthesized before incorporation into silica films, good control over the size distribution and emission tunability of the NCs in the composites were obtained. Figure 5.3 shows the emission profiles of three different CdS/ZnS NC-silica composite films. The narrow spectral widths of the fluorescence emission of the NCs (FWHM $\sim 25 - 30\ \text{nm}$) are preserved upon incorporation into the film. No significant deep-trap emission is observed, suggesting that the incorporation process does not appreciably perturb the surface quality of the overcoated NCs. ASE at room temperature was achieved by exciting the films with the frequency-doubled output of a regeneratively amplified titanium-sapphire (Ti-sapph) laser, although other laser systems can also be used (See Appendix B). This provided excitation centered at $400\ \text{nm}$

with a pulsewidth of 100 fs and a repetition rate of 1 kHz. The narrower (FWHM $\sim 5 - 7$ nm) ASE counterpart of each fluorescence spectrum appears on the lower energy side of the fluorescence.

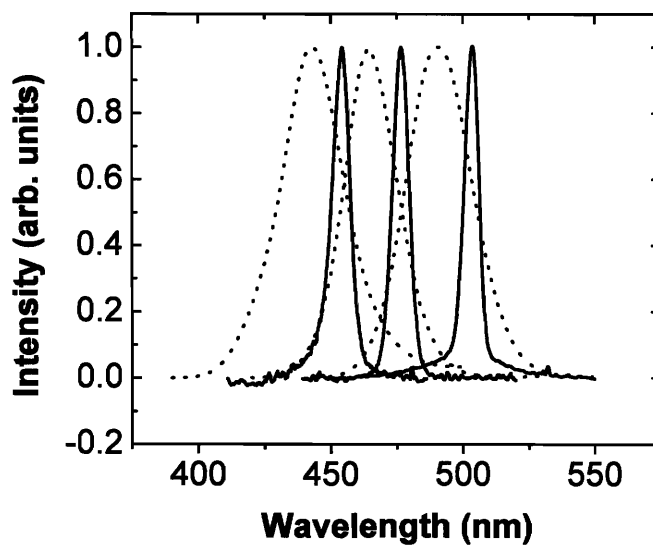


Figure 5.3 Tunable fluorescence of CdS/ZnS NC-silica films (dotted lines). Their corresponding room temperature ASE spectra (solid lines), which occur at 454, 477, and 503 nm feature dramatically reduced linewidths (from ~ 25 to ~ 5 nm)

5.4.3 Photostability study

The photostability of the CdS/ZnS NC-silica film was evaluated by monitoring the ASE intensity as a function of time. Figure 5.4 shows the decline in the ASE intensity over the course of 45 min of continuous excitation at 400 nm using the Ti:Sapph laser system at 1 kHz, equivalent to 2.7×10^6 laser shots. The presence of ASE after such a large number of laser shots illustrates the high optical stability of the NC-silica film. Owing to this high photostability of the NC-silica composite, threshold data could be

obtained reliably and reproducibly within the same sample. The mean number of electron-hole pairs injected into a NC immediately after an excitation pulse was then estimated to be ~ 2 using a NC absorption cross section of $5.28 \times 10^{-15} \text{ cm}^2$ and a pump fluence of $4.02 \times 10^{14} \text{ photons / cm}^2$ at threshold. This suggests that the optical gain from CdS/ZnS results primarily from the presence of biexcitons, as theoretically predicted⁹. This is consistent with the observed redshift of the ASE transitions with respect to the fluorescence, which can be attributed to a combination of re-absorption in the film¹⁴ and a negative biexciton binding energy.^{15,16}

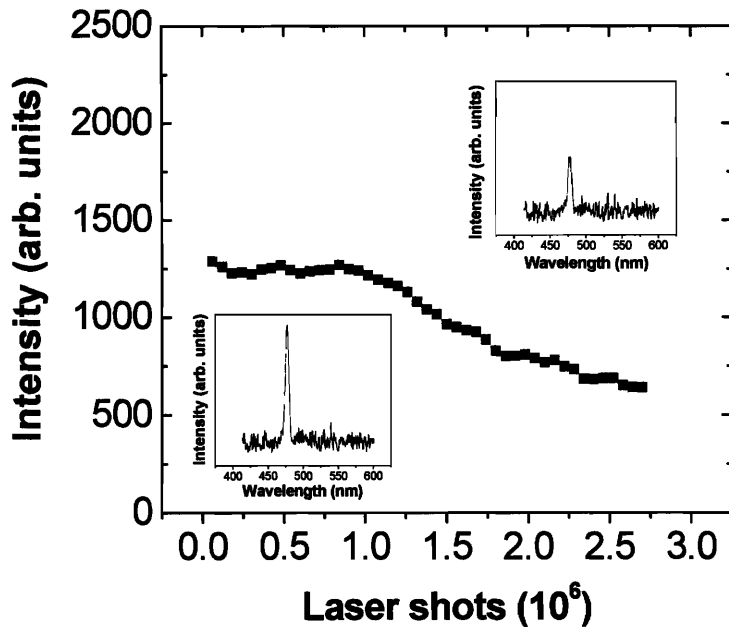


Figure 5.4 Plot of the room-temperature ASE intensity as a function of number of laser shots. The left and right insets show the ASE emission at 1.8×10^5 and 2.4×10^6 laser shots, respectively.

5.4.4 Variable Stripe Length Measurements

Variable stripe length (VSL) measurements were subsequently performed at room temperature in order to determine the biexciton modal gain, as illustrated in Figure 5.5. The curve was fitted (solid line) to $I \propto e^{g l_a (1 - e^{-z/l_a})}$, where I , g , and z are the ASE intensity, biexciton modal gain, and stripe length, respectively, and l_a is defined as the optical gain lifetime multiplied by the speed of light in the amplifying medium. The equation takes into account the saturation of the gain through the parameter l_a . Close examination of l_a reveals a very fast optical gain lifetime on the order of ~ 1 ps, which is comparable to previous studies¹⁷ on CdSe NCs of comparable size. This fast optical gain lifetime, attributed to Auger relaxation processes that deplete gain, accounts for the observed saturation in the ASE intensity.¹⁷ The maximal gain in a composite film of 3.3 nm radius CdS/ZnS NCs in silica was found to be $\sim 100 \text{ cm}^{-1}$ (this figure represents the modal gain per unit stripe length in a waveguide mode), on the same order as that of high quality CdSe NCs in titania films.¹⁸ This gain results from the high loading fraction of NCs into the sol-gel matrix, which in this work is $\sim 10\%$. Indeed, the high loading fraction accounts for the increased refractive index of the silica film ($n \sim 1.7$ as determined by ellipsometry), affording enough index contrast between the film and glass substrate for the film to serve as a waveguide.

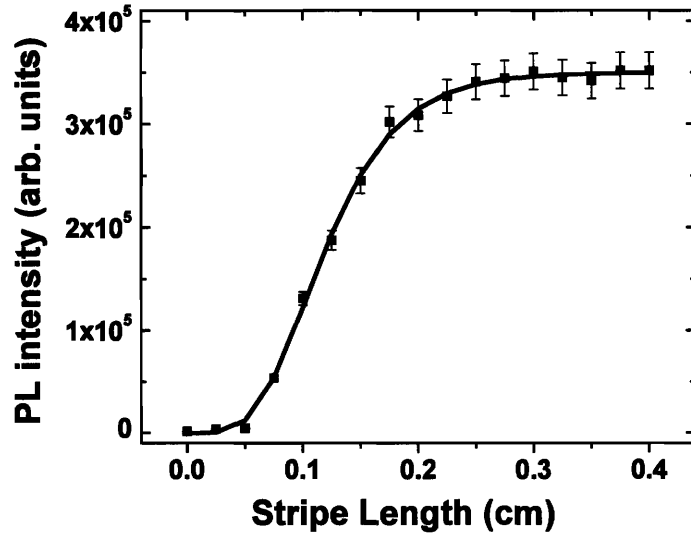


Figure 5.5 Linear plot of the ASE intensity as a function of stripe length obtained from VSL measurements on a CdS/ZnS-silica film at room temperature. The fitted curve (solid line) gives a biexciton modal gain of $\sim 100 \text{ cm}^{-1}$.

5.4.5 Coupling to a Feedback Structure

Optically pumped lasing was achieved by coupling the CdS/ZnS NC-silica composite to a spherical resonator. NC-silica coated spherical resonators were produced according to the procedure¹⁹ elaborated in Chapter 3, in which the NC-sol mixture is spin coated in the presence of commercially available silica microspheres onto a substrate. Figure 5.6 shows microscope images of a typical microsphere resonator under white and UV light excitation. The images were taken using a Nikon ME600 fluorescence microscope.

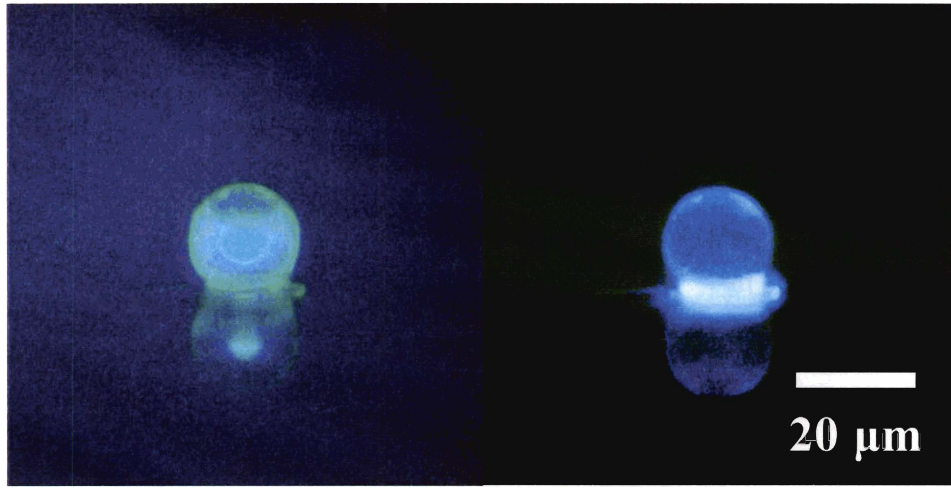


Figure 5.6 Fluorescence microscope images of a typical 20 μm diameter CdS/ZnS NC-microsphere composite under white (left image) and UV (right image) light excitation. The bright halo in the fluorescence image on the right is due to slight agglomeration of the NC-sol at the base of the microsphere during spin casting.

A home-built imaging/dispersive far-field fluorescence microscope coupled to the frequency-doubled output of the Ti:Sapph regenerative amplifier was used to excite and detect lasing from the microsphere-NC composites. Lasing was obtained at room temperature by exciting individual microspheres above threshold, as indicated in the spectra of Figure 5.7. The development of narrow (FWHM < 1 nm), evenly spaced peaks (characteristic of whispering gallery modes²⁰) within the gain spectrum of the NCs depicts the onset of lasing. Clear threshold behavior is readily seen in Figure 5.8, which shows a superlinear increase in emission intensity at ~ 60 μW (corresponding to a flux density of ~ 3.7 mJ/cm^2). The insets show the emission spectra of the NC-microsphere composite below and above threshold. A resolution-limited Q factor (where $Q = \lambda / \Delta\lambda$) of > 600 was obtained from the spectra in Figure 5.7, which is reasonable considering radiative losses from self-absorption and scattering from surface defects in the cavity.

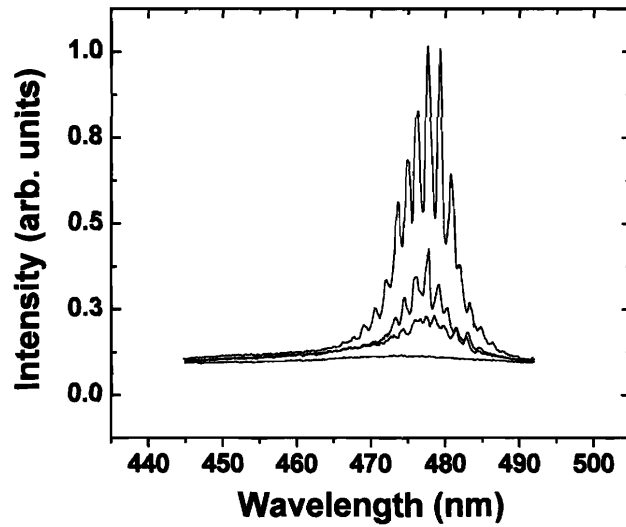


Figure 5.7 Lasing spectra from the NC-microspheres at increasing pump intensities. The Q factor is approximately 600.

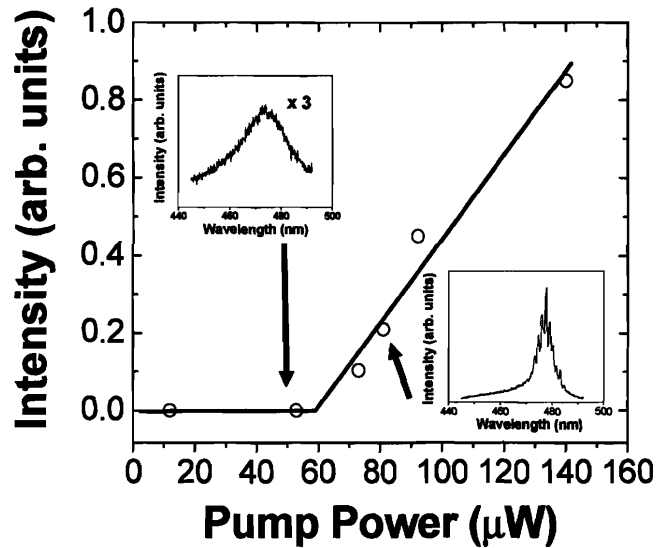


Figure 5.8 The integrated lasing intensity (after subtracting the contribution from background fluorescence) in Figure 5.7 plotted at various pump powers shows clear threshold behavior. The insets on the left and right are the actual emission spectra of the data points indicated by the arrows.

5.5 Conclusion

In this chapter a facile method of incorporating high-quality CdS/ZnS NCs into a silica matrix was presented. The ease of fabricating these CdS/ZnS NC-silica composites obviates the need for expensive techniques such as ion-beam synthesis,²¹ thus providing a cost effective route to a host of possible applications and studies involving the nonlinear optical behavior of these NCs. This was exemplified by the demonstration of stable room-temperature ASE, tunable within a range of blue wavelengths. The absence of deep-trap emission and stability of the ASE allowed for the determination of the biexcitonic origin of the optical gain, and also facilitated VSL measurements of the modal gain at room temperature. It was further showed that blue NC microcavity lasers may easily be produced through the simple strategy of spin coating the CdS/ZnS NC-sol mixture in the presence of microspheres. These blue-emitting spherical resonators open up a new spectral window, providing room-temperature NC-based lasers access across the entire visible range.

5.6 References

1. V. I. Klimov, A. A. Mikhailovsky, Su Xu, A. Malko, J. A. Hollingsworth, C. A. Leatherdale, H. -J. Eisler, M. G. Bawendi, *Science* **2000**, *290*, 314
2. H. -J. Eisler, V. C. Sundar, M. G. Bawendi, M. Walsh, H. I. Smith, V. I. Klimov, *Appl. Phys. Lett.* **2002**, *80*, 4614
3. V. I. Klimov and M. G. Bawendi, *MRS Bull.* **2001**, *26*, 998
4. V. I. Klimov, A. A. Mikhailovsky, D. W. McBranch, C. A. Leatherdale, M. G. Bawendi, *Science* **2000**, *287*, 1011
5. S. A. Ivanov, J. Nanda, A. Piryatinski, M. Achermann, L. P. Balet, I. V. Bezel, P. O. Anikeeva, S. Tretiak, V. I. Klimov, *J. Phys. Chem. B* **2004**, *108*, 10625
6. J. He, W. Ji, G. H. Ma, S. H. Tang, J. I. Elim, W. X. Sun, Z. H. Zhang, W. S. chin, *J. Appl. Phys.* **2004**, *95*, 6381
7. H. Du, G. Q. Xu, W. S. Chin, L. Huang, W. Ji, *Chem. Mater.* **2002**, *14*, 4473
8. Yu. P. Rakovich, M. V. Artemyev, A. G. Rolo, M. I. Vasilevskiy, M. J. Gomes, *Phys. Status Solidi B* **2001**, *224*, 319
9. J. T. Andrews, P. Sen, *J. Appl. Phys.* **2002**, *91*, 2827
10. J. Butty, N. Peyghambarian, Y. H. Kao, J. D. Mackenzie, *Appl. Phys. Lett.* **1996**, *69*, 3224
11. K. Kang, K. Daneshvar, *J. Appl. Phys.* **2004**, *95*, 646
12. J. S. Steckel, J. P. Zimmer, S. Coe-Sullivan, N. E. Stott, V. Bulović, M. G. Bawendi, *Angew. Chem. Int. Ed.* **2004**, *43*, 2154
13. J. S. Steckel, Ph.D. Dissertation, Massachusetts Institute of Technology, **2006**

14. V. C. Sundar, H. –J. Eisler, M. G. Bawendi, *Adv. Mater.* (Weinheim, Ger.) **2002**, *14*, 739
15. J. –Michel Caruge, Y. Chan, V. C. Sundar, H. –J. Eisler, M. G. Bawendi, *Phys. Rev. B* **2004**, *70*, 085316
16. M. Achermann, J. A. Hollingsworth, V. I. Klimov, *Phys. Rev. B* **2003**, *68*, 245302
17. A. V. Malko, A. A. Mikhailovsky, M. A. Petruska, J. A. Hollingsworth, H. Htoon, M. G. Bawendi, V. I. Klimov, *Appl. Phys. Lett.* **2002**, *81*, 1303
18. M. A. Petruska, A. V. Malko, P. M. Voyles, V. I. Klimov, *Adv. Mater.* (Weinheim Ger.) **2003**, *15*, 610
19. P. T. Snee, Y. Chan, D. G. Nocera, M. G. Bawendi, *Adv. Mater.* (Weinheim Ger.) **2005**, *17*, 1131
20. V. Lefèvre-Seguin, *Opt. Mater.* (Amsterdam, Neth.) **1999**, *11*, 153
21. D. Matsuura, Y. Kanemitsu, T. Kushida, C. W. White, J. D. Budai, A. Meldrum, *Appl. Phys. Lett.* **2000**, *77*, 2289

Appendix A to Chapter 5

Incorporating Core CdS NCs into Silica Films

Core CdS NCs were processed from growth solution and incorporated into a silica film using the procedures listed for core-shell CdS/ZnS NCs in section 5.3.2. Interestingly enough, ethanol solubilization of core CdS NCs was achieved through the sole use of AP, though oleylamine and THF were also added following the protocol established for CdS/ZnS NCs. Addition of the silica precursor APS resulted in a relatively viscous sol that was spin-coated onto a glass substrate. A two-part heating step on a hot plate was then applied to complete the condensation of the silica network, affording clear CdS NC-silica composite films with smooth surface morphology. Figure 5.A.1 compares the emission spectra of CdS NCs before and after incorporation into a silica film. The amount of deep-trap emission relative to the band-edge fluorescence is notably increased, suggesting that the surface of core CdS NCs is significantly exacerbated by the incorporation process. This may be contrasted with Figure 5.3, which depicts the emission spectra of core-shell CdS/ZnS NCs in silica films. The absence of deep-trap emission from core-shell NCs after incorporation into the silica matrix may be attributed to the ZnS shell, which offers some protection against external chemical processing.

Optical excitation of CdS NC-silica composite films with a frequency doubled, regeneratively amplified Ti:Sapph (1 kHz repetition rate, 100 fs pulse width) resulted in room temperature ASE, as shown in Figure 5.A.2. While core CdS NCs are not particularly attractive as NC-based gain media owing to their spectrally broad deep-trap emission, it is interesting to note that the presence of these surface trap states does not

appear to prevent the achievement of ASE. This is consistent with the notion that optical gain from CdS NCs stem solely from the presence of biexcitons which have short, Auger-dominated lifetimes.

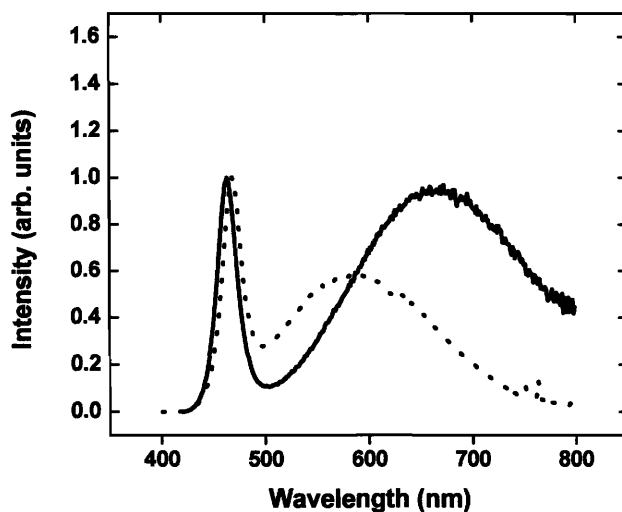


Figure 5.A.1 The emission profiles of core CdS NCs in hexane (dotted line) and in a silica film (solid line). It is interesting to note that the deep-trap emission is redshifted with respect to the band-edge emission after incorporation.

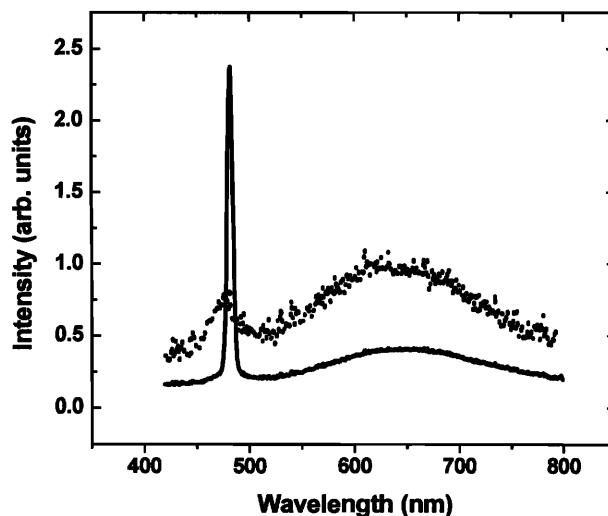


Figure 5.A.2 Room temperature emission spectra from a CdS NC-silica film below (dotted line) and above (solid line) threshold. The ASE component is centered at 481 nm with a FWHM of ~ 6 nm.

Appendix B to Chapter 5

Achieving ASE from CdS/ZnS-silica Composites using a Nanosecond Excitation Source

Although all nonlinear emission spectra described in the main text of Chapter 5 were obtained using a frequency-doubled, regeneratively amplified Ti:Sapph (1 kHz repetition rate, 100 fs pulsewidth), stimulated emission in as-synthesized CdS/ZnS-silica composites was also achieved using a frequency-tripled Nd:YAG (50 Hz repetition rate, 10 ns pulsewidth) as the excitation source. Figure 5.B.1 shows ASE at room temperature from a CdS/ZnS-silica film optically pumped by a Nd:YAG at 355 nm. This presents a more cost effective optical excitation scheme to observing or demonstrating lasing from these NC-based gain media. Some caution, however, must be exercised in using a nanosecond pulsed laser system to investigate quantitatively the nonlinear optical behavior of these NC-based composites, since the biexciton lifetime of these strongly-confined NCs is likely dominated by Auger processes and may be comparable to the pulsewidth of the excitation source. This would present complications in experiments such as determining the number of electron-hole pairs injected into a NC per pulse at threshold due to possible re-excitation issues.

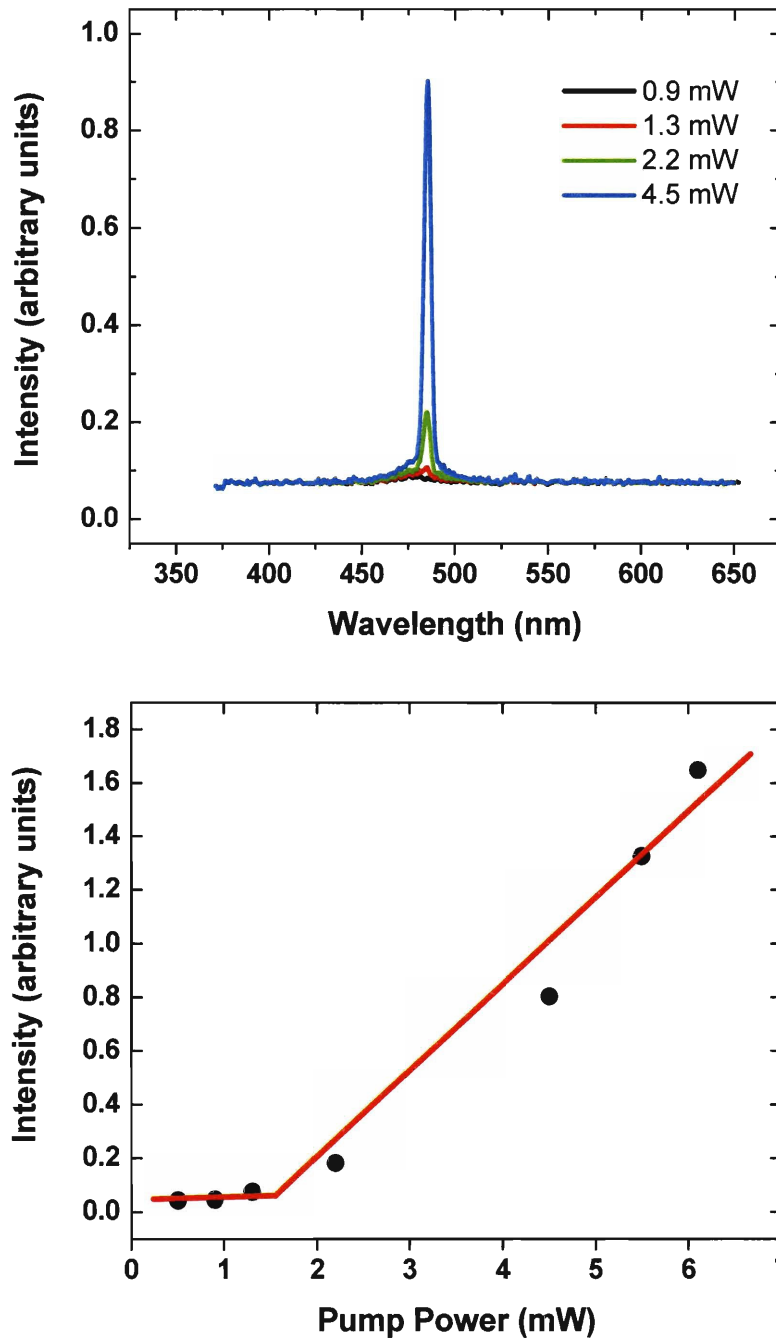


Figure 5.B.1 *Top*: Room temperature ASE spectra of CdS/ZnS-silica films optically pumped using a frequency-tripled Nd:YAG (50 Hz repetition rate, 10 ns pulsewidth). The ASE peak is at 485 nm with a FWHM of ~ 4.2 nm. *Bottom*: Corresponding threshold curve. In this case the threshold is 1.5 mW (30 mJ/pulse) over an excitation area of $\sim 5.0 \times 10^{-3}$ cm².

Chapter 6

Stimulated Emission and Lasing from Multiexcitonic States in Semiconductor Nanocrystals*

6.1 Introduction

The previous chapters addressed the biexcitonic origin of the optical gain in colloidal semiconductor nanocrystals (NCs). Amplified spontaneous emission (ASE) and lasing from the band-edge transition in core-shell CdSe/ZnS NCs were amply demonstrated in NC-doped sol-gel derived slabguides and microcavities, emerging from the lower energy side of the fluorescence spectrum due to a negative biexciton binding energy and re-absorption. More specifically, the light amplification originates from a two electron-hole pair state ($N=2$), where the two electrons and two holes occupy the lowest $1S_e$ electronic and $1S_{3/2}$ hole states of the core CdSe NC respectively, while fluorescence is derived from the radiative recombination of a single electron-hole pair at the $1S_{3/2}$ - $1S_e$ transition. An obvious question that arises is: would it be possible to observe emission from transitions higher in energy than $1S_{3/2}$ - $1S_e$ in these quantum confined CdSe NCs? Multiexciton states (broadly defined as possessing 2 or more electron-hole pairs) in epitaxially grown semiconductor quantum dots (QDs) have been exploited to produce strongly correlated photon pairs,¹ nonclassical optical field states² and to demonstrate the optical entanglement of excitons.³ There is clearly an impetus to achieve multiphoton emission in NCs, which generally have stronger carrier confinement than self-assembled

* Much of this chapter has appeared in print (Y. Chan et. al. *Appl. Phys. Lett.* **2004**, *85*, 2460 and J. -M. Caruge et. al. *Phys. Rev. B* **2004**, *70*, 085316)

or Stranski-Krastanov QDs as a result of their smaller sizes. However, apart from stimulated emission from the biexcitonic state, there have been relatively few reports,⁴⁻⁶ to our knowledge, on the observation of multiexcitonic emission in colloidal CdSe nanocrystals or nanorods prior to the journal publications of this chapter.

The elusive nature of observing emission from multiexcitonic transitions becomes less puzzling when one considers the fast, coulomb mediated non-radiative Auger recombination processes which dominate multiexciton relaxation in these strongly confined NCs. As mentioned in Chapter 1, the biexciton Auger relaxation time is very fast, and high resolution time resolved experiments have shown that its dynamics depend strongly on the NC radius.⁷ For example, the biexciton Auger relaxation time going from a 4.2 nm to a 2.3 nm radius CdSe NC decreases by factor of ~ 8 : from 360 ps to 42 ps. Since the recombination process of multiple electron-hole (e-h) pairs in a NC occurs as a sequence of quantized steps from N to $N-1$, $N-2$ and finally to the 1 e-h pair state, it is reasonable to expect that the relaxation time for a 3 or more e-h pair state to be much faster than that of a 2 e-h pair (biexciton) state. Figure 6.1 compares the extracted decay dynamics of multiexciton states in a 2.3 nm radius CdSe NC from transient absorption (TA) data. It is evident that the 4 e-h pair state and the 3 e-h pair state have a faster relaxation time compared to the 2 e-h pair state, which in turn has a much faster relaxation time than the 1 e-h pair state. These extremely fast Auger relaxation processes in NCs efficiently quench multiexciton emission within picoseconds, leading to negligible multiexciton quantum yields.

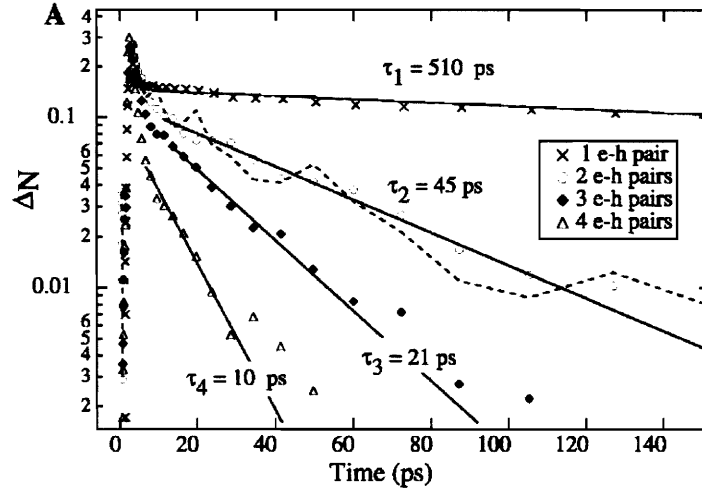


Figure 6.1 Dynamics of 1-, 2-, 3-, and 4- e-h pair states (symbols) extracted from TA data for a 2.3 nm CdSe NC. Figure is reproduced from Ref. [7].

This chapter addresses the challenge of observing and characterizing emission from multiexcitonic states in colloidal CdSe NCs. Transient photoluminescence is employed to spectrally resolve the emission from 1, 2, and 3 e-h pair states in CdSe NCs with radii ranging from 2.3 nm to 5.2 nm. The power dependence of the triexciton, biexciton and single exciton emission intensities are reported. Optical excitation of CdSe/ZnS core-shell NCs in a titania matrix allowed for the achievement of simultaneous amplified spontaneous emission (ASE) from both the $1S_{3/2}-1S_e$ and $1P_{3/2}-1P_e$ transitions. The achievement of amplified spontaneous emission from the $1P_e$ state suggests that the $1P_e$ sixfold degeneracy may be lifted by the e-h exchange interaction. Variable stripe length (VSL) measurements on a CdSe/ZnS-titania slabguide show that the gain from the $1P_{3/2}-1P_e$ transition is approximately twice that of the $1S_{3/2}-1S_e$ transition for 4.2 nm radius core-shell CdSe/ZnS NCs. Finally, two-state lasing from both multiexcitonic

transitions is achieved by embossing the CdSe/ZnS-titania film with a distributed feedback (DFB) structure.

6.2 Experimental

6.2.1 Synthesis of core and core-shell CdSe/ZnS NCs

Core CdSe NCs were synthesized according to previously established methods.^{8,9} For the synthesis of core-shell CdSe/ZnS NCs, the as-synthesized CdSe cores were first processed from growth solution using 2 cycles of precipitation in methanol/butanol and re-dispersal in hexane. The cores were then overcoated with a shell of ZnS according to procedures described in a previous report.¹⁰

6.2.2 Incorporation of CdSe/ZnS NCs into titania and fabrication of NC-titania DFB structures

A detailed description for incorporating core-shell CdSe/ZnS NCs into titania in high volume fraction is given in Chapter 3. The fabrication of NC-titania DFB structures proceeded by first spin-coating the relatively viscous NC-titania sol onto a precleaned glass substrate, which resulted in NC-doped titania waveguides with thicknesses between 200 nm and 500 nm (depending on the spin rate) and optical refractive indices between 1.7 and 1.85 (depending on the NC loading fraction). The films described in this chapter generally have a thickness of ~ 300 nm with a NC loading fraction of $\sim 10\%$. A polydimethylsiloxane (PDMS) stamp onto which the grating grooves of a lithographically patterned silicon wafer have been previously transferred is used to print the surface of the NC-titania waveguide, as described more elaborately in Chapter 3.

6.2.3 Optical measurements

For the transient PL measurements, low concentrations of highly luminescent core CdSe NCs were dispersed in hexane in a 1 mm path length quartz cuvette. The NCs were excited by a frequency-doubled regenerative titanium-sapphire amplifier, delivering 100 fs long pulses at 400 nm at a repetition rate of 1 kHz. Within our pump fluence, up to 10 e-h pairs could be injected into the NCs on average. The mean number of e-h pairs is given by

$$\bar{n} = \frac{\sigma \lambda P}{hcA} = \alpha P \quad (6.1)$$

where σ , λ , h , c , A and P are the NC absorption cross-section¹¹ at 400 nm, the excitation wavelength, the Planck constant, the speed of light, the beam cross-sectional area and the pump power respectively. The room temperature PL was collected with a 5 cm focal length lens, dispersed with a 100 grooves/mm grating and directly detected with a streak camera. The time resolution of the detection setup was 18 ps for the shortest experimental time range.

For fluorescence and ASE measurements, films of NC-titania were either mounted onto a cryostat and cooled to 80 K or studied at room temperature. The NC-films were optically excited perpendicular to their plane using the output from a frequency doubled, regeneratively amplified Ti:Sapph laser. The excitation beam is focused into a thin stripe through the use of a cylindrical lens. Emission from the NC-titania slabguide is collected in the direction of waveguiding and optically coupled into a spectrometer attached to a CW CCD cooled camera.

6.3 Characterization of the multiexcitonic transition

6.3.1 Transient photoluminescence measurements

Streak camera measurements on dilute hexane solutions of CdSe NCs of various radii were performed in order to observe the fast dynamics of multiexcitonic emission. Figure 6.2 shows a three dimensional transient PL spectrum for a 2.3 nm radius CdSe NC sample over a 1.1 ns time window. The pump fluence was adjusted such that 4 e-h pairs were injected into the NCs on average. The PL intensity is coded in white, with the brighter areas corresponding to higher PL intensity. Figure 6.3 shows PL spectra extracted from Figure 6.2 at 20 ps (stars) and 800 ps (circles) after excitation using a 40 ps integration window. It is readily seen that, shortly after excitation, a second emission peak is present at energy higher than the usual band edge emission. Close examination of the pump fluence reveals that the higher energy peak is only present at high excitation intensities, indicative of its multiexcitonic origin. The energy splitting between the two peaks, Δ , is about 0.25 eV. Increasing the NC radius from 2.3 nm to 4.3 nm decreases Δ by a factor of 2, as depicted in Figure 6.4. This decrease in Δ is not mainly due to a significant variation of the band edge Stokes shift. We obtained band edge Stokes shifts between 10 and 25 meV for NC radii ranging from 2.3 to 5.2 nm, which are consistent with nonresonant Stokes shift values reported by Kuno et. al.¹² Figure 6.5 displays the band edge emission spectrum for a 2.3 nm radius CdSe NC 20 ps (squares) and 800 ps (triangles) after excitation. Since the band edge peak comprises of both single and biexciton emission, the observed 20 meV positive energy shift with time is evidence for the negative binding energy of the biexciton, as previously reported.⁴

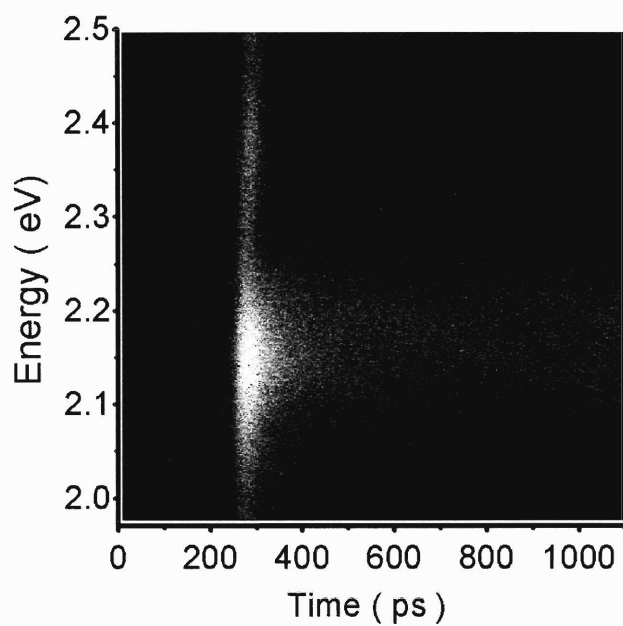


Figure 6.2 3D transient PL spectrum recorded on a 1.1 ns timescale for a 2.3 nm radius NC sample. The PL intensity is color coded in white, with the brighter areas corresponding to higher PL intensity.

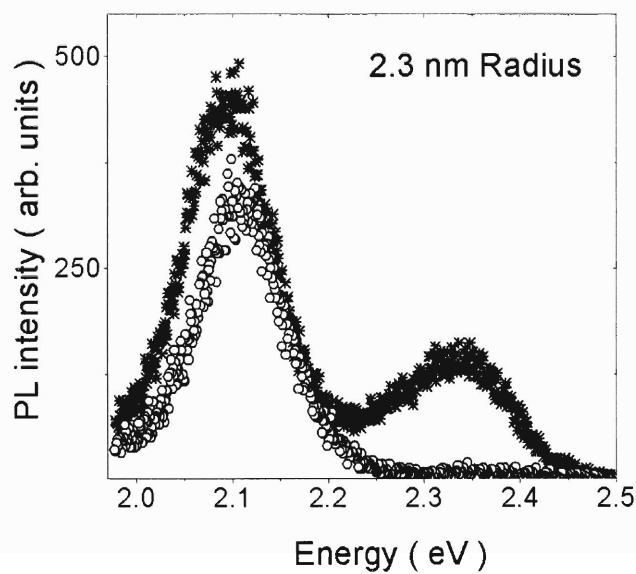


Figure 6.3 PL spectra 20 ps (stars) and 800 ps (circles) after excitation extracted from Figure 6.2. A prominent peak at higher energy is evident at early times.

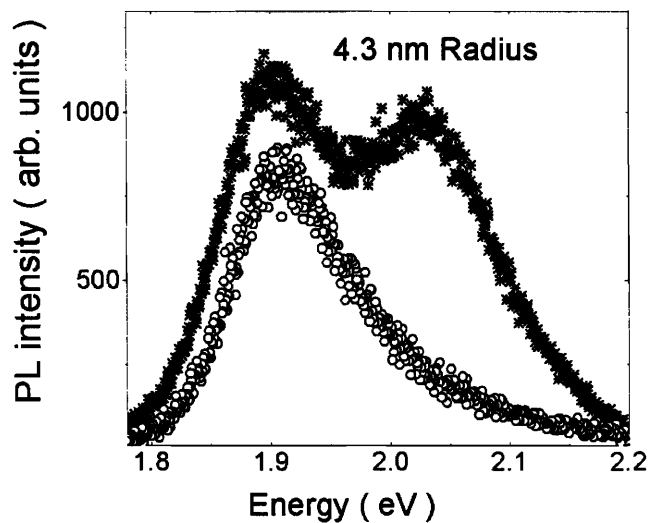


Figure 6.4 PL spectra of 4.3 nm radius CdSe NCs 20 ps (stars) and 800 ps (circles) after excitation. The presence of a peak at higher energy is readily seen at early times.

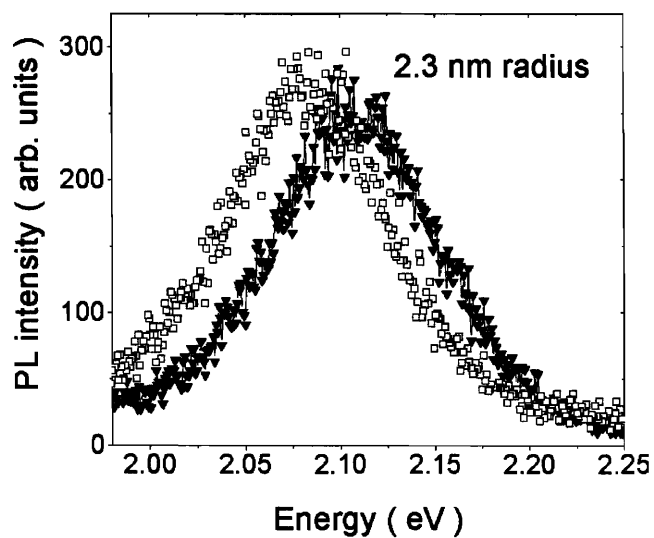


Figure 6.5 Band edge spectra of 2.3 nm CdSe NCs 60 ps (squares) and 800 ps (triangles) after excitation. The blue shift in energy at later times may be attributed to a negative biexciton binding energy.

6.3.2 Lifetime measurements

The transient PL data allowed for the determination of the relaxation time of each emission band. Figure 6.6 presents the extracted dynamics at high excitation intensities, of the band edge emission peak for 3.4 nm (circles) and 2.3 nm (diamonds) radius CdSe NCs. As our measured single exciton lifetime is 14 ns, we assign the fast band edge dynamics, observed on a 1 ns timescale, to biexciton relaxation. The measured biexciton lifetimes, τ_2 , are 150 ps (3.4 nm radius NCs) and 50 ps (2.3 nm radius NCs), consistent with previous reported values.^{4,7} Because the higher energy band is spectrally distinct from the band edge emission, extracting its relaxation dynamics from the transient PL spectrum is relatively straightforward. Figure 6.7 reveals a 50 ps relaxation time for the higher energy band for 3.4 nm radius NCs. The faster carrier decay dynamics for the higher energy band in the 3.4 nm radius sample is expected for Auger recombination involving an increased number of e-h pairs,¹³ suggesting that the higher energy band arises from processes involving more than 2 e-h pairs.

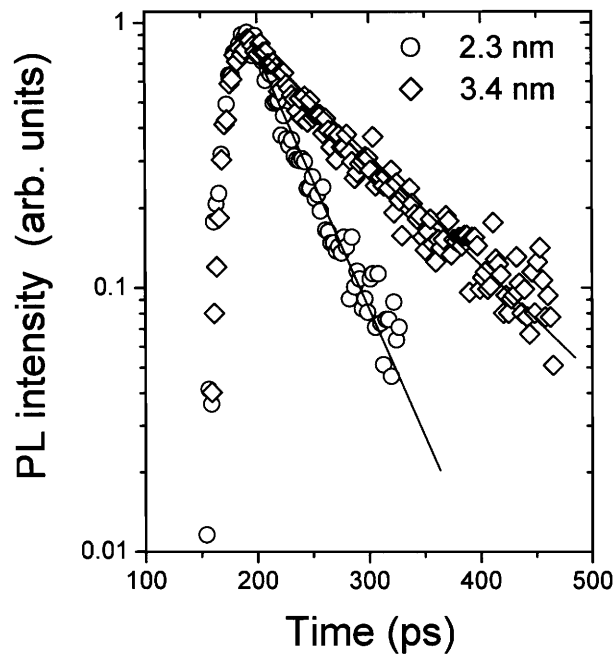


Figure 6.6 The biexciton decay dynamics of 2.3 nm (circles) and 3.4 nm (diamonds) radius NCs.

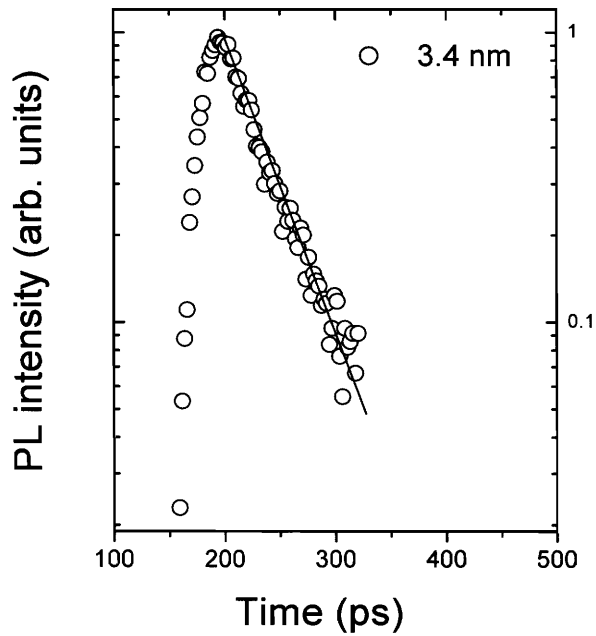


Figure 6.7 The PL decay curve (circles) of the multiexcitonic band for a 3.4 nm radius NC sample.

6.3.3 Analysis of the energy splitting, Δ

The energy splitting, Δ , between the band edge transition and the higher energy multiexciton transition was tabulated for a range of NC radii. Figure 6.8 summarizes the evolution of Δ as a function of NC size. In order to determine the origin of the multiexcitonic band, the size evolution of Δ was compared with single exciton absorption spectra of CdSe NCs, reported previously by Norris *et. al.*¹⁴ Figure 6.9 provides a comparison between Δ (squares) and the position of the $1P_{3/2}-1P_e$ transition (triangles) relative to the $1S_{3/2}-1S_h$ band edge transition. Since the PLE data in reference [13] were obtained at low temperature (10 K), we use the energy of the first excited state of the NCs, instead of its size, to obtain the relative energy of the $1P_{3/2}-1P_e$ transition from reference [14]. This is to take into account the increase of the effective band gap of the NC with temperature.¹⁵ For example, the extracted 0.31 eV spacing for the 2.3 nm NC sample is comparable to the room temperature value reported in reference [16]. The position of the $1P_{3/2}-1P_e$ transition was also measured by performing room temperature linear absorption measurements on three different-sized NC samples. The good agreement between low temperature data from reference [14] and room temperature data from our linear absorption measurements validates the $1P_{3/2}-1P_e$ transition curve shown in Figure 6.8. Within our size range, we obtain an approximate 50 meV energy difference between Δ and the relative position of the $1P_{3/2}-1P_e$ transition. The correlation between Δ and the $1P_{3/2}-1P_e$ energy transition suggests that the observed multiexcitonic band originates from a 3 e-h pair state: 2 electrons in the first $1S_e$ electronic state, 2 holes in the $1S_{3/2}$ state, a third electron in the $1P_e$ electronic state and a third hole in the $1P_{3/2}$ state. The 50 meV energy offset between Δ and the $1P_{3/2}-1P_e$ energy transition may result from

the triexciton (3 e-h pair) binding energy and a Stokes shift due to the fine structure of the $1P_{3/2}-1P_e$ transition.

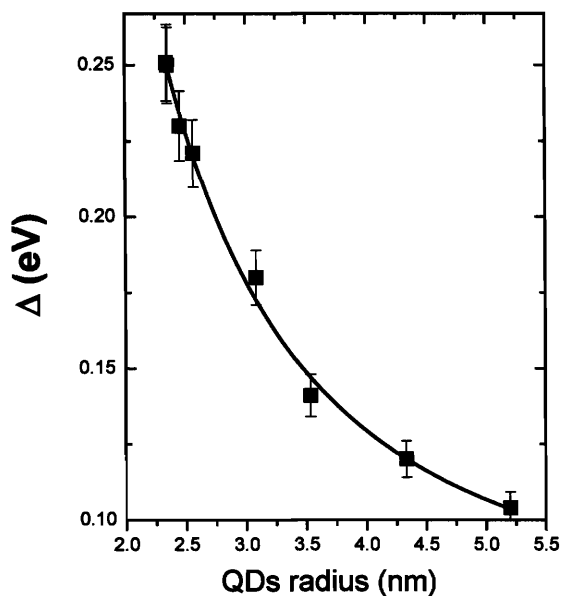


Figure 6.8 A plot of the energy splitting, Δ , versus NC radius. The solid line is a guide to the eye.

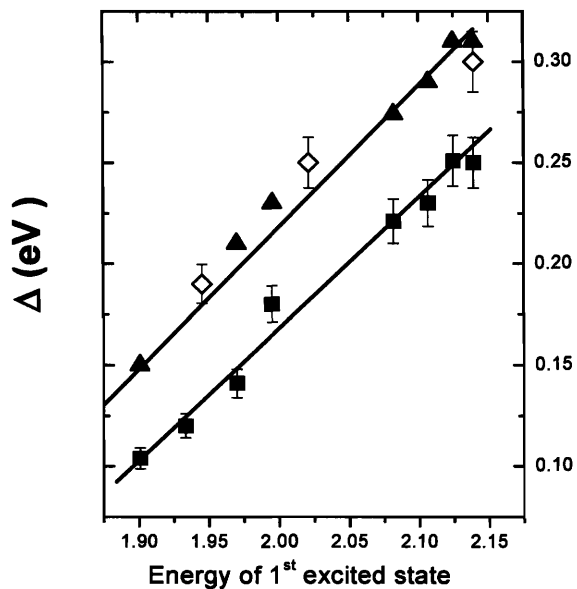


Figure 6.9 A comparison between Δ (squares) and the $1P_{3/2}-1P_e$ transition (triangles) relative to the $1S_{3/2}-1S_e$ band edge transition. The room temperature absorption measurements (diamonds) for three distinct NC radii appear to be consistent with the low temperature data of reference [14].

6.3.4 Analysis of the power dependence of the emission bands

We obtain from the transient PL measurements the power dependence of the single exciton, biexciton and multiexciton emission band for a 2.3 nm CdSe NC sample. We assume a Poisson distribution $p(n) = \bar{n}^n e^{-\bar{n}} / n!$ for the number, n , of e-h pairs injected into a NC after a short excitation pulse*, and \bar{n} is given by Equation 6.1. The single exciton PL intensity at time $t \gg \tau_2$ (where τ_2 is the biexciton lifetime) is proportional to the probability of generating more than 0 e-h pairs per NC immediately after an excitation pulse. The single exciton PL intensity, $I_1(P)$, can thus be expressed as

$$I_1(P) = C_1(1 - p(0)) = C_1(1 - e^{-\alpha P}) \quad (6.2)$$

where C_1 and α are two fitting parameters. It is readily seen in Figure 6.10 that the solid line based on Equation 6.2 closely reproduces the intensity saturation curve of the single exciton for the 2.3 nm NC sample. The fit gives $\alpha = 0.56$, which leads to an absorption cross-section (using Equation 6.1 with $A = 0.032 \text{ cm}^2$) of $\sigma = 6 \times 10^{-15} \text{ cm}^2$, consistent with the $5 \times 10^{-15} \text{ cm}^2$ value previously reported for CdSe NCs of the same size.¹¹

Since the multiexcitonic band is well separated from the band edge emission peak, its power dependence can be obtained directly by acquiring its time-integrated area over a 1 ns window. To minimize errors due to the weak overlap between the two peaks (especially in larger samples), we use a 10 nm (25 meV) integration window on the higher energy side of the emission peak. If we assume, as in reference [4], that the band originates from a charged biexciton, the time integrated PL intensity $I_2(P)$ should then be

* This approximation is valid if we neglect recombination during the pump pulse, which is reasonable given that the pulse width of the excitation source is ~100 fs.

proportional to the probability of generating more than 1 e-h pair per NC after each excitation pulse. This is given by

$$I_2(P) = C_2[1 - p(0) - p(1)] = C_2[1 - (1 + \alpha P)e^{-\alpha P}] \quad (6.3)$$

where C_2 is the only fitting parameter and α has already been determined from the single exciton saturation curve. As illustrated by the crosses in Figure 6.11, Equation 6.3 does not reproduce the power dependence of the multiexcitonic band. We thus conclude that the observed multiexcitonic transition does not originate primarily from the presence of charged biexcitons.

We therefore consider that the multiexcitonic band originates from a 3 e-h pair recombination mechanism. The time integrated PL intensity, $I_3(P)$, should then be proportional to the probability of generating more than 2 e-h pairs per NC after an excitation pulse, and can be expressed as

$$I_3(P) = C_3[1 - p(0) - p(1) - p(2)] = C_3 \left[1 - \left(1 + \alpha P + \frac{\alpha^2 P^2}{2!} \right) e^{-\alpha P} \right] \quad (6.4)$$

where C_3 is the only fitting parameter. As shown by the solid line in Figure 6.11, Equation 6.4 closely reproduces the power dependence of the multiexciton emission band. We thus conclude that the multiexcitonic band originates from a 3 e-h pair, or triexciton emission process.

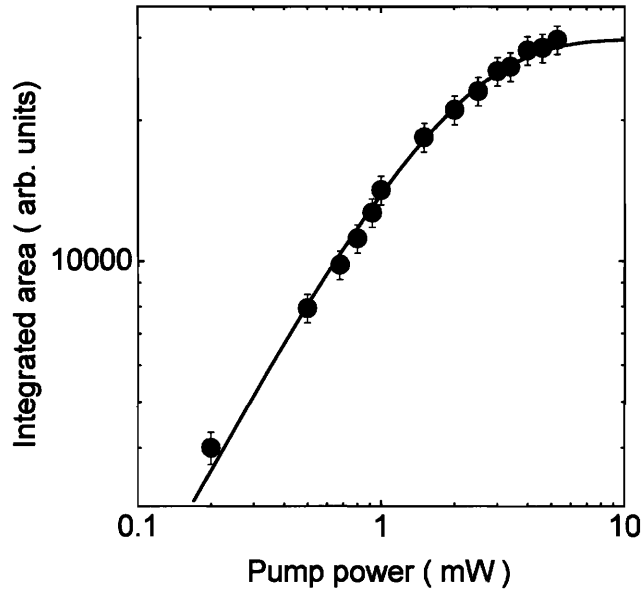


Figure 6.10 The single exciton saturation curve. Single exciton spectra are taken 1 ns after excitation. The solid line (least squares fit) shows that Equation 6.2 reproduces the saturation curve.

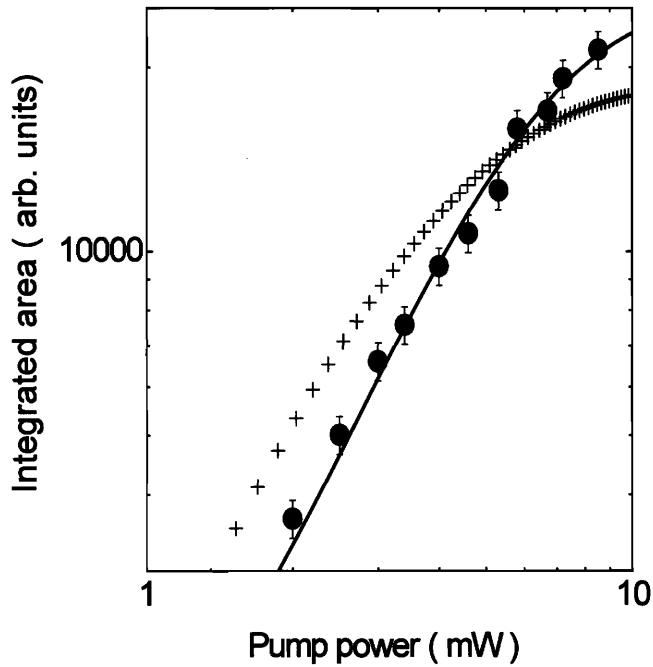


Figure 6.11 Power dependence of the multiexcitonic band (circles). The crosses and solid line are least square fits to Equation 6.3 and Equation 6.4 respectively.

The derivation of the biexciton PL spectrum and its power dependence from the transient PL data is not as straightforward since its emission peak is not spectrally distinct from that of the single exciton. Since the band edge emission comprises of a mixture of both single and biexciton emission, a subtractive procedure is exacted to remove the contribution from the single exciton at time $t \ll \tau_2$. Indeed, as the biexciton lifetime for a 2.3 nm CdSe NC is 50 ps (as shown in Figure 6.6), only a small portion of the initial biexciton population will contribute to the single exciton spectrum at time $t=1$ ps, for example. This fraction is given by $1 - \exp(-1/50) = 0.02$ (2%). At time $t=20$ ps this fraction is 32%, which is significant. We thus calculate the evolution of the single exciton population as a function of time and pump power by first solving a linear set of coupled rate equations which describe the NC multiparticle dynamics.⁷ Let f_N be the fraction of NCs having N e-h pairs at time t . Then we have

$$\frac{df_N}{dt} = \Gamma_{N+1}f_{N+1} - \Gamma_N f_N,$$

$$\sum_N f_N = 1, \quad (6.5)$$

where Γ_N is the N e-h pair relaxation rate. The initial conditions for the linear set of equations are $f_N(t=0) = p(N)$. The following approximation is then made: We limit our calculation to a maximum of 3 e-h pairs, thus obviating rate equations higher than $N=3$ (i.e. $\frac{df_4}{dt}, \frac{df_5}{dt}, \dots$ etc.). We further assume that $\frac{df_3}{dt} \approx -\Gamma_3 f_3$, thus effectively decoupling the expression for $\frac{df_2}{dt}$ from terms higher than $\Gamma_3 f_3$. This approximation holds true at moderate pump power, where the probability of injecting more than 3 e-h pairs into a NC

is small. We thus have the following general solution to Equation 6.5 for the single exciton population

$$f_1(t) = Ae^{-\Gamma_1 t} + Be^{-\Gamma_2 t} + Ce^{-\Gamma_3 t} \quad (6.6)$$

for which A, B and C can be solved by applying the initial conditions to give

$$A = p(1) - B - C, \quad B = \frac{\Gamma_2}{\Gamma_2 - \Gamma_1} \left[p(2) + \frac{\Gamma_3 p(3)}{\Gamma_3 - \Gamma_2} \right], \quad C = \frac{\Gamma_2 \Gamma_3 p(3)}{(\Gamma_1 - \Gamma_3)(\Gamma_2 - \Gamma_3)}$$

We can then calculate the contribution of the single exciton to the band edge PL spectrum at time t by rescaling the band edge spectrum obtained at time $t_1 \gg \tau_2$ by the ratio $f_1(t)/f_1(t_1)$. Figure 6.12 shows the transient PL spectrum (in circles) obtained 20 ps after excitation for a 2.3 nm radius NC sample. The solid line shows the same PL spectrum after subtraction of the single exciton contribution: the peaks thus comprise of biexciton and triexciton emission bands. A plot of the single exciton contribution to the PL spectrum at $t = 20$ ps (diamonds) and at 300 ps (circles) is given in Figure 6.13. At 300 ps the saturation curve of the single exciton is retrieved. At shorter times, the single exciton contribution levels off and even decays. The drop is due to the expected “Poissonian decay” (shown in crosses) of the probability to generate 1 e-h pair per NC after an excitation pulse. The difference between the expected (crosses) and observed (diamonds) decays may be attributed to the contribution from the relaxation of multiexcitonic states. The biexciton emission power dependence can now be plotted according to Equation 6.3 based on the subtracted data illustrated in Figure 6.12. Figure 6.14 shows the fit to the biexciton emission intensity. A summary of the power dependence of all three emission bands, normalized to $P = 1$ mW is given in Figure 6.15.

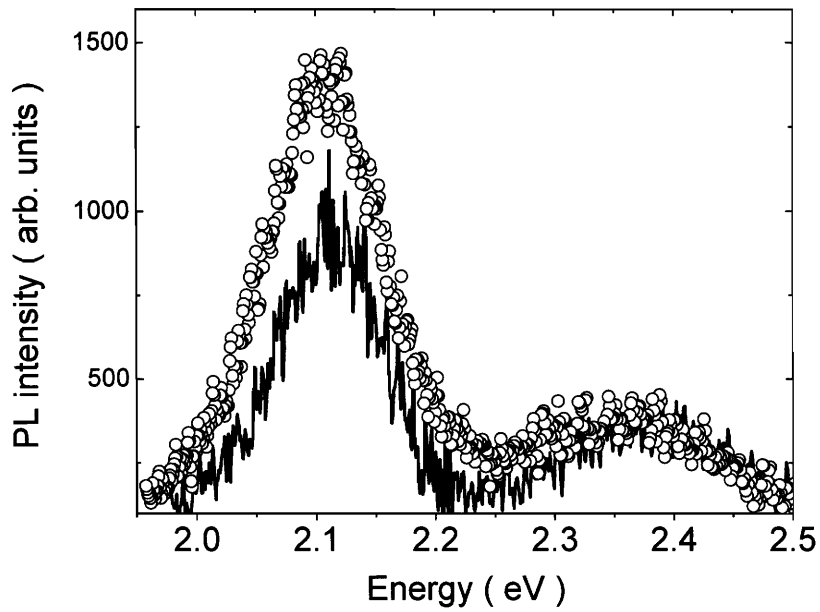


Figure 6.12 The PL spectra of a 2.3 nm CdSe NC 20 ps after excitation before (circles) and after (solid line) subtraction of the single exciton contribution.

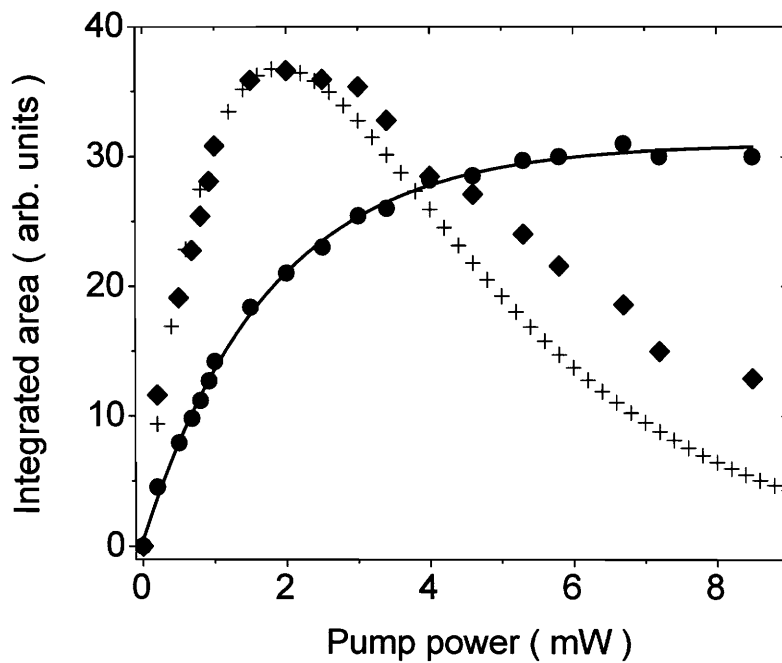


Figure 6.13 The calculated contribution of the single exciton emission to the PL spectrum 20 ps (diamonds) and 300 ps (circles) after an excitation pulse. The rescaled Poissonian probability (crosses) to generate 1 e-h pair per NC after an excitation pulse is also given for comparison.

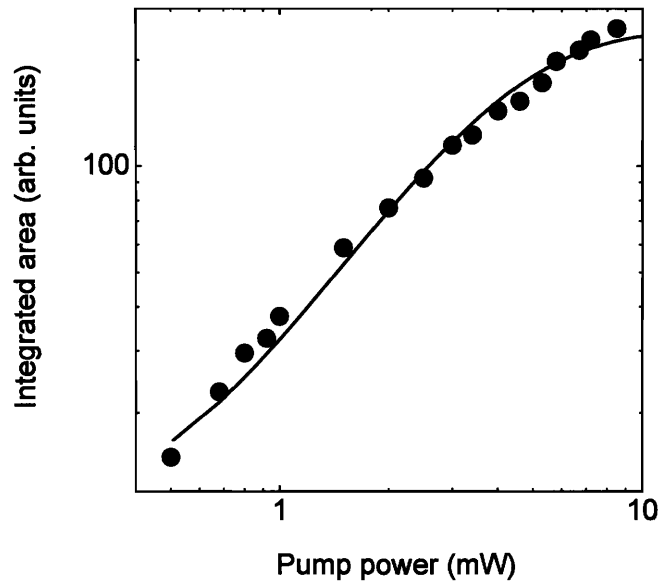


Figure 6.14 Biexciton power dependence. The solid line is a least squares fit using Equation 6.3.

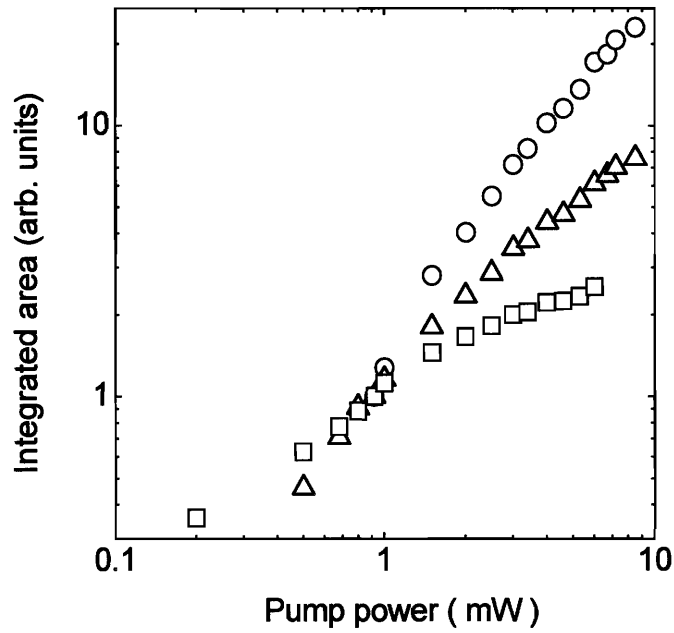


Figure 6.15 Normalized power dependence of the single exciton (squares), biexciton (triangles) and the multiexcitonic band (circles); the 3 different slopes suggest that the 3 bands originate from 3 different emission processes.

6.3.5 Amplified Spontaneous Emission measurements

Slabguides of NC-titania composites were studied under excitation from a frequency-doubled regeneratively amplified Ti:Sapph laser. These NC-titania composites possess NCs in high volume fraction and have a refractive index of about 1.7 as measured by ellipsometry. The thickness of the films are tunable by varying the spin speed during the spin coating process and are typically ~ 250 nm. The 400 nm excitation light is focused onto the film and the detected PL is spectrally analyzed with a CW CCD cooled camera. Figure 6.16 shows the linear PL spectrum of a NC-titania film comprising of 3.1 nm radius CdSe/ZnS core-shell NCs. Above a certain intensity threshold the usual biexciton ASE peak (triangles) is observed, emerging to the red side of the linear PL spectrum as illustrated in Figure 6.17. Increasing the pump power gives rise to a second, higher energy ASE peak (stars). The position of the second ASE peak coincides with the position of the multiexcitonic band, observed in the transient PL spectrum. Figure 6.18 summarizes the evolution of the integrated area below the first (triangles) and second (circles) peak as a function of pump power. The two distinct threshold values correspond to 2.2 and 4 e-h pairs injected on average into a NC. Figure 6.19 shows that the 2 ASE peaks, from both bands, are also observed for NCs with a larger radius (5.2 nm). Within our waveguide optical confinement factor, simultaneous ASE from both the biexciton and multiexciton band was only achievable for CdSe/ZnS NCs with radii larger than 3.1 nm. This is expected since the Auger recombination time for multiexcitons is much faster than that of the biexciton.

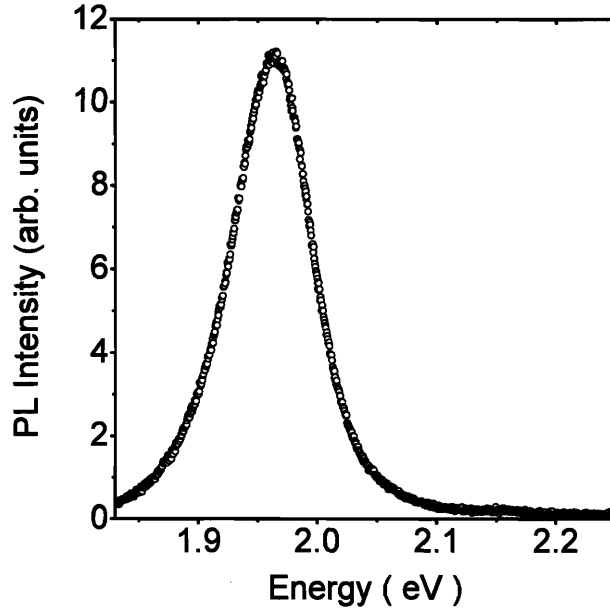


Figure 6.16 Linear PL spectrum of a 3.1 nm radius NC-doped titania thin film.

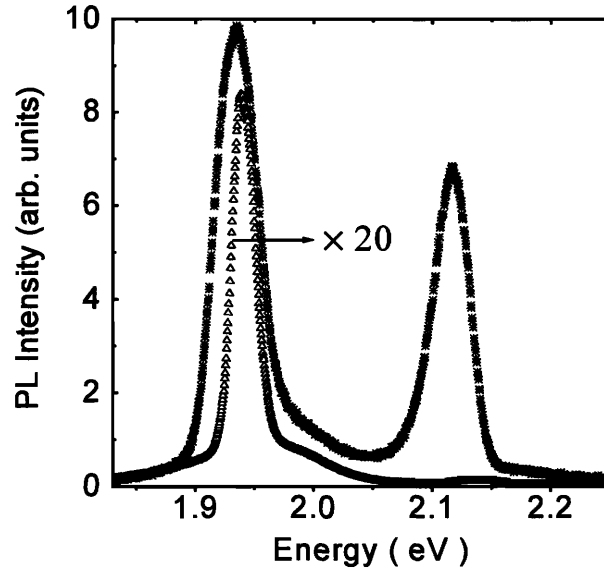


Figure 6.17 The corresponding PL spectrum for biexciton ASE (triangles) with a threshold of ~ 2.2 e-h pairs injected on average per NC. Simultaneous ASE from both the biexcitonic and multiexcitonic transition (stars) at a threshold of 4 e-h pairs injected on average per NC is also achieved. The FWHM of the two peaks are on the order of 30 meV (10 nm).

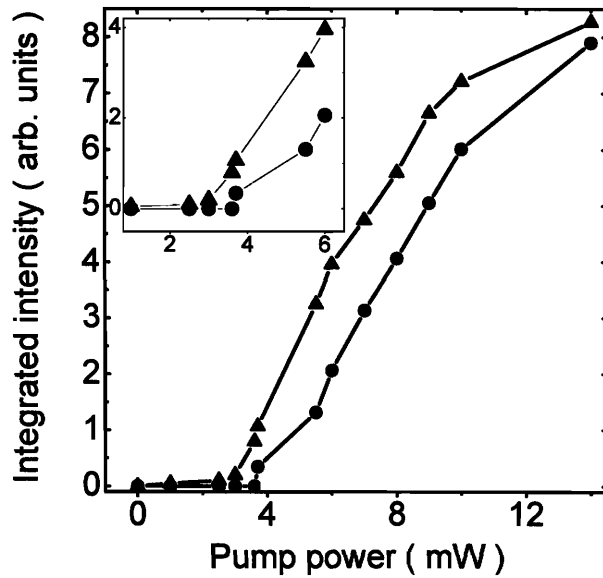


Figure 6.18 Power dependence plot of the integrated area under the biexcitonic (triangles) and multiexcitonic (circles) peak. The inset is an area of the plot enlarged to show more clearly the two distinct thresholds.

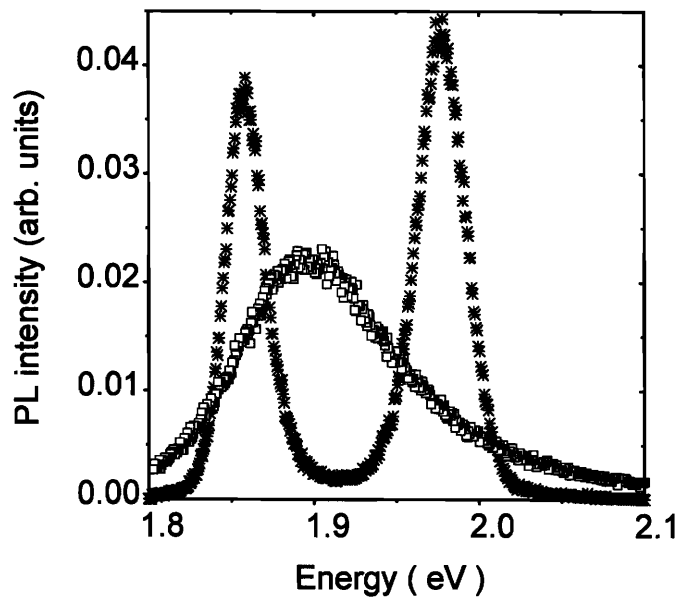


Figure 6.19 Simultaneous ASE (stars) from the biexcitonic and multiexcitonic states from a 5.2 nm CdSe/ZnS NC-titania film. The PL spectrum (squares) at low pump intensity is given for comparison.

The size evolution of the energy spacing parameter Δ obtained from transient PL measurements is further supported by the simultaneous ASE data. Indeed, the energy spacing between the 2 narrow (~ 10 nm FWHM) ASE peaks is 0.18 eV and 0.12 eV for 3.1 and 5.2 nm radius NCs, in good agreement with the values shown in Figures 6.8 and 6.9. The combined evidence from both the energy spacings and the power dependence of the multiexcitonic band lead us to conclude that the observed emission is due to a triexciton recombination process from a $1P_{3/2}-1P_e$ transition. However, since intraband relaxation processes for holes and electrons take place on a subpicosecond timescale,^{17,18} which is faster than the triexciton lifetime, a hole in the $1P_{3/2}$ state should quickly relax to the lowest $1S_{3/2}$ state. As the recombination of an electron in a $1P$ state and a hole in the $1S$ state is a forbidden transition, triexciton emission should not be observed.

To explicate the conundrum above, the following explanation is proposed: to a first approximation, the crystal field splitting energy Δ_{cf} (~ 25 meV for bulk CdSe) plays an important role in determining the relative energies of the $1S$ and $1P$ hole states. If the effect of confinement, Δ_{conf} is such that the energy difference between $1S$ and $1P$ states is greater than Δ_{cf} , then the hole states of the highest energies would be a two-fold spin degenerate $1S$ state from the heavy hole band, followed by a two-fold spin degenerate $1S$ state from the light hole band. Correspondingly, if Δ_{conf} is such that the splitting between the $1S$ and $1P$ hole states is less than Δ_{cf} , then the hole state with the second highest energy would be a $1P$ state from the heavy hole band.¹⁹ Thus in smaller NCs, $\Delta_{conf} > \Delta_{cf}$, and is consistent with the fact that cooling a 2.3 nm radius NC sample to 77 K resulted in a significant decrease in the triexciton PL intensity. However, in large NCs it is possible that $\Delta_{conf} \leq \Delta_{cf}$, and recombination with the electron in the $1P_e$ state would be allowed.

The observation of ASE from the $1P_{3/2}-1P_e$ transition is surprising due to the expectedly high degeneracy of the $1P_e$ electronic state. We speculate that the e-h exchange interaction, which plays an important role in such strongly confined NCs,²⁰ partially lifts the degeneracy of the $1P_e$ electronic state. This exchange interaction should lift the degeneracy by splitting the $1P_e$ energy levels into different sub-levels with spin 0, 1, 2, and 3. Furthermore, the observation of ASE from the $1P_{3/2}-1P_e$ transition is only possible if the ASE build up time is shorter than the gain relaxation time,²¹ which in this case is dominated by the $N \geq 3$ e-h pair Auger recombination rate. This may explain our inability to observe ASE from the $1P_{3/2}-1P_e$ transition in NCs with radii smaller than 3.1 nm, owing to their faster optical gain relaxation times. The ASE build up time is related to the NC loading fraction and the optical confinement factor of the wave-guiding media. Increasing the NC loading fraction (although there is a limit as it cannot be higher than close-packed films of the same capping ligands), or use of higher quality factor microcavities should facilitate the achievement of ASE from multiexcitonic states in NCs with radii smaller than 3.1 nm.

6.3.6 Variable stripe length measurements

The modal gain of a NC-titania slabguide comprising of 4.2 nm radius CdSe/ZnS core-shell NCs was studied at room temperature. Figure 6.20 shows its linear PL spectrum (stars) below ASE threshold, centered around 660 nm with a FWHM of 30 nm. A narrow (8 nm FWHM) biexcitonic ASE peak (circles) develops above threshold, emerging on the lower energy side of the linear PL spectrum due to the negative biexciton binding energy and reabsorption²² of amplified light in the heavily doped NC-

titania waveguide. At even higher pump excitation intensities, the multiexcitonic peak (squares) develops at 45 nm to the blue of the position of the biexcitonic ASE peak. A broadening (due to higher gain) and a slight blueshift (less reabsorption due to the bleaching of the band edge transition) of the biexciton ASE peak are also observed. Figure 6.21 illustrates the evolution of the integrated area below the first (diamonds) and second (circles) ASE peak as a function of pump power. Two different threshold values corresponding to 1.5 and 4.2 e-h pairs injected on average per NC are evident. The saturation of the biexciton ASE signal (around 8 mW) may be attributed to the saturation of the biexciton gain, i.e. the saturation of the biexciton population. As shown by the power dependence data, within the pump powers of our experiment, the biexcitonic ASE emission does not vanish with the emergence of the second ASE.

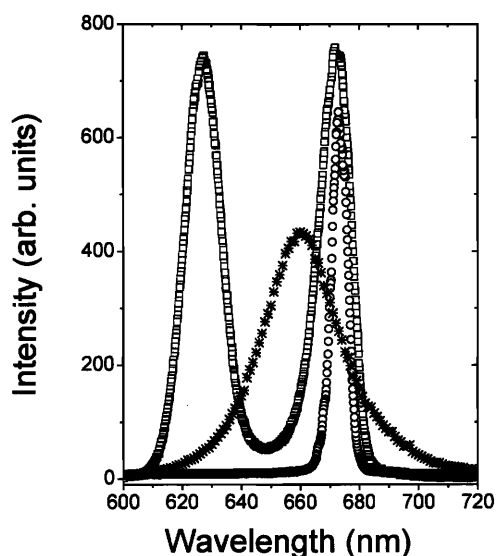


Figure 6.20 Linear PL spectrum (stars), below threshold of a NC-titania film incorporating 4.2 nm radius CdSe/ZnS NCs. The development of biexcitonic ASE (circles) is seen above threshold, followed by simultaneous ASE (squares) from both the biexcitonic and multiexcitonic states at higher pump intensities. Note that the amplitudes of both peaks are the same for a particular stripe length of excitation.

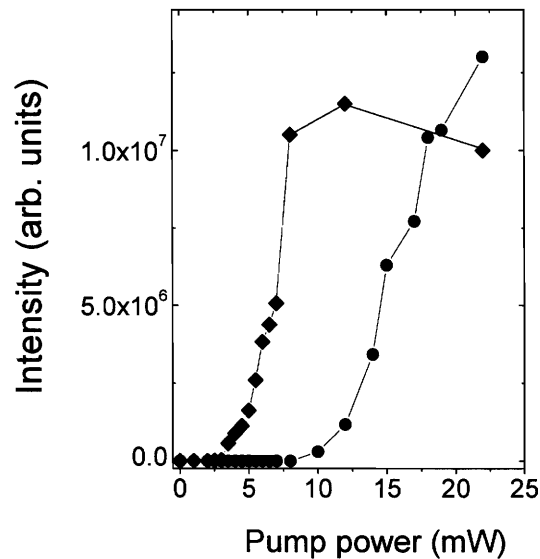


Figure 6.21 Power dependence of the integrated area under the biexcitonic and multiexcitonic ASE peaks. The development of ASE from the $1P_e$ state does not appear to affect the biexcitonic ground state ASE within the range of pump powers shown.

We employ a standard variable stripe length measurement (VSL) technique to extract the modal gain profile of the $1S_{3/2}-1S_e$ biexciton transition and the multiexciton $1P_{3/2}-1P_e$ transition. Figure 6.22 displays the evolution of the ASE intensity at 628 nm (circles) and 673 nm (diamonds) as a function of stripe length. The faster saturation of the ASE emission at 628 nm indicates that the amplification from the $1P_{3/2}-1P_e$ transition takes place at a shorter stripe length than that of the biexciton transition. Figure 6.23 depicts the modal gain profile of the NC-titania slabguide as a function of wavelength, and reveals a maximal gain of 70 cm^{-1} from the $1P_{3/2}-1P_e$ transition, which is nearly twice that of the 40 cm^{-1} gain from the biexcitonic state. This result is surprising since the $1P_{3/2}-1P_e$ gain relaxation is dominated by a $N \geq 3$ e-h pair Auger relaxation time ($< 150 \text{ ps}$ for

4.2 nm radius CdSe NCs⁷), which is shorter than the biexciton Auger relaxation time (~ 350 ps for 4.2 nm radius CdSe NCs⁷). However, this result is consistent with the ASE spectra shown in Figure 6.20. Indeed, as light amplification from the $1P_{3/2}-1P_e$ transition takes place on a smaller stripe length than that of the biexciton transition, only a stronger $1P_{3/2}-1P_e$ gain can explain the same amplitude observed for both ASE peaks at a particular stripe length of excitation.

We further confirm that the measured gain difference is not due to higher cavity losses at 673 nm. Assuming a film thickness of 300 nm and an optical refractive index of 1.7, a simple asymmetric waveguide dispersion curve calculation²³ shows that the critical angles at 673 nm and 628 nm are nearly identical at $\sim 75^\circ$, which leads to similar confinement factors. We can thus conclude that cavity losses at the film-glass and film-air interfaces are identical for both wavelengths. The gain data reveal a large discrepancy between the stimulated emission rate for the $1S_{3/2}-1S_e$ (biexciton) as well as the $1P_{3/2}-1P_e$ (multiexciton) transitions. We speculate that this difference may be due to a higher $1P_{3/2}-1P_e$ multiexcitonic ($N \geq 3$) absorption cross-section. Indeed, while previous theoretical²⁴ and experimental¹⁴ data suggest that the single exciton band edge and $1P_{3/2}-1P_e$ transition oscillator strengths are comparable, discrepancies in oscillator strength may appear in the multiexcitonic regime, where the multiparticle coulombic interaction can significantly alter transition matrix elements.

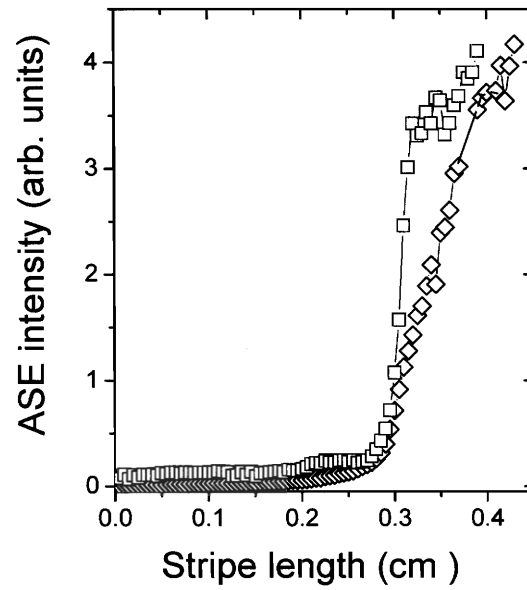


Figure 6.22 The ASE emission intensity as a function of excitation stripe length for a NC-titania slabguide comprising of 4.2 nm CdSe/ZnS core-shell NCs. The figure shows the biexciton and $1P_{3,2}-1P_e$ ASE intensities at 678 nm (diamonds) and 628 nm (squares), respectively.

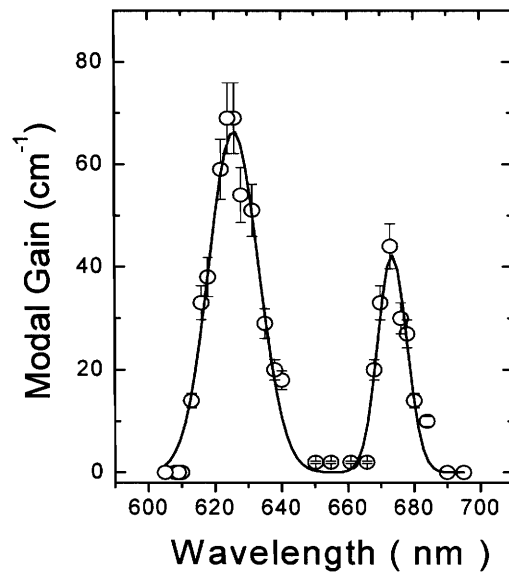


Figure 6.23 The corresponding modal gain profile of the NC-titania slabguide

6.4 Lasing from multiexcitonic states in NCs

Although simultaneous two-state lasing was recently observed in epitaxially grown self-assembled InAs quantum dots,²⁵ this was, to our knowledge, not demonstrated in colloidal NCs prior to this work. The NC-titania films comprising of 4.2 nm CdSe/ZnS core-shell NCs were embossed with a 360 nm grating pattern via soft lithographic techniques described in Chapter 3. The grating spacing of 360 nm is used to satisfy the Bragg condition for the biexciton ASE peak at 673 nm. Despite the slight Bragg mismatch at 628 nm the same grating is used to provide feedback for the $1P_{3/2}-1P_e$ lasing transition. Figures 6.24 and 6.25 illustrate the room temperature lasing spectra from the printed NC-titania DFB structure at two different detection angles. The non-collinear fashion in which the two distinct lasing wavelengths are emitted may be attributed to the slight Bragg mismatch. When matched with the stop band of the DFB grating a strong reduction in the linewidth of both ASE peaks is seen: 1 and 2 nm linewidths for the biexciton and the multiexciton lasing transitions respectively. The larger linewidth for the $1P_{3/2}-1P_e$ lasing transition is likely due to the inability to fulfill the Bragg condition at 628 nm. Within the pump fluences used in our experiment, we observe that the ground state biexciton lasing is not affected by lasing from the $1P_{3/2}-1P_e$ transition.

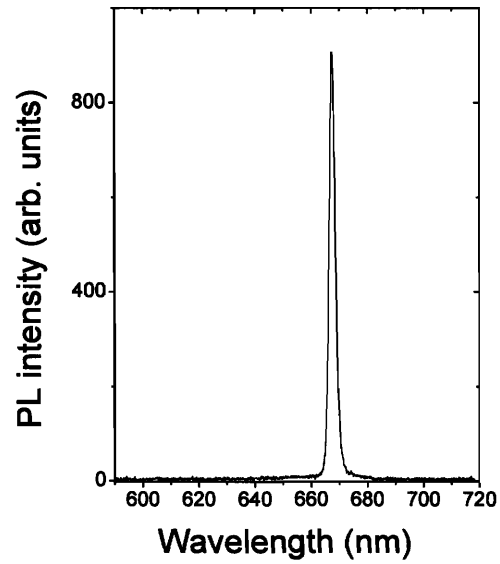


Figure 6.24 Lasing spectra of the NC-titania DFB composite laser when the grating stop band is matched to the biexciton ASE.

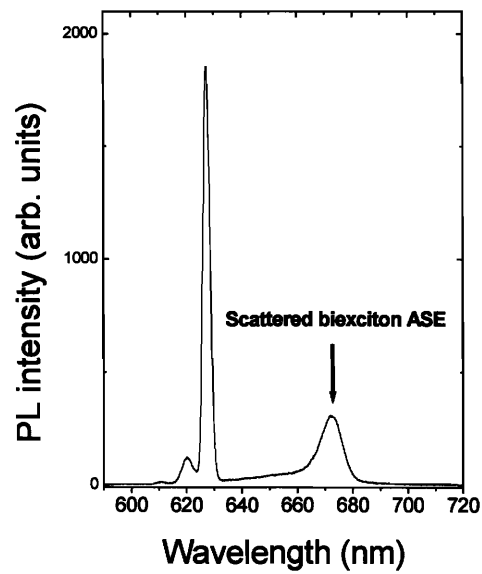


Figure 6.25 Lasing from the $1P_{3,2}-1P_e$ transition at 628 nm at a different detection angle than Figure 6.24. The peak at 673 nm originates from scattered biexcitonic ASE.

6.5 Summary and conclusions

Through the use of transient PL measurements, the multiexcitonic band observed on the higher energy side of the band edge emission peak in CdSe NCs under high excitation intensities was characterized and attributed to a triexciton recombination process arising from a $1P_{3/2}-1P_e$ transition. This triexciton emission may be facilitated by crystal field splitting energies which significantly mix the energy levels of the $1S_{3/2}$ and $1P_{3/2}$ hole states. The energy level assignment for the triexciton is further corroborated by ASE data from NC-titania composites, which show energy spacings consistent with those found using transient PL. Two interesting observations were made: Firstly, the very achievement of ASE from the $1P_{3/2}-1P_e$ transition with a threshold of ~ 4 e-h pairs suggest that the high degeneracy of the $1P_e$ electronic state (six-fold, in principle) is lifted, possibly due to e-h exchange interactions. Secondly, the surprisingly higher peak gain of the $1P_{3/2}-1P_e$ transition compared to the $1S_{3/2}-1S_e$ transition from VSL measurements lead us to speculate that the difference may be due to a higher $1P_{3/2}-1P_e$ absorption cross-section. Finally, through the use of soft-lithography, the NC-titania composite films were embossed with a DFB structure to enable room temperature lasing at both biexcitonic and multiexcitonic transitions simultaneously.

To conclude, multiexcitonic emission and lasing from the $1P_{3/2}-1P_e$ transition in colloidal CdSe NCs have been observed and characterized. It is perhaps fitting to say that the success of achieving stimulated emission and lasing from multiexcitonic states hinged upon the high volume fraction incorporation of CdSe/ZnS NCs into thermally robust sol-gel derived titania matrices. Extension of this work to produce room temperature ordered multiphoton emission from multiexciton states in single CdSe/CdZnS core-shell

NCs has already been undertaken,²⁶ suggesting the utility of single NCs as sources for nonclassical light generation. The outlook on continued work on multiexciton dynamics in NCs thus appears to be a promising, if not busy one.

6.6 References

1. E. Moreau, I. Robert, L. Manin, V. Thierry-Mieg, J. M. Gerard, I. Abram, *Phys. Rev. Lett.* **2001**, *87*, 183601
2. O. Benson, C. Santori, M. Pelton, Y. Yamamoto, *Phys. Rev. Lett.* **2000**, *84*, 2513
3. G. Chen, N. H. Bonadeo, D. G. Steel, D. Gammon, D. S. Katzer, D. Park, L. J. Sham, *Science* **2000**, *289*, 1906
4. M. Achermann, J. A. Hollingsworth, V. I. Klimov, *Phys. Rev. B* **2003**, *68*, 245302
5. H. Htoon, J. A. Hollingsworth, A. V. Malko, R. Dickerson, V. I. Klimov, *Appl. Phys. Lett.* **2003**, *82*, 4776
6. H. Htoon, J. A. Hollingsworth, R. Dickerson, V. I. Klimov, *Phys. Rev. Lett.* **2003**, *91*, 227401
7. V. Klimov, A. A. Mikhailovsky, D. W. McBranch, C. A. Leatherdale, M. G. Bawendi, *Science* **2000**, *287*, 1011
8. B. R. Fisher, H. -J. Eisler, N. E. Stott, M. G. Bawendi, *J. Phys. Chem. B* **2004**, *108*, 143
9. N. E. Stott, Ph.D. Dissertation, Massachusetts Institute of Technology, **2004**
10. B. O. Dabbousi, J. Rodriguez-Viejo, F. V. Mikulec, J. R. Heine, H. Mattoussi, R. Ober, K. F. Jensen, M. G. Bawendi, *J. Phys. Chem. B* **1997**, *101*, 9463
11. C. A. Leatherdale, W. -K. Woo, F. V. Mikulec, M. G. Bawendi, *J. Phys. Chem. B* **2002**, *106*, 7619
12. M. Kuno, J. K. Lee, B. O. Dabbousi, F. V. Mikulec, M. G. Bawendi, *J. Chem. Phys.* **1997**, *106*, 9869
13. V. I. Klimov, *J. Phys. Chem. B* **2000**, *104*, 6112

14. D. J. Norris, M. G. Bawendi, *Phys. Rev. B* **1996**, *53*, 16338
15. T. Vossmeier, L. Katsikas, M. Giersig, I. G. Popovic, K. Diesner, A. Chemseddine, A. Eychmuller, H. Weller, *J. Phys. Chem.* **1994**, *98*, 7665
16. P. Guyot-Sionnest, M. A. Hines, *Appl. Phys. Lett.* **1997**, *72*, 686
17. V. Klimov, A. A. Mikhailovsky, D. W. McBranch, C. A. Leatherdale, M. G. Bawendi, *Phys. Rev. B* **2000**, *61*, R13349
18. U. Woggon, H. Giessen, F. Gindele, O. Wind, B. Fluegel, N. Peyghambarian, *Phys. Rev. B*, **1996**, *54*, 17681
19. B. Fisher, J. –M. Caruge, Y. Chan, J. Halpert, M. G. Bawendi, *Chem. Phys.* **2005**, *318*, 71
20. Al. L. Efros, M. Rosen, M. Kuno, M. Nirmal, D. J. Norris, M. Bawendi, *Phys. Rev. B* **1996**, *54*, 4843
21. V. I. Klimov, A. A. Mikhailovsky, S. Xu, A. Malko, J. A. Hollingsworth, C. A. Leatherdale, H. –J. Eisler, M. G. Bawendi, *Science* **2000**, *290*, 314
22. V. C. Sundar, H. –J. Eisler, M. G. Bawendi, *Adv. Mater.* **2002**, *14*, 739
23. B. E. A. Saleh, M. C. Teich, *Fundamentals of Photonics* (Wiley-Interscience, New York, 1991), p. 249
24. J. B. Xia, *Phys. Rev. B* **1989**, *40*, 8500
25. A. Markus, J. X. Chen, C. Paranthoen, A. Fiore, C. Platz, O. Gauthier-Lafaye, *Appl. Phys. Lett.* **2003**, *82*, 1818
26. B. Fisher, J. –M. Caruge, D. Zehnder, M. G. Bawendi, *Phys. Rev. Lett.* **2005**, *94*, 087403

Chapter 7

Concluding Remarks

This thesis broadly explored the chemistry and physics of wet-chemically synthesized semiconductor nanocrystals (NCs) doped in sol-gel derived structures, and in some instances enabled potentially novel applications. It was shown in Chapter 2 that growing a shell of silica or titania on Stöber microspheres in the presence of appropriately derivatized CdSe/ZnS NCs allowed for their uniform incorporation into the shell. The utility of these well-characterized, sub-micron diameter NC-silica microspheres in *in-vivo* imaging was demonstrated and extending their role as a size-tunable and photostable chromophore to other applications such as flow visualization in microfluidics to map out velocity profiles of particulates is certainly a distinct possibility. Another avenue for exploration would be in the area of photonics, since the NC-titania coated microspheres offer a good refractive index contrast ($n \sim 1.7$) with air, and their monodispersity permits them to close-pack into 3D structures. Although each individual sphere is too small to support whispering gallery modes (WGMs) and is thus inadequate as a laser cavity, their assembly into a photonic pseudogap structure may have interesting consequences. For example, Maskalay et. al., have recently shown that inverse opal structures of CdSe NC-titania show gain enhancement and significantly reduced ASE thresholds.¹

The development of CdSe/ZnS NC lasers was described in Chapter 3, and facile processes to introduce optical feedback to NC-titania structures were developed. From

soft-lithographically embossed distributed feedback (DFB) structures to large NC-titania coated microspheres exhibiting whispering gallery mode (WGM) lasing, NC-based gain media have indeed come a long way since their inception as close-packed films showing amplified spontaneous emission at low temperature.² However, composites of NC-titania were found to be unsuitable for any practical application since exposure to moisture results in their rapid structural and photophysical degradation, as shown in Chapter 4. A new synthetic strategy employing a combination of different silica precursors subsequently addressed this issue, and the ensuing NC-silica composites were found to be robust in a variety of solvent environments. Fabrication techniques developed for NC-titania composites could easily be transferred to NC-silica composites to yield NC-silica DFB and WGM lasers which were found to be optically responsive towards an aqueous environment of amines. These composites have the potential to be interfaced with microfluidic systems to produce non-linear optical chemosensors,³ although it should be emphasized that much work needs to be done in increasing both the sensitivity and chemical specificity of the device. One method of enhancing the chemical sensitivity of the composite is to increase its porosity. Increasing the porosity of silica films can be achieved through the addition of block co-polymers to the acid-catalyzed condensation of tetraethylorthosilica (TEOS).^{4,5} These mesoporous silica films can be extremely smooth, as illustrated in Figure 7.1, and the inclusion of NCs into these films should raise their relatively low refractive indices to make them better waveguides. However, new methodologies to obviate the use of acid-catalysis must be invented in order to be compatible with the current NC incorporation process.

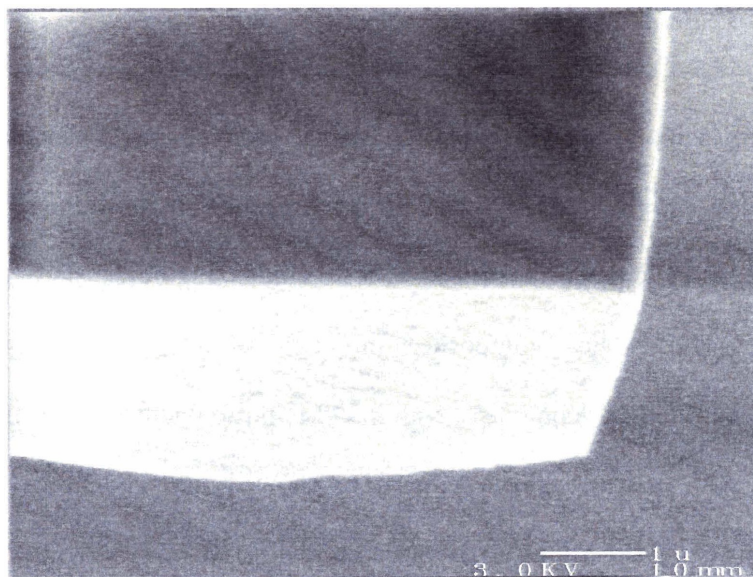
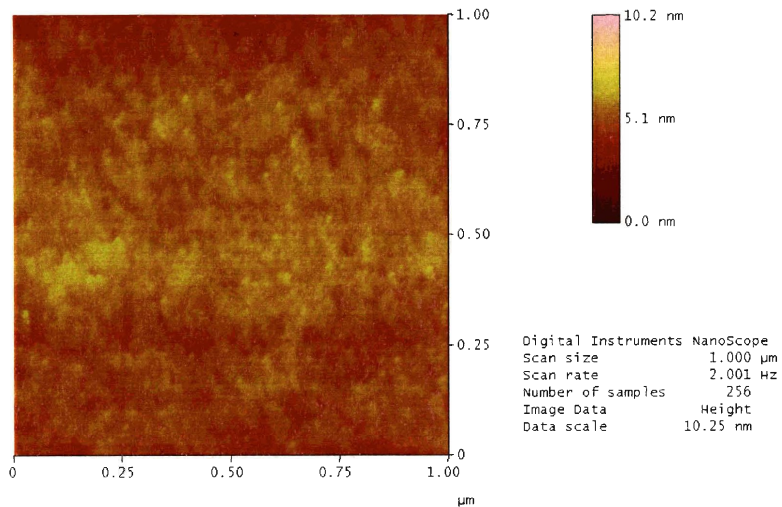


Figure 7.1 AFM (top) and SEM (bottom) images of a mesoporous silica film made by adding poly(ethylene oxide)-b-poly(propylene oxide)-b-poly(ethylene oxide) (commonly known as P123) to an acid-catalyzed solution of TEOS according to reference [4]. The surface roughness (RMS) as depicted by the AFM image is 0.3 nm.

Much effort was spent on making the surface chemistry of different NCs compatible with sol-gel processes. We showed in Chapter 5 that the surface chemistry of as-synthesized core-shell CdS/ZnS NCs rendered them incompatible with the standard protocols used to incorporate CdSe/ZnS NCs into sol-gel matrices. This was overcome through a judicious modification of the incorporation procedure and blue NC lasing at room temperature from core-shell CdS/ZnS NCs in silica was achieved. Although extension of the incorporation procedure into silica to produce stimulated emission in other semiconductor NCs such as PbSe and InAs has not been as successful, uniform and smooth-looking films were achieved. A typical procedure for producing such films is as follows: to 28 mg of PbSe NCs, 56 mg of tetrahydrofuran, 150 mg of 6-amino-1-hexanol (50% wt/wt in ethanol) and 80 mg of 16-hydroxy-hexadecanoic acid is added, resulting in a clear but dark solution. To this solution, 30 mg of aminopropyltrimethoxysilane is added, and the resulting mixture is stirred for 5 mins and spin-coated onto a glass slide. Annealing on a hot plate proceeded at 100 °C for ~ 2 mins. Figure 7.2 shows the emission spectra from a PbSe-silica composite film excited using a frequency-doubled, regeneratively amplified Ti:Sapph laser with a 100 fs pulse width and a 1 kHz repetition rate. Although ASE was not achieved, the films showed thermal stability even at high excitation intensities ($\sim 20 \mu\text{J/pulse}$ over an area of $5 \times 10^{-3} \text{ cm}^2$). While ASE in PbSe NCs stabilized in titania have been reported,⁶ there is still impetus to develop and implement silica as a more robust host matrix for reasons enumerated in Chapter 4. The incorporation of different semiconductor NCs into sol-gel derived matrices should not only be able to extend the spectral window of NC-based lasers, but would also present a stable platform in which to investigate their nonlinear optical properties.

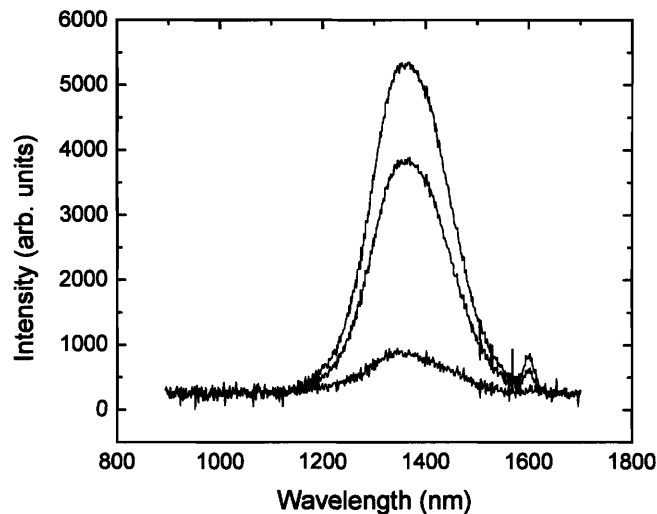


Figure 7.2 Emission spectra of PbSe NCs incorporated into a silica matrix. Although excitation intensities were as high as $20 \mu\text{J}/\text{pulse}$ over an area of $5 \times 10^{-3} \text{ cm}^2$, no ASE was observed. The small peak at 1600 nm is a harmonic of the excitation source.

The observation of ASE from multiexcitonic states in CdSe/ZnS NCs was, in many ways a surprising result, especially since the quantum yield of such states would be expectedly low due to highly efficient Auger relaxation processes. The multiexcitonic emission was subsequently determined as originating from a $1P_{3/2}-1P_e$ transition, and the flexibility of the titania facilitated the embossing with a grating pattern to produce a multiexcitonic distributed feedback NC-laser. The work described in Chapter 6 is thus an example of how the incorporation of CdSe/ZnS NCs into sol-gel derived microcavities can result in the observation of interesting nonlinear optical behavior. It would be interesting to perform a similar investigation on CdS/ZnS-silica composites to see if any multiexcitonic emission may be observed, thus possibly lending insight into the nature of the electronic transitions in CdS NCs.

References

1. G. R. Maskaly, M. A. Petruska, J. Nanda, I. V. Bezel, R. D. Schaller, H. Htoon, J. M. Pietryga, V. I. Klimov, *Adv. Mater.* **2006**, *18*, 343
2. V. I. Klimov, A. A. Mikhailovsky, S. Xu, A. Malko, J. A. Hollingsworth, C. A. Leatherdale, H. Eisler, M. G. Bawendi, *Science* **2000**, *290*, 314
3. A. W. Wun, P. T. Snee, Y. Chan, M. G. Bawendi, D. G. Nocera, *J. Mater. Chem.* **2005**, *15*, 2697
4. P. Yang, G. Wirnsberger, H. C. Huang, S. R. Cordero, M. D. McGehee, B. Scott, T. Deng, G. M. Whitesides, B. F. Chmelka, S. K. Buratto, G. D. Stucky, *Science* **2000**, *287*, 465
5. D. Zhao, J. Feng, Q. Huo, N. Melosh, G. H. Fredrickson, B. F. Chmelka, G. D. Stucky, *Science* **1998**, *279*, 548
6. R. D. Schaller, M. A. Petruska, V. I. Klimov, *J. Phys. Chem. B* **2003**, *107*, 13765

YINTHAI CHAN

Massachusetts Institute of Technology
400 Main Street, 18-080
Cambridge, MA 02139
(617) 253-8594

70 Pacific St. Apt.606
Cambridge, MA 02139
(617) 452-5154
ytchan77@mit.edu

EDUCATION

Massachusetts Institute of Technology Cambridge, MA

Candidate for Ph.D in Physical Chemistry 2001-present
"The Physics and Chemistry of Semiconductor Nanocrystals in Sol-gel Derived Optical Microcavities."
Thesis advisor: Professor Mounji G. Bawendi
Cumulative GPA: 5.0/5.0

University of California, Berkeley Berkeley, CA

B.S. in Chemistry 1998-2000
Cumulative GPA: 3.8/4.0, High Honors

EXPERIENCE

Massachusetts Institute of Technology Cambridge, MA

Research Assistant 2001-present
Co-invented novel procedure for incorporating CdSe/ZnS and CdS/ZnS nanocrystals into the shells of monodisperse sub-micron diameter silica microspheres. Extended the procedure to include shells of titania. Co-invented novel procedure for producing hundreds of nanocrystal-based spherical resonators in a single spin-coating process. These spherical resonators exhibit whispering gallery mode lasing at room temperature.
Co-discovered the presence of multiexcitonic emission and stimulated emission in a titania film of CdSe nanocrystals.
Demonstrated room temperature lasing at a range of blue wavelengths using CdS/ZnS nanocrystals in a sol-gel derived silica matrix.

Massachusetts Institute of Technology Cambridge, MA

Teaching Assistant 2001-2002
Courses taught: Principles of Chemical Science; Thermodynamics and Kinetics

University of California, Berkeley Berkeley, CA

Undergraduate Research Assistant under Professor A. Paul Alivisatos 2000-2001
Covalently linked oligonucleotides to semiconductor nanocrystals and exposed them to gold surfaces containing complementary oligonucleotides.

University of California, Berkeley Berkeley, CA

Reader for introductory astronomy 1999-2000

AWARDS

Graduate student award for excellence in teaching, Department of Chemistry, Massachusetts Institute of Technology, 2002. Dean's list, College of Chemistry, University of California, Berkeley, 2000.

MEMBERSHIPS

American Chemical Society. Materials Resesarch Society. Alpha Chi Sigma Class of 2000.

List of Publications

- Caruge, J.-M.; Chan, Y.; Sundar, V.; Eisler, H.-J.; Bawendi, M.G., "Transient photoluminescence and simultaneous amplified spontaneous emission from multiexcitonic states in CdSe quantum dots", *Physical Review B*, **70**, 085316 (2004).
- Chan, Y.; Caruge, J.-M.; Snee, P.T.; Bawendi, M.G., "Multiexcitonic two-state lasing in a CdSe nanocrystal laser", *Applied Physics Letters*, **85**, 2451 (2004).
- Chan, Y.; Zimmer, J.P.; Stroh, M.; Steckel, J.S.; Jain R.K.; Bawendi M.G., "Incorporation of luminescent nanocrystals into monodisperse core-shell silica microspheres", *Advanced Materials*, **16**, 2092 (2004).
- Sundar, V.C.; Eisler, H.-J.; Deng, T.; Chan, Y.; Thomas, E.L.; Bawendi, M.G., "Soft-lithographically embossed multilayered distributed-feedback nanocrystal lasers", *Advanced Materials*, **16**, 2137 (2004).
- Chan, Y.; Steckel, J.S.; Snee, P.T.; Caruge, J.-M.; Hodgkiss, J.M.; Nocera, D.G.; Bawendi, M.G., "Blue semiconductor nanocrystal laser", *Applied Physics Letters*, **86**, 073102 (2005).

*This work was featured in *Photonics Spectra* (April 2005) and *Laser Focus World* (May 2005)

- Snee, P.T.; Chan, Y.; Nocera, D.G.; Bawendi, M.G., "Whispering-gallery-mode lasing from a semiconductor nanocrystal/microsphere resonator composite", *Advanced Materials*, **17**, 1131 (2005).
 - Vezenov, D.V.; Mayers, B.T.; Conroy, R.S.; Whitesides, G.M.; Snee, P.T.; Chan, Y.; Nocera, D.G.; Bawendi, M.G., "A low-threshold, high-efficiency microfluidic waveguide laser," *Journal of the American Chemical Society*, **127**, 8952 (2005)
 - Wun, A.W.; Snee, P.T.; Chan, Y.; Bawendi, M.G.; Nocera, D.G., "Non-linear transduction strategies for chemo/biosensing on small length scales," *Journal of Materials Chemistry*, **15**, 2697 (2005).
 - Fisher, B.R.; Caruge, J.-M.; Chan, Y.; Halpert, J.E.; Bawendi, M.G., "Multiexciton fluorescence from semiconductor nanocrystals," *Chemical Physics*, **318**, 71 (2005)
 - Chan, Y.; Snee, P.T.; Caruge, J.-M.; Yen, B.K.H.; Nair, G.P.; Nocera, D.G.; Bawendi, M.G., "A solvent stable nanocrystal-silica composite laser," *Journal of the American Chemical Society*, **128**, 3146 (2006)
- *This work was featured in *Chemical & Engineering News* (February 2006)
- Chan, Y.; Yen, B.K.H.; Zimmer, J.P.; Nair, G.P.; Bawendi, M.G., "An all-optical method of determining the absorption cross-section of luminescent semiconductor nanocrystals," (in prep.)

List of Patents

- Chan, Y.; Zimmer, J.P.; Bawendi, M.G. "Incorporation of Nanocrystals into Core-Shell Microspheres," U.S. Patent Application Number 10/898554, filed July 26, 2004.
- Chan, Y.; Zimmer, J.P.; Insin, N.; Tracy, J.B.; Bawendi, M.G. "Microspheres Including Nanoparticles," Patent Cooperation Treaty (PCT) Application Number US0525593, filed July 20, 2005.
- Snee, P.T.; Chan, Y.; Nocera, D.G.; Bawendi, M.G., "Whispering Gallery Mode Laser and Sensor," U.S. Patent Application Number 11/288321, filed Nov 29, 2005.

Presentations

- **Chan Y.**, "Applications of Semiconductor Nanocrystals in Sol-gel Derived Microcavities" Graduate Student Seminar Series, Center for Integrated Photonics, MIT, 2006 (oral presentation)
- **Chan Y.**, "Applications through nanocrystal-doped sol-gel microcavities" Harrison Spectroscopy Laboratory Annual Meeting, MIT, 2006 (oral presentation).
- **Chan Y.**, "New applications and insights through nanocrystal-doped sol-gel structures," Graduate student seminar, MIT, 2005 (oral presentation).
- **Chan Y.**; Caruge, J.-M.; Snee, P.T.; Nocera, D.G.; Bawendi, M.G., "Colloidal semiconductor nanocrystal lasers," Materials Processing Center – Materials Day, MIT, 2004 (poster presentation).
- **Chan, Y.**; Steckel, J.S.; Snee, P.T.; Caruge, J.-M.; Hodgkiss, J.M.; Nocera, D.G.; Bawendi, M.G., "Blue semiconductor nanocrystal laser," Materials Research Society, Boston, 2004 (oral presentation).
- Caruge, J.-M.; **Chan, Y.**; Sundar, V.; Eisler, H.-J.; Bawendi, M.G., "Photophysics of charged CdSe quantum dots," Materials Research Society, San Francisco, 2004 (poster presentation)

References

Prof. Mounji G. Bawendi
Professor, Dept. of Chemistry, MIT
77 Massachusetts Ave, 6-221
Cambridge, MA 02139
Phone: (617) 253-9796
mgb@mit.edu

Prof. Daniel G. Nocera
Professor, Dept. of Chemistry, MIT
77 Massachusetts Ave, 6-335
Cambridge, MA 02139
Phone: (617) 253-5537
nocera@mit.edu

Prof. A. Paul Alivisatos
Professor, Dept. of Chemistry
University of California, Berkeley
D43 Hildebrand
Berkeley, CA 94720
Phone: (510) 643-7371
alivis@berkeley.edu

Prof. Preston T. Snee
Assistant Professor, Dept. of Chemistry
University of Illinois, Chicago
845 West Taylor Street
Chicago, IL 60607
Phone: (617)253-8594
sneep@mit.edu

Acknowledgements

I would first like to thank my parents, Kah Khiong and Cecilia, for their love and support through the many years in graduate school that I was away from my home in Singapore. Their relentless encouragement enabled me to trudge through the most difficult times of my life, and without which this thesis would not be possible. My career in science can probably be attributed to my dad, whose own role as an excellent experimental scientist had inspired me to abandon the suit and tie in favor of the ever-trendy VWR white lab coat. I also thank Yoke Kwan for being a wonderful big sister who always offered a listening ear when I needed it in spite of my frequent ranting about life's ordeals.

I am very thankful to my thesis advisor, Mounqi for his great tolerance and ever-patient disposition, always offering friendly instruction despite my countless displays of ignorance. I am especially grateful for the financially stress-free environment he has provided the group, and the encouragement to actively pursue our own ideas. This intellectual freedom has undoubtedly helped to fashion and develop my skills as an independent researcher. I must say I am glad Mounqi abandoned the lure of riches on Wall Street long ago to assume the role of a most excellent scientific advisor.

To my colleagues in the Bawendi group, it has been a very rewarding 5 years. It must be somewhat difficult, I imagine, putting up with my various idiosyncrasies and I would like to express my heartfelt gratitude to my stalwart colleagues for their immense patience. I want to thank my colleagues and long-time collaborators Jean-Michel and Preston in particular, for their guidance in the lab. Their mentorship has seen me through the many technical difficulties in my graduate career, and to which I am deeply indebted. I would also like to thank John, Jonny, Brian and Dave, who shared with me a strong camaraderie that has made the past 5 years in the dungeons of Building 18 so much better both professionally and socially. I'm quite proud to have been one of the founding members of the lunch and coffee gang, and in the good hands of Jon and Venda I am confident that more cohesive interactions will be fostered between group members. I certainly hope the collaborative atmosphere in the group will continue to flourish.

Much credit has to be given to my friends outside of the lab, who have weathered many of my complaints about the hardships of life, and whose words of encouragement always lifted my spirits whenever failed experiments in the research lab sunk them. I thank Grace, Jelena and Justin who have been with me since our early days of struggling with p-chem classes. I would also like to acknowledge Palex, Lynn, Songya, Vivien and Wenchao for their support and encouragement, and in some instances, home-cooked food when I forgot to buy dinner. I am also grateful to Bingru for her support through many difficult times I faced throughout most of graduate school. I thank Jujin, Ivy and Hiroyo for their friendship and for making Friday night dinners something I could always look forward to. Last but not least, I would like to thank Rie for being the light at the end of the tunnel in my graduate career, making the future brighter and happier than I could have expected.